PROVISION OF POINT-SOURCE WATER BY AIR-GAP MEMBRANE DISTILLATION

Final Report to the

Water Research Commission

by

RD Sanderson[1], C Aldrich[2], L Lorenzen[2] and BF Chemaly[1]

[1]Institute for Polymer Science, University of Stellenbosch,
Private Bag X1, Matieland 7602 RSA
[2]Department of Chemical Engineering, University of Stellenbosch,
Private Bag X1, Matieland 7602 RSA

WRC Report No. 591/1/97
ISBN 1 86845 295 6

February 1997

ACKNOWLEDGEMENTS

I would like to thank the following people without whom this study would have been impossible:

DR. R.D. SANDERSON, DR. C. ALDRICH and PROF. L. LORENZEN, my promotors, for all their help and support.

INSTITUTE OF POLYMER SCIENCE and **DEPARTMENT OF CHEMICAL ENGINEERING** for financial support.

The **STAFF** of the **DEPARTMENT OF CHEMICAL AND METALLURGICAL ENGINEERING** for all their help.

The **STAFF** of the **INSTITUTE FOR POLYMER SCIENCE** for all their help.

Mr. F. LANCHASTER for help in preparing this document.

To my **MOTHER**, for all her love and support.

To my **FRIENDS**, for making Stellenbosch such an unforgettable experience.

To **OUR HEAVENLY FATHER** for providing me the opportunity and the strength.

PROVISION OF POINT-SOURCE WATER BY AIR-GAP MEMBRANE DISTILLATION

EXECUTIVE SUMMARY

Report to the Water Research Commission

by

R.D. Sanderson[1], C. Aldrich[2], L. Lorenzen[2] and B.F. Chemaly[1]

[1]*Institute for Polymer Science, University of Stellenbosch, Private Bag X1,* Matieland 7602 RSA

[2]Department of Chemical Engineering, University of Stellenbosch, Private Bag X1, Matieland 7602, RSA

INTRODUCTION

In many areas of South Africa there is no reliable water supply. In most of these areas there is, however, access to large quantities of brackish ground water or contaminated water which is generally non-potable. There exists a need therefore for a membrane desalination unit which could make use of the abundant supply of solar energy to desalinate these water supplies to produce potable water.

Apart from being both portable and cheap, the proposed unit should be both simple to operate and require only low maintenance costs. These requirements call for a system that will appeal to a very broad market, ranging from agriculture to hiking. This report describes the designing of such a device and initial results.

In order to understand the transport phenomena in such a unit, a mathematical model had to be derived. Such a model may also be used to predict the permeate flux of such a unit under various operating conditions.

BACKGROUND

In order to produce a distillate of quality energy is required to separate the different species present in the feed to the distillation unit. A principle governing factor is the cost of the energy required to produce the thermal driving force. Generally, separation by membrane distillation has been found to be competitive in situations where some source of waste energy is available or where electricity is expensive. The advantage of using a solar distillation unit to produce water which is safe for human consumption, lies in the fact that solar energy is used as the only source of energy and it is readily available. In most areas where there is a lack or shortage of reliable water, there is access to large quantities of brackish, non-potable water. The combination of abundant quantities of solar energy and the availability of non-potable water, gives rise to the possibility of economically desalinating such water to produce water of potable standard.

Membrane distillation is a process by which water in a salt solution is evaporated through a porous membrane **[1]**. The vapour condenses on a coolant surface on the other side of the membrane. The two liquid surfaces; the heated salt solution and the condensate, are separated by a porous hydrophobic membrane. Surface tension forces withhold liquids from the pores and prevent contact of the two streams. It can be said that the main purpose of the membrane in membrane distillation is as a physical support for the vapour-liquid interface **[2]**.

The temperature difference, causing a corresponding vapour pressure difference across the membrane, provides the driving force for the membrane distillation process. Evaporation will occur at the solution surface if the vapour pressure on the solution side is greater than the vapour pressure at the condensate surface. Vapour then diffuses through the pores to the cooler surface, where it condenses.

There are basically two categories in which membrane distillation (MD) can be categorised. These are Direct Contact Membrane Distillation (DCMD) and Air Gap Membrane Distillation (AGMD) **[3]**. In both cases the liquid feed flows over the one side of the membrane and the evaporation surface is immobilised at one membrane surface. In DCMD the condensation surface is localised at the downstream side of the membrane, while in AGMD condensation of the distillate

takes place over a cold surface separated from the membrane by an additional gap of an inert gas, typically air. In DCMD the distance between the evaporation and the condensing surfaces is separated only by the membrane, resulting in low mass and heat transfer. In AGMD, on the contrary, the evaporation and condensing surfaces are separated by a much larger distance hence giving rise to a much larger heat and mass resistance. The very narrow gas gap in the DCMD set-up gives rise to a small temperature difference between the two surfaces, creating a small driving force for mass transfer. The larger air gap in the AGMD set-up, on the other hand, gives rise to a larger temperature difference and consequently a large partial pressure difference. An increase in the air-gap thickness is beneficial in all cases as far as the heat losses are concerned; however, it can result in an increase or in a decrease of the water distillation rate from a salt solution.

MOTIVATION

Membrane distillation is a rapidly growing field gaining wide attention from membrane experts such as Enrico Drioli in Italy, Marcel Mulder in the Netherlands, Tony Fane in Australia, Sydney Loeb in Israel, and many others in the USA, and even more in Japan. The biggest use of membrane distillation is the stripping of water in the concentration of foods or biostreams, at room temperature. Prof. Tony Fane of the Membrane Research Centre at the University of New South Wales in Australia has a solar membrane distillation plant at the university.

The potential value of successful results of this research are not restricted to South Africa, but could have international implications, especially into Africa.

There is also a need to have a small storable device that can provide drinkable water in an emergency, or that can provide water at any site far from a water reticulation system.

Companies such as ESKOM were interested as they needed pure water for washing purposes at distant substations. Farmers in Botswana were interested as they have no means for providing water for their stock in distant areas of their

farms. In an emergency at sea it is important to have a means for distilling drinking water, even by body heat.

This is a very new field of research, becoming increasingly viable as improved membranes become available. (The best membranes were considered to be the Enka polypropylene, the Goretex polytetrafluoroethylene, the ATO Pebax films, the GKSS Pebax films and the ICI polyurethane film).

OBJECTIVES

The original objectives included the following:

Construction of a foldable, storable, membrane distillation bag which could be used in emergencies, to meet daily requirements of sterile and desalinated water, and a unit to produce 1 - 10 litres of such water per day, by the use of solar heat, body heat, heat from hot rocks or cooling by wind.

Construction of a movable membrane air-gap distillation unit operated by solar heat and air-cooling which could be used on farms to desalinate brack borehole water in quantities of 100 or more litres per day.

The membrane distillation bag should be a small pocket-sized pouch or bag that could be filled with sea, saline or polluted water and which, in short term, could distill this water to produce a potable product.

The membrane air-gap distillation unit should be a larger movable structure that could be placed, for extended periods of time, in a solar environment and which could continuously deliver desalinated water, for long periods of time.

RESULTS

An air-gap membrane distillation unit was designed and assembled. Experimental details are given elsewhere **[4, 5]**. Using a two-level, four-factor full factorial design, it was found that the variables temperature of the brine, the air-gap width and the temperature of the cooling water had the most significant effects on the response variable and the production rate of desalinated water. By increasing the

brine water temperature and by decreasing the cooling water temperature, the mass flux was maximised. There was an experimental relationship between the mass flux and temperature of the brine feed. The air-gap and the concentration of the brine solution did, however, also affect the mass flux.

The effect of changes in the temperature of the condensing surface was not as significant as changes in the temperature of the salt solution. If the air-gap was saturated with water-vapour, it is obvious that the temperature of the condensing surface would have a noticeable effect on the permeation rate. The lower the temperature of the condensing surface, the faster the water-vapour would condense. This would influence the saturation of the water-vapour in the air-gap, and diffusion would be able to take place at a faster rate through the specific membrane and under the specific conditions.

Both a fundamental model and an empirical model were derived for the transport phenomena in air-gap membrane distillation.

The fundamental model was inclined to deviate from the experimental results, especially at high feed concentrations and at high temperatures. (These deviations were considered to possibly be due to the facts that: the permeability was assumed to be concentration independent and the vapour pressure that was extrapolated for salt concentrations above 26% (wt.). On a typical South African summer's day, the temperature of the water can reach temperatures as high as 52°C. If a larger water volume was used, the same temperature would be reached, but it would take longer to reach this temperature. A brine water temperature of this magnitude could result in a mass flux of about half a litre per hour. In instances where this process might be applied in emergency to obtain fresh water, a flux of this magnitude would be adequate in the short term.

The salt rejection of this process varied between 99.69% - 99.94% and, for a continuous system, no fouling occurred over short periods of time.

CONCLUSIONS AND RECOMMENDATIONS

Air-gap membrane distillation units have successfully been made with a transfer area of 400 cm^2. They might be used by hikers, campers and people living in rural areas without access to fresh water. A shortcoming was, however, the fact that the air-gap membrane distillation units had variables that were difficult to control. From the data obtained from the alternative set-up, the conclusion could be drawn that this would be a viable process if a low mass flux is required and sunlight or some other source of waste heat is available. When sunlight was used as an energy source, the feed could be heated to temperatures of up to 52°C. If these distillation units were to be used only for emergency purposes, this method of fresh water production would be viable. The permeate was of a quality that met the requirements for human consumption, since the salt rejection achieved by this process was greater than 99.6%.

There was a good correlation between the predicted and experimental results. The fundamental model could be used with confidence to predict the performance of air-gap membrane distillation. The fundamental model had a correlation coefficient (R^2) of 0.9156, while the empirical model had a correlation coefficient (R^2) of 0.9026. At high brine concentrations, where the fundamental model tends to deviate from the experimental data, the empirical model can be used to predict the performance of the air-gap membrane distillation unit. Below 3% (wt.) NaCl solution, both the models correlate the experimental data quite accurately, whilst the empirical model produces better results when the air gap width is changed. Conversely, it was found that the fundamental model made better predictions of the experimental data when the flowrates of the brine solution and the cooling water were varied. The mass flux can therefore be very accurately predicted when the advantages and disadvantages of both these models are taken into account.

There was a near linear relationship between the vapour pressure difference and the mass flux, showing that the vapour pressure difference was the driving force in the process.

REFERENCES

1. A.S. Johnson, R. Wimmerstedt, A.C. Harryson. Membrane Distillation: A theoretical study of evaporation through microporous membranes, *Desalination*, **56**, 237-249 (1985).

2. S. Bandini, C. Gostoli, G.C. Sarti. Role of heat and mass transfer in membrane distillation process, *Desalination*, **81**, 91-105 (1991).

3. I. Basini, G. D'Angelo, M. Gobbi, G.C. Sarti, C. Gostoli. A desalination process through sweeping gas membrane distillation, *Desalination*, **64**, 246-257 (1987).

4. B.F. Chemaly. Modelling of the transport phenomena in an airgap membrane distillation unit, M.Sc.-thesis, University of Stellenbosch, November 1995.

5. B.F. Chemaly. Point source water, Institute for Polymer Science, University of Stellenbosch, In-house report.

TABLE OF CONTENTS

LIST OF SYMBOLS viii

LIST OF TABLE xiii

LIST OF FIGURES xviii

CHAPTER 1 1
INTRODUCTION 1

CHAPTER 2 3
LITERATURE SURVEY 3
2.1 Membrane Distillation 3
2.1.1 Historical Background 6
2.1.2 Direct Contact Membrane Distillation 7
2.1.3 Air Gap Membrane Distillation 15
2.1.4 Sweeping Gas Membrane Distillation 20
2.1.5 Vacuum Enhanced Membrane Distillation 23
2.2 Transport Inefficiencies 25
2.2.1 Temperature Polarisation 25
2.2.2 Concentration Polarisation 27
2.3 Heat efficiency of Membrane Distillation 30
2.4 Solar Radiation as Energy Source 31
2.5 Summary 32

CHAPTER 3 33
EXPERIMENTAL 33
3.1 Air Gap Membrane Distillation Units 33
3.2 Air Gap Membrane Distillation 34
3.2.1 The factorial design 36
3.2.2 Statistical interpretation of the results 36
3.3 Permeability coefficient of the Membrane 38
3.4 Solar Radiation 39
3.5 Summary 39

CHAPTER 4 41
MODELLING OF THE TRANSPORT PHENOMENA IN AIR GAP MEMBRANE DISTILLATION 41
4.1 Physical Properties 41
4.1.1 Physical Properties of Aqueous NaCl solution 41
4.1.2 Physical Properties of Water 45
4.1.3 Physical Properties of Air 46
4.2 Transport Phenomena 46
4.2.1 Mass Transfer in Air Gap Membrane Distillation 46
4.2.2 Heat Transfer in Air Gap Membrane Distillation 53
4.3 Solving the Model Equations 58
4.3.1 Correlation between Predicted and Experimental Results 60
4.4 Empirical Modelling 60
4.4 Sensitivity Analysis 61
4.4.1 Temperature Polarisation 61
4.4.2 Concentration Polarisation 62
4.4.3 Heat flux in Air Gap Membrane Distillation 63
4.4.4. Heat Efficiency in Air Gap Membrane Distillation 64
4.5 Summary 65

CHAPTER 5 84
DISCUSSION OF RESULTS 84
5.1 Temperature Variation Experiments 84
5.2 Feed Concentration Experiments 85
5.3 Experiments on the Diffusion Path 86
5.3.1 Air Gap Experiments 86
5.3.2 Membrane Thickness 87
5.4 Velocity Experiments 88
5.5 Model Evaluation 89
5.5.1 Fundamental Model 89
5.5.2 Empirical Model 90
5.6 Product Quality 91
5.6 Time Dependency of the Flux 92
5.8 Effect of Other Salts on the Mass Flux 92
5.9 Solar Radiation as Energy Source for Membrane Distillation 93
5.10 Distillation Units 93
5.11 Summary 94

CHAPTER 6 108
CONCLUSIONS AND RECOMMENDATIONS 108

REFERENCES 110

APPENDIX A 116
TABLES OF RESULTS

APPENDIX B 139
FIGURES

APPENDIX C 142
TURBO PASCAL PROGRAM

APPENDIX D 155
PUBLICATIONS

LIST OF SYMBOLS

A	Transfer area [m^2].
c_{21}	Concentration of the water at the water/membrane interface [mol/m^3].
c_{22}	Concentration of the water vapour at the water/membrane interface [mol/m^3].
c_g	Specific heat of the vapour [kJ/kg.K].
c_l	Specific heat of the fluid [kJ/kg.K].
c_m	Molality.
$c_{p,g}$	Specific heat capacity of water vapour [kJ/kg.K].
$c_{p,l}$	Specific heat capacity of water [kJ/kg.K].
c_{pG}	Specific heat capacity of gas stream (SGMD).
c_{pL}	Specific heat capacity of feed (SGMD).
$c_{w,l}$	Concentration of the water at the brine/membrane interface (SGMD) [mol/m^3].
$c_{w,G}$	Concentration of the water vapour in the gas stream (SGMD) [mol/m^3].
d	Thickness of the condensing surface [m].
D	Diffusion coefficient [m^2/s].
D_{AB}	Diffusion coefficient of water vapour through air [m^2/s].
D_{eff}	Effective diffusion coefficient [m^2/s].
D_K	Knudsen diffusion coefficient [m^2/s].
E	Heat efficiency.
g	Gravitational acceleration [m/s^2].
G	Gas flow rate.
Gr	Grashof number.
h_a	Free convection coefficient [$W/m^2.K$].
h_l	Heat transfer coefficient in the brine feed [$W/m^2.K$].
h_{cw}	Cooling water convection heat transfer coefficient [$W/m^2.K$].
h_{fg}	Latent heat of evaporation [kJ/kg].
h'_{fg}	Modified latent heat of evaporation [kJ/kg].
h_L	Condensation heat transfer coefficient [W/K].

h_m Average mass transfer coefficient [m/s].

h_o Heat transfer coefficient in the cooling water [W/m^2.K].

H Overall heat transfer coefficient for the membrane [W/K].

I Ionic strength.

J Mass flux [m/s].

Ja Jacob number.

k Mass transfer coefficient.

k_{air} Thermal conductivity of air [W/m.K].

k_c Gas phase mass transfer coefficient [m/s].

k_{cs} Conduction coefficient of condensing surface [W/m.K].

k_d Effective conduction coefficient through the total diffusion gap [W/m.K].

k_f Conduction coefficient [W/m.K].

k_g Conductivity of the gas in the membrane pores [W/m.K].

k_L Conduction heat transfer coefficient for condensate [W/m.K].

k_m Membrane mass transfer coefficient [m/s].

k_{mem} Thermal conductivity of the membrane [W/m.K].

k_s Conductivity of the membrane itself [W/m.K].

k_{ss} Thermal conductivity of stainless steel [W/m.K].

k_w Thermal conductivity of water [W/m.K].

K Thermally driven mass transfer coefficient [Pa.s/g].

K_c Overall mass transfer coefficient [Pa.s/g].

K_D Diffusion mass transfer coefficient [m/s].

K_K Knudsen mass transfer coefficient[m/s].

K_m Membrane permeability.

l Length of the condensing plate [m].

l_1 Thickness of the membrane [m].

l_2 Air gap width [m].

L Length of the membrane parallel to the flow direction [m].

L Mass flow of the heated solution (SGMD).

M Molecular mass [g/mol].

M_r Molecular mass of water [g/mol].

M_w Molecular mass of water [g/mol].

n Ionic concentration of the ionic species [g-ion/1000g water].

n_{pore} Pore density.

N Mass flux [g/m^2.s].

Nu Nusselt number.

p Vapour pressure [Pa].

p_{BM} Logarithmic mean pressure of the air in the air gap [Pa].

p_2 Vapour pressure at the membrane surface (upstream) [Pa].

p_3 Vapour pressure at the membrane surface (downstream) [Pa].

P Total pressure in the air gap [Pa].

P_{av} Average permeability coefficient [g.m.m^{-2}.s^{-1}.Pa^{-1}].

Pr Prandl number.

q_{pore} Flow through a single pore.

Q Heat flux [W].

Q_{cond} Heat flux due to conduction across the membrane [W].

Q_{vap} Heat flux associated with the evaporation [W].

r Radius of a membrane pore [m].

R Universal gas constant [J/mol.K].

R_{m1} Mass transfer resistance due to the concentration boundary layer [s.mol/m^3.g].

R_{m2} Mass transfer resistance due to the membrane [s.mol/m^3.g].

R_{m3} Mass transfer resistances due to the air gap [s.mol/m^3.g].

R_{11} Heat transfer resistance due to convection in boundary layer (brine) [K/W].

R_{12} Heat transfer resistance due to enthalpy change [K/W].

R_{1t} Effective resistance between R_{11} and R_{11} [K/W].

R_{c1} Heat transfer resistance due to conduction (membrane) [K/W].

R_{c2} Heat transfer resistance due to conduction (air gap) [K/W].

R_{22} Heat transfer resistance due to enthalpy change (membrane) [K/W].

R_{221} Heat transfer resistance due to enthalpy change (air gap) [K/W].

R_{23} Heat transfer resistance due to evaporation [K/W].

R_{zt} Effective resistance across diffusion path [K/W].

R_3 Heat transfer resistance due to condensate [K/W].

R_4 Heat transfer resistance due to condensing surface [K/W]

R_5 Heat transfer resistance due to boundary layer (cooling water) [K/W].

Re Reynolds number.

S Solubility [$g.m.m^{-4}.Pa^{-1}$].

Sc Schmidt number.

Sh Sherwood number.

T Temperature [K].

T_m Average temperature [K].

T_s Temperatures at the surface of the plate [K].

T_{sat} Saturation temperature [K].

u_b Linear velocity of the brine solution [m/s].

u_c Linear velocity of the cooling water [m/s].

U_G Overall heat transfer coefficient [W/m.K].

v Valence of ions.

y mole fraction of the solvent.

Y_{lm} Mole fraction of air (log mean) present in the pores.

Greek symbols

χ Tortuosity factor.

δ Membrane thickness [m].

ε Porosity of the membrane.

η Dynamic viscosity of the gas [cP].

λ Latent heat of evaporation [J/g].

μ Dynamic viscosity [cP].

ν Kinematic viscosity of the brine solution [Pa.s].

ρ Density [kg/m^3].

τ Temperature polarisation coefficient.

Subscripts

1	Brine feed (bulk).
2	Membrane surface (upstream).
3	Membrane surface (downstream).
4	Condensate surface.
5	Condensing surface (condensate side).
6	Condensing surface (cooling water side).
7	Cooling water (bulk).
b	Brine feed.
c	Cooling water.

LIST OF FIGURES

Membrane distillation concept 3

Temperature and concentration distribution in direct contact membrane distillation. 8

Heat transfer in direct contact membrane distillation 13

Schematic representation of air gap membrane distillation 15

Schematic representation of sweeping gas membrane distillation 21

Vacuum enhanced membrane distillation 26

A schematic of concentration polarisation 28

Simple solar still 31

Air gap membrane distillation unit 33

Experimental air gap membrane distillation set-up 34

Permeability of the membrane 38

Radiation of a black container 39

Air gap membrane distillation 41

Dependency of density on temperature and concentration of brine 43

Dependency of vapour pressure on temperature and concentration of brine 44

Dependency of viscosity on temperature and concentration of brine 45

Heat transfer in air gap membrane distillation 58

..... 58

..... 59

..... 66

..... 66

..... 67

..... 67

..... 68

..... 68

..... 69

e feed

..... 69

ling

..... 70

ine feed

..... 70

..... 71

..... 71

Fig. 4.20 Concentration at the membrane surface as the Reynolds number of the brine feed changes. 72

Fig. 4.21 Concentration at the membrane surface as the Reynolds number of the cooling water changes. 72

Fig 4.22 Heat efficiency as the temperature of the brine feed is changed at various air gap widths..... 73

Fig 4.23 Heat efficiency as the temperature of the cooling water is changed at various air gap widths..... 73

Fig 4.24 Heat efficiency as the concentration of the brine feed is changed..... 74

Fig 4.25 Heat efficiency as the air gap width is changed. 74

Fig 4.26 Heat efficiency as the membrane thickness is changed..... 75

Fig 4.27 Heat efficiency as the Reynolds number of the brine feed is changed. 75

Fig 4.28 Heat efficiency as the Reynolds number of the cooling water is changed. ... 76

Fig. 4.29 Mass and heat flux as the temperature of the brine feed changes 76

Fig. 4.30 Mass and heat flux as the temperature of the cooling water changes 77

Fig. 4.31 Mass and heat flux as the concentration of the feed changes. 77

Fig. 4.32 Mass and heat flux as the air gap width changes. 78

Fig. 4.33 Mass and heat flux as the membrane thickness changes..... 78

Fig. 4.34 Mass and heat flux as the Reynolds number (brine feed) changes 79

Fig. 4.35 Mass and heat flux as the Reynolds number (cooling water) changes. 79

Fig. 4.36 Heat transfer resistances as the temperature of the brine solution changes.. 80

Fig. 4.37 Heat transfer resistances as the temperature of the cooling water changes.. 80

Fig. 4.38 Heat transfer resistances as the concentration of the brine solution

changes 81

Fig. 4.39 Heat transfer resistances as the air gap width changes. 81

Fig. 4.40 Heat transfer resistances as the membrane thickness changes 82

Fig. 4.41 Heat transfer resistances as the Reynolds number(brine) changes. 82

Fig. 4.42 Heat transfer resistances as the Reynolds number (cooling water) changes. 83

Fig 5.1 Loss in driving force by concentration polarisation 86

Fig 5.2 Comparison between the experimental and predicted results (fundamental model). (R^2 = 0.9156) 89

Fig 5.3 Comparison between the experimental and predicted results (empirical model) R^2 = 0.90258 90

Fig. 5.4 Relationship between the mass flux and the vapour pressure difference across the diffusion path 96

Fig 5.5 Mass flux as the temperature of the brine feed changes (R^2 = 0.9951). 96

Fig. 5.6 Mass flux as the temperature of the brine solution increases (R^2 = 0.9955). 97

Fig 5.7 Mass flux as the temperature of the brine increases (R^2 = 0.9315) 97

Fig. 5.8 Mass flux as the temperature of the cooling water changes (R^2 = 0.9560). . 98

Fig. 5.9 Mass flux as the temperature difference between the bulk liquids stays constant at 15 K (R^2 = 0.982). 98

Fig. 5.10 Mass flux as the air gap width changes (R^2 = 0.8873). 99

Fig. 5.11 Mass flux as the air gap width changes (R^2 = 0.9710). 99

Fig. 5.12 Mass flux as the air gap width changes (R^2 =0.9582) 100

Fig. 5.13 Mass flux as the air gap width changes (R^2 = 0.9431). 100

Fig. 5.14 Mass flux as the concentration of the feed changes (R^2 = 0.9937). 101

Fig. 5.15 Mass flux as the concentration changes (R^2 = 0.8537). 101

Fig. 5.16 Mass flux as the concentration changes (R^2 = 0.9710) 102

Fig. 5.17 Mass flux as the concentration changes (R^2 = 0.9620). 102

Fig. 5.18 Mass flux as the concentration changes (R^2 = 0.9582). 103

Fig. 5.19 Mass flux as the concentration changes (R^2 = 0.9430). 103

Fig. 5.20 Heating of water by direct sunlight 104

Fig. 5.21 Relationship between mass flux and the velocity of the feed 104

Fig. 5.22 Relationship between mass flux and the velocity of the feed 105

Fig. 5.23 Change in mass transfer resistances as the temperature of the brine increases. 105

Fig. 5.24 Dependency of the permeability coefficient and permeation rate on temperature. 106

Fig. 5.25 Permeate quality as the concentration of the feed changes 106

Fig. 5.26 Change in convection coefficient as the Reynolds number of the feed changes. 107

Fig. 5.27 Dependency of mass flux on time 107

Fig. B1 Air gap membrane distillation module (upstream side) 139

Fig. B2 Air gap membrane distillation module (downstream side) 140

Fig. B3 Photograph of air gap membrane distillation Unit 141

LIST OF TABLES

Table 3.1 Factorial design variables and the levels 36

Table 3.2 Experimental runs with responses of the factorial design 36

Table 3.3 Analysis of variance 37

Table 3.4 Experiments conducted 38

Table 4.1 Constants for density correlations 42

Table 4.2 Constants for vapour pressure correlations 43

Table 4.3 Constants for viscosity correlations 45

Table 4.4 Constants for physical properties correlations 46

Table 4.5 Empirical modelling coefficients 60

Table 5.1 Effect of membrane width on the permeation flux and the product quality.. 87

Table 5.2 Results for the permeation experiments on the membrane. 88

Table 5.3 Effect of different salts on the mass flux 92

Table 5.4 Radiation of sunlight on water in a black container. 93

Table 5.5 Results from distillation unit. 94

Table A1 Results when the cooling water temperature is varied 116

Table A2 Results when the temperature of the brine is varied for distilled water..... 116

Table A3 Results when the temperature of the brine is varied at various NaCl concentrations 117

Table A4 Results when the concentration of the NaCl and the air gap thickness is varied 118

Table A5 Results when the concentration of the NaCl and the air gap thickness is varied 119

Table A6 Results when the temperatures of the brine solution and the cooling water is varied 120

Table A7 Results when the concentration of the NaCl is varied 120

Table A8 Results when the linear velocity of the cooling water and the brine solution is varied 121

Table A9 Results when the membrane thickness is varied 121

Table A10 Results from the factorial design 122

Table A11 Results from the fundamental model 123

Table A12 Results from the fundamental model 123

Table A13 Results from the fundamental model 124

Table A14 Results from the fundamental model 124

Table A15 Results from the fundamental model 125

Table A16 Results from the fundamental model 125

Table A17 Results from the fundamental model 126

Table A18 Results from the fundamental model 126

Table A19 Results from the fundamental model 126

Table A20 Results from the fundamental model 127

Table A21 Mass transfer resistances 127

Table A22 Mass transfer resistances 127

Table A23 Mass transfer resistances 128

Table A24 Mass transfer resistances 129

Table A25 Mass transfer resistances 130

Table A26 Mass transfer resistances 130

Table A27 Mass transfer resistances 131

Table A28 Mass transfer resistances 131

Table A29 Mass transfer resistances 131

Table A30 Mass transfer resistances 132

Table A31 Heat transfer resistances 133

Table A32 Heat transfer resistances 133

Table A33 Heat transfer resistances 134

Table A34 Heat transfer resistances 135

Table A35 Heat transfer resistances 136

Table A36 Heat transfer resistances 137

Table A37 Heat transfer resistances 137

Table A38 Heat transfer resistances 138

Table A39 Heat transfer resistances 138

Table A40 Heat transfer resistances 138

CHAPTER 1

INTRODUCTION

In many areas of South Africa there is no reliable supply of fresh drinkable water, but in most of these areas there is access to large quantities of brackish ground water or contaminated water which is generally non-potable. A need therefore exists for a unit which could make use of the abundant supply of solar energy to desalinate this water to produce potable water. Such an unit should also be of use offshore as to desalinate seawater.

In order to produce a distillate of quality, energy is required to separate the different non-volatile species which are to be found in the feed to the distillation unit. The principal factor is the cost of the energy needed to produce the thermal driving force. Generally, membrane distillation is found to be competitive in situations where some source of waste energy is available or where electricity is expensive. The advantage of using a solar distillation unit to produce water which is safe for human consumption, is that solar energy is the only source of energy that is readily available. In most areas where there is a lack or shortage of reliable water, there is access to large quantities of brackish, non-potable water. The combination of abundant quantities of solar energy as well as non-potable water, gives rise to the possibility of desalinating the water economically in order to produce water of a potable standard.

The proposed unit should be both simple to operate and the maintenance costs should be low if made portable and inexpensive. Such features would make such a system appealing to a very broad market ranging from agriculture to hiking. It could be considered an emergency rescue pack as well.

In this thesis, the design of such an unit , as well as the derivation of a mathematical model of the unit is presented. Unfortunately, it is very difficult to control the variables in such a distillation unit and an alternative set-up was designed to produce results which could be compared with the predicted data.

Membrane distillation is defined as the evaporation of water vapour through a hydrophobic, porous membrane with heated contaminated water in contact with the membrane. The downstream side of the membrane is either in contact with the permeate (direct contact membrane distillation or DCMD) or in contact with a stagnant layer of air which is in contact with a cooled condensing surface (air gap membrane distillation or AGMD). In this project, a hydrophilic, non porous membrane was used in air gap membrane distillation instead of a hydrophobic membrane. In the literature, models exist for air gap membrane distillation using porous, hydrophobic membranes, but no model could be found where the modelling was extended for the use of a dense, hydrophilic membrane.

CHAPTER 2

LITERATURE SURVEY

In this chapter, a literature survey will be conducted on membrane distillation. Models will be discussed for the different types of membrane distillation. Furthermore, transport inefficiencies, such as temperature polarisation and concentration polarisation will be investigated, as well as the heat efficiency in membrane distillation. The use of solar radiation as an energy source for desalination will be investigated as well.

2.1 Membrane Distillation

Membrane distillation (MD) is a temperature driven process in which two phases are separated by a porous, hydrophobic (non wettable) membrane (Jönsson *et al.*, 1985), where a membrane is defined as a selective barrier between two phases, the term 'selective' being inherent to a membrane or a membrane process (Mulder, 1991). Since the process is non isothermal, the water vapour migrates through the membrane from the heated side to the cooled side due to a transmembrane temperature gradient (see fig. 2.1) (Jönsson *et al.*, 1985).

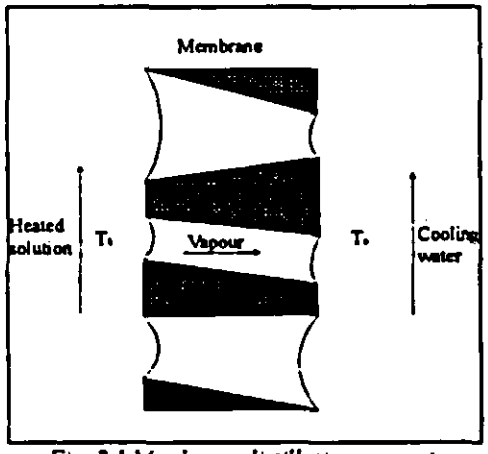

Fig. 2.1 Membrane distillation concept.

This water vapour transport occurs at atmospheric pressure and the temperatures may be much lower than the boiling point of the solution (Carlsson *et al.*, 1983). Because of the liquid repulsing properties of the membrane material, the liquid phase is kept outside the pores as long as the pressure of the liquid does not exceed the minimum entry pressure of the porous partition,

that is, the liquid phases are kept out of the pores by capillary forces (Sarti *et al.*, 1985). The role of the membrane is peculiar insofar as the membrane does not contribute to the separation due to its selectivity, but rather acts as a physical support for a liquid vapour interface (Bandini *et al.*, 1991; Gostolli *et al.*, 1989) and it aids in achieving a larger vertical liquid area (Andersson *et al.*, 1985). The separation mechanism in this process is the vapour-liquid equilibrium and the driving force for membrane distillation is the transmembrane vapour pressure difference (Jönsson *et al.*, 1985). After the vapour has passed through the membrane, it condenses, and the condensate is totally or partially devoid of all components present in the mother liquid that lack a measurable vapour pressure, for example, Na^+ and Cl^- (Andersson *et al.*, 1985). The net flux is in the direction of the decreasing temperature, that is, from the warm solution to the cold solution. The main requirement for membrane distillation is that the membrane must not be wetted, that is, only vapour is present in the pores. In order to prevent the wetting of the membrane, the pores should be small (0.1 μm-0.5 μm), the surface energy of the membrane should be high and the surface tension of the liquid should be high. Typical membranes that are normally used for membrane distillation are polytetrafluoroethylene (PTFE), polypropylene (PP), polyethylene (PE) and polyvinylidene (PVDF). These materials are used for their sensitivity to vapour, not liquid (Banat *et al.*, 1994). Andersson *et al.* (1985) reported that no membrane has been developed especially for membrane distillation, so there is a great potential for improvement. This problem still exists.

Different types of membrane distillation are available: i) direct contact membrane distillation, ii) air gap membrane distillation, iii) vacuum enhanced membrane distillation and iv) sweeping gas membrane distillation.

Membrane distillation is a process with a large variety of applications. It is primarily used for the desalination of sea water and brackish water (Jönsson *et al.*, 1985), water removal from blood, milk and fruit juice, the separation of alcohol-water mixtures (Gostolli *et al.*, 1989) and to concentrate to high osmotic pressures aqueous solutions of substances sensitive to high temperatures (Drioli *et al.*, 1987). Since effective permeate rates can be

obtained at 50° C-100° C, membrane distillation can be effectively used for the separation and concentration of solutions with non volatile components (Kurokawa *et al.*, 1990). The main advantages of membrane distillation over conventional distillation are:

- lower operating costs (Banat *et al.*, 1994),
- the possibility of overcoming corrosion problems by using plastic equipment (Banat *et al.*, 1994; Jönsson *et al.*, 1985),
- mist elimination (Banat *et al.*, 1994; Hanbury *et al.*, 1985; Jönsson *et al.*, 1985),
- the configuration of the evaporation surface can be made similar to various membrane modules, with a compact area density,
- product is very pure,
- waste energy and solar energy can be used as an energy source (Jönsson *et al.*, 1985),
- the marginal decrease of flux with high concentrations encourages the use of membrane distillation for high concentration solutions (Banat *et al.*, 1994).

Fane *et al.* (1987) found in an evaluation of membrane distillation for the production of distilled or potable water, that production costs are very sensitive to feed temperatures. For a modest scale plant with a capacity of 5000 kg/h, the production costs could be similar to that of reverse osmosis (RO), while for a smaller plant with membrane distillation coupled to a solar heater, the production cost would be marginally higher than for reverse osmosis, but it could offer practical advantages in arid or rural locations.

Membrane distillation has the drawback of high membrane cost and the problem of membrane wetting (Hanbury *et al.*, 1985). To prevent the phenomenon of membrane wetting, composite membranes in which a hydrophilic layer is coated on a hydrophobic membrane are used, as described by Cheng *et al.* in a series of patents. Hanbury *et al.* (1985) claimed that for membrane distillation to become economically viable, the price of

the membrane has to be reduced considerably and, second, much higher heat transfer coefficients have to be achieved. To achieve better heat transfer coefficients, the only method would be to use acid treatment and highly degassed feeds to reduce the partial pressure of the gas in the membrane pores. Hanbury *et al.* (1985) concluded that membrane distillation based on PTFE membranes is unlikely to be economically viable.

2.1.1 Historical Background

The transport of liquids under non isothermal conditions through membranes has been known since the beginning of the century. At first, the membranes used were dense membranes which gave very small mass fluxes; this was known as thermo-osmosis and this process had very little industrial application.

In the 1960s, larger fluxes were obtained for the non isothermal transport of vapour through hydrophobic, porous membranes (Ortiz de Zárate *et al.*, 1993). Van Haute and Hynderycks in Europe (Van Haute *et al.*, 1967) and Findley (Findley, 1967; Findley *et al*, 1969) in the United States made major contributions to this field by investigating seawater desalination through a hydrophobic membrane.

This process obtained renewed attention in 1982 when Gore proposed a spiral type module using a Gore Tex membrane and calling the process "Gore-Tex Membrane Distillation" (Gore, 1982). The Swedish Development Co. also reported test results in 1983 (Carlson, 1983). Enka presented a hollow fibre "Trans Membrane Distillation" module in 1984. At the Second World Congress on Desalination and Water Re-use in 1985, held in Bermuda, several papers on this topic were presented (Sarti *et al.*, 1985). The renewal of interest in this process led to the development of polytetrafluoroethylene (PTFE) membranes and polypropylene (PP) membranes that can be used for membrane distillation. The Chigasaki Laboratory of the Water Re-Use Promotion Center has been studying sea water desalination since April 1985. The modules they used were plate-and-frame type with both hydrophobic and hydrophilic membranes (Kubota *et al.*, 1988; Ohta *et al.*, 1990). In 1988, Kubota *et al.* (1988) noticed that the heat efficiency was improved

in the desalination of sea water by the introduction of an air gap in the plate-and-frame module.

2.1.2 Direct Contact Membrane Distillation

Direct contact membrane distillation (DCMD), as the name indicates, is a membrane distillation process in which a liquid phase is in contact with both sides of the membrane. As mentioned, the hydrophobic membrane allows only vapour to penetrate the membrane (see fig. 2.1). Furthermore, it is assumed that there is liquid-vapour equilibrium between the vapour in the pores and the adjacent liquid at the entrance of the membrane pores.

Due to liquid contact at either sides of the membrane, the evaporation and condensation surface are very close to each other, and as a consequence a high conduction flux parallels the mass flux. This reduces the effective temperature difference across the membrane greatly with respect to the bulk temperature difference (Gostolli *et al.*, 1989). According to Schofield *et al.* (1990b), heat losses in direct contact membrane distillation due to conduction amount to 20 %-40 % of the total heat input. The temperature and concentration distribution in direct contact membrane distillation is illustrated in fig. 2.2.

Schofield *et al.* (1990a) claimed that membrane distillation is limited by heat transfer if the module design does not give adequate heat transfer to the membrane surface, and that direct contact membrane distillation gives better control of the film heat transfer than other types of membrane distillation. Conversely, the process will be mass transfer limited if the membrane permeability is too low.

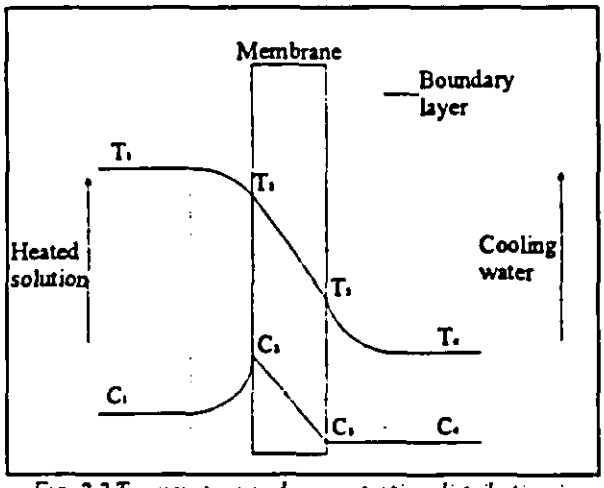

Fig. 2.2 Temperature and concentration distribution in direct contact membrane distillation.

Membrane distillation is a process in which heat transfer and mass transfer take place simultaneously. Mass transfer takes place by the convective and diffusive transport of water vapour across the microporous membrane. The convective transport across the membrane can be described either by the Knudsen flow model or by the Poiseuille flow model, the former being dominant when the pore size is smaller than the mean free molecular path of the gaseous water molecules (Schofield *et al.*, 1987). This is because the molecules collide much more often with the walls of the pores than with each other. The resistance to diffusion can thus be attributed to the collisions of the molecules with the walls rather than with each other, as in ordinary diffusion (Sherwood *et al.*, 1975). Since the mean free molecular path of water vapour is about 0.3 μm at 60° C and this is similar to the size of a typical membrane pore (0.1 μm-0.5 μm), both the abovementioned models must be considered (Jönsson *et al.*, 1985; Schofield *et al.*, 1987). A pore size of 0.5 μm is too large for pure Knudsen flow (Schofield *et al.*, 1990a). In both these models, the main resistance to mass transport is induced by the membrane structure, since it is assumed that no air is present in the membrane pores (Fane *et al.*, 1987).

According to Schofield *et al.* (1990a), gas permeation experiments were conducted on a range of membranes to determine whether the governing mechanism in direct contact membrane distillation is Knudsen or Poiseuille flow. Experiments were conducted on three different flat sheet hydrophobic microporous membranes, with pore sizes of 0.1 μm, 0.2 μm and 0.45 μm. Initial experiments involved the measurement of the gas permeation rate versus pressure drop for helium and air at subatmospheric pressures, to asses the applicability of Poiseuille or Knudsen flow to the chosen membranes. It was found that

for gas permeation, Knudsen diffusion is predominantly the transport mechanism. The Knudsen model can be expressed as

$$N = \frac{D_K \varepsilon}{\chi} \frac{\Delta c}{\delta} \qquad (2.1)$$

where N is the mass flux, D_K is the Knudsen diffusion coefficient, ε is the porosity of the membrane, χ is the tortuosity factor, δ is the membrane thickness and Δc is the concentration difference across the membrane. The first term ($D_K\varepsilon/\chi$) in eqn. (2.1) is the corrected Knudsen diffusion coefficient for a microporous membrane, which is the ratio of the flux per unit of the total face area to the concentration gradient normal to the face, while the second term is the concentration driving force (Schofield *et al.*, 1987; Sherwood *et al.*, 1975).

The Knudsen diffusion coefficient can be expressed as

$$D_K = \frac{2r}{3}\left(\frac{8RT}{\pi M}\right)^{0.5} \qquad (2.2)$$

where $(8RT/\pi M)^{0.5}$ is the mean molecular speed and r is the radius of the pore. Since the vapour pressure and temperature of the water vapour in the membrane are relatively low, ideal gas behaviour can be assumed.

$$c = \frac{PM}{RT} \qquad (2.3)$$

By substituting eqn. (2.2)-(2.3) into eqn. (2.1), the mass flux (N) can be expressed as

$$N = 1.064 \frac{r\varepsilon}{\chi\delta}\left(\frac{M}{RT}\right)^{0.5} \Delta p \qquad (2.4)$$

where M is the molecular mass of water, R is the gas constant, T is temperature and ΔP is the vapour pressure difference of water vapour across the membrane (Sherwood *et al.*, 1987). Equation 2.4 is for gas permeation through an isotropic, microporous membrane (Schofield *et al.*, 1990a).

The Poiseuille flow model describes the flow of a gas through a porous structure. The Poiseuille flow model for a capillary is expressed as

$$N = q_{pore} n_{pore} \frac{MP_m}{RT} \tag{2.5}$$

where q_{pore} is the flow through a single pore and n_{pore} is the pore density. Furthermore, q_{pore} and n_{pore} are expressed as

$$q_{pore} = \frac{\pi r^4 \Delta p}{8\eta\delta\chi} \tag{2.6}$$

and

$$n_{pore} = \frac{\varepsilon}{\pi r^2} \tag{2.7}$$

where η is the dynamic viscosity of the gas, δ is the membrane thickness, χ is the tortuosity factor, ε is the porosity of the membrane and r is the radius of the membrane pores. Substituting eqn. (2.6)-(2.7) into eqn. (2.5), the Poiseuille flow (Schofield *et al.*, 1987) for a microporous membrane can be expressed as

$$N = \frac{1}{8}\frac{r^2\varepsilon}{\chi}\frac{1}{\eta}\frac{MP_m}{RT}\frac{\Delta p}{\delta} \tag{2.8}$$

Unfortunately, the Knudsen and Poiseuille flow models have their limitations, since δ, ε and r must be predetermined from experimental gas fluxes through the given membrane.

The transport of gas through a microporous membrane in direct contact membrane distillation can also be seen as a process of diffusion through a stagnant gas film, because the presence of air in the pores depends on the solubility of air in water (Bandini *et al.*, 1991; Schofield *et al.*, 1987). The solubility of air in water is of the order of 10 ppm (Schofield *et al.*, 1990c), implying that the flux of air is many orders of magnitude smaller than that of the vapour flux. Accordingly, the air establishes a pressure gradient opposing

the vapour flux. Diffusion will be dominant if a significant amount of air is present in the membrane pores. The assumption can be made that molecular diffusion (or ordinary diffusion) is the prevailing mechanism in direct contact membrane distillation because of the air in the pores. Molecular diffusion takes place when the water molecules move at high speeds, although they travel extremely short distances before they collide with other molecules. This causes the molecules to be deflected in random directions. Consequently, the migration of the molecules is very slow, except at very low molecular densities (Sherwood *et al.*, 1975). The mass flux (N) through the microporous membrane is given by

$$N = \frac{1}{Y_{lm}} \frac{D\varepsilon}{\chi\delta} \frac{M}{RT} \Delta p \qquad (2.9)$$

where Y_{lm} is the mole fraction of air (log mean) in the pores (Schofield *et al.*, 1987). For isotropic porous materials, the effective diffusion coefficient is $D_{eff} = D\varepsilon/\chi$ (Schofield *et al*, 1990a). When the partial pressure of the air present in the membrane pores is very low, $Y_{lm} \rightarrow 0$, so eqn. (2.9) is undefined.

Equations (2.4), (2.8) and (2.9) can be simplified to

$$N = K\Delta p \qquad (2.10)$$

where K is a thermally driven mass transfer coefficient for the specific system. Equation (2.10) simply states that flux (N) = Permeability (K) x driving force (ΔP). From eqn. (2.4), eqn. (2.8) and eqn. (2.9), it can be seen that K is temperature dependent. If diffusive transport prevails, the average air content of the pores, Y_{lm}, will be the controlling factor (Schofield *et al.*, 1987). The partial pressure of air within the membrane pores can be reduced by deaerating the feed, or by reducing the pressure of the liquids bounding the membrane (i.e. limiting the total gas pressure in the pores). By deaeration, the flux can be enhanced 20 %-50 %. If convection transport prevails, K will be strongly dependent on the pore geometry (Schofield *et al.*, 1990c).

Schofield *et al.* (1987) found that diffusive as well as convective transfer of water vapour occur, and in an attempt to account for both of these transport mechanisms it was suggested that the combined mass transfer coefficient (K_c) should be calculated as follows

$$K_c = \left(\frac{Y_{ln}}{K_D} + \frac{1}{K_K} \right)^{-1} \qquad (2.11)$$

where Y_{ln} is the mole fraction of air (log mean), K_D is the diffusion mass transfer coefficient and K_K is the Knudsen mass transfer coefficient.

For small differences in temperature across the membrane, the following relation can be used

$$\left. \frac{dp}{dT} \right|_{T_m} = \frac{\Delta p}{\Delta T} \qquad (2.12)$$

According to Schofield *et al.* (1987), this relation is very accurate for temperature differences smaller than 10 °C. Equation (2.12) is evaluated at the average temperature across the membrane (T_m,). Since it is not possible to measure the vapour pressure in the membrane pores, it would be better to express the vapour pressure difference as a temperature difference. The mass flux (N) can be expressed as

$$N = K \left. \frac{dp}{dT} \right|_{T_m} \Delta T \qquad (2.13)$$

The Clausius Clapeyron equation can be used to evaluate dp/dT.

$$\left. \frac{dp}{dT} \right|_{T_m} = \left. \frac{p \lambda M}{RT^2} \right|_{T_m} \qquad (2.14)$$

where λ is the latent heat of vaporisation at the average temperature (T_m). Owing to the vapour liquid equilibrium in the membrane pores, the Antoine equation can be used to determine the vapour pressure at temperature the average temperature (T_m)(Schofield *et al.*, 1987).

$$p = \exp(23.238 - \frac{3841}{T_m - 45}) \qquad (2.15)$$

The heat transfer in direct contact membrane distillation can best be visualised by examining the electrical analog as shown in fig. 2.3.

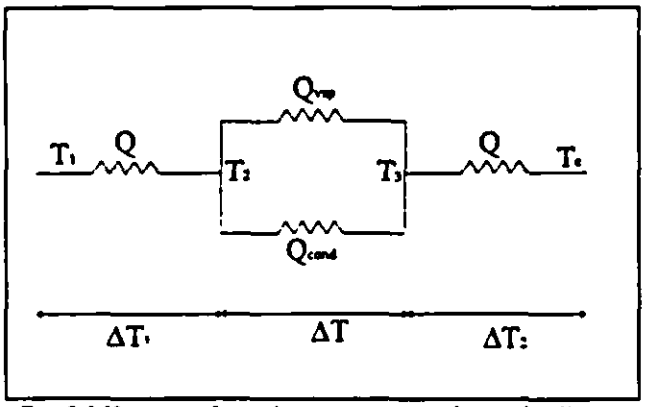

Fig. 2.3 Heat transfer in direct contact membrane distillation.

The heat transfer from the bulk solution to the membrane surface is given by following expression

$$Q = h_1 (T_1 - T_2) \qquad (2.16)$$

where h_1 is the heat transfer coefficient of the heated solution. The film heat transfer coefficients h_1 and h_o can be determined from heat transfer theory if the fluid dynamics are well defined or can be determined experimentally (Schofield *et al.*, 1987). From fig. 2.3 the heat flux through the membrane associated with conduction and evaporation is in parallel. Consequently, the sensible heat (Q) can be expressed as

$$Q = Q_{cond} + Q_{vap} \qquad (2.17)$$

where Q_{cond} is the heat flux due to conduction across the gas filled membrane and Q_{vap} is the heat flux associated with the evaporation.

The latent heat is simply

$$Q_{vap} = N\lambda = K\frac{dp}{dT}\Big|_{T_m}\Delta T\lambda \qquad (2.18)$$

and the heat loss due to conduction is

$$Q_{cond} = \frac{k_{mem}}{\delta}\Delta T \qquad (2.19)$$

where δ is the membrane thickness and k_{mem} is the effective thermal conductivity of the membrane calculated from the solid and gas conductivities by

$$k_{mem} = \varepsilon k_g + (1-\varepsilon)k_s \qquad (2.20)$$

where k_g is the conductivity of the gas in the membrane pores, k_s is the conductivity of the membrane itself, and ε is the porosity of the membrane

Substitution of eqn. (2.18) and eqn. (2.19) into eqn. (2.17), yields

$$Q = H\Delta T \qquad (2.21)$$

where

$$H = K\frac{dP}{dT}\Big|_{T_m}\lambda + \frac{k_m}{\delta} \qquad (2.22)$$

is the overall heat transfer coefficient for the membrane.

From eqn. (2.21) and eqn. (2.22) it can be seen that for a constant heat flux (Q) that the heat required for evaporation can be increased if the conduction losses are minimised.

Due to a temperature difference between the membrane surface (T_3) and the cooling water, there is a heat flux between these two regions. Hence

$$Q = h_c(T_3 - T_c) \qquad (2.23)$$

where h_o is the heat transfer coefficient on the condensing side (Schofield *et al.*, 1987).

2.1.3 Air Gap Membrane Distillation

Air gap membrane distillation (AGMD) is the membrane distillation process in which the evaporation and condensation surfaces are separated by an air gap, that is, they are separated further from each other than in direct contact membrane distillation (fig. 2.4). This phenomenon leads to an increase in mass transfer and heat transfer resistances and, by changing the air gap width the distillation rate is influenced (Gostolli *et al.*, 1989).

The air gap was initially introduced to membrane distillation for the minimisation of the conduction losses and to maintain the maximum temperature difference between the membrane surface and the condensing surface. Air gap membrane distillation (AGMD) is a relatively recent process compared to direct contact membrane distillation, and consequently not as much research has been conducted on the former process as on direct contact membrane distillation.

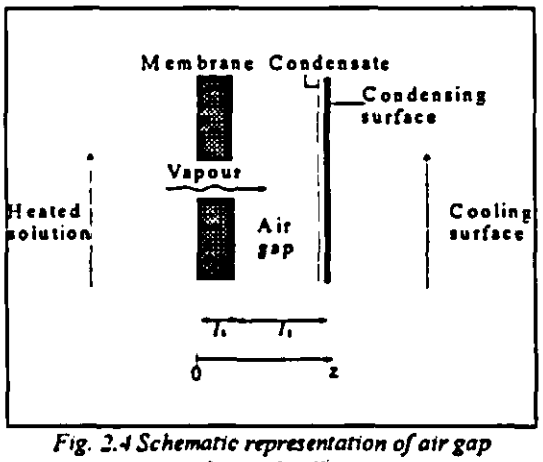

Fig. 2.4 Schematic representation of air gap membrane distillation.

To simplify the transport phenomena in air gap membrane distillation, it can be divided into the following steps:

i) Heat is transported from the bulk fluid to the membrane surface.

ii) Water evaporates at the membrane surface from the hot solution.

iii) Water vapour diffuses through the membrane pores.

iv) Water vapour diffuses through the air gap.

v) Water vapour condenses on the condensing surface.

vi) Heat is transported through the condensate to the condensing surface.

vii) Heat is transported through the condensing surface.

viii) Heat is transported from the condensing surface to the coolant.

In the modelling of the transport phenomena in air gap membrane distillation, Jönsson *et al.* (1985) assumed that the temperature of the bulk was equal to that of the membrane surface and the temperature of the condensate equal to that of the coolant. These assumptions cannot be made without expecting a substantial error in the distillation rate, since temperature polarisation plays an important role in membrane distillation.

Since the membrane is in contact with a stagnant layer of air, the valid assumption can be made that the membrane pores are filled with air. As in direct contact membrane distillation, where molecular transport is the prevailing mechanism, the mass transport through the total diffusion path (x) can be expressed as

$$N = \frac{\boldsymbol{D}c}{1 - y_a} \frac{dy_a}{dx} \qquad (2.24)$$

where $\boldsymbol{D}$ is the diffusion coefficient, c is the concentration of the solvent and y is the mole fraction of the solvent.

In order to be able to integrate this equation, the following boundary conditions are necessary

$$x = 0, \qquad y_A = y_{Am}$$

$$x = x, \qquad y_A = y_{Al}$$

At steady state, the magnitude of the flux does not vary with distance, thus $dN/dx = 0$; hence eqn. (2.24) can be integrated to obtain the following expression.

$$N = \frac{c\boldsymbol{D}}{x} \ln \frac{1 - y_{Al}}{1 - y_{Am}} \qquad (2.25)$$

The heat transfer between the heated bulk fluid and the membrane surface is the same as that in direct contact membrane distillation.

$$Q = (h_1 + Nc_l)(T_1 - T_2) \qquad (2.26)$$

where h_l is the convection heat transfer coefficient, N is the flux, c_l is the specific heat capacity of the fluid and T_1 and T_2 are the temperatures of the bulk fluid and the membrane surface, respectively.

Kimura *et al.* (1987) assumed that no liquids are present in the membrane pores. The water evaporates at the entrance of the membrane pores and the vapour diffuses through the air filled pores to and through the air gap. The vapour contains a certain amount of heat due to its enthalpy. Since the membrane is stationary with no bulk motion, there is conduction of heat through the membrane. In order to simplify the heat transfer, Kimura *et al.* (1987) decided to combine the heat transfer through the membrane and air gap into one step, an approach also followed by Kurokawa *et al.* (1990). Since the membrane pores are filled with air, the thermal conductivity of air is used. The diffusion path (x) is defined as the air gap width together with the membrane thickness (Kimura *et al.*, 1987). The heat transfer through the membrane is

$$Q = (\frac{k_d}{x} + Nc_g)(T_2 - T_4) + N\lambda \qquad (2.27)$$

where k_d is the effective conduction coefficient through the total diffusion gap, c_g is the specific heat capacity of the vapour, and T_4 is the temperature of the condensate.

Kurokawa *et al.* (1990) reported that for an air gap less than 5mm, the heat transfer and mass transfer are controlled by conduction across the diffusion path and for an air gap larger than 5mm, the heat and mass transfer are controlled by free convection. He also found that the permeate characteristics are affected by the width of the air gap.

To evaluate the free convection heat transfer coefficient (h_a) of the vapour in the air gap, the air gap can be approximated as a gap between two vertical plates. The Nusselt

number (Nu), in terms of the Grashof number (Gr) and the Prandtl number (Pr), is given by

$$Nu = \frac{c}{(l/z)^{1/9}}(\mathrm{Pr}.Gr)^{n} \qquad (2.28)$$

$2.1\times10^{5}<Gr<1.1\times10^{7}$	c=0.07	n=1/3
$2.0\times10^{-4}<Gr<2.1\times10^{5}$	c = 0.20	n=1/4

where l is the length of the plate.

Owing to the analogy between heat and mass transfer, the Nusselt number (Nu) can be replaced by the Sherwood number (Sh) and the Prandtl number (Pr) can be replaced by the Schmidt number (Sc).

$$Sh = \frac{c}{(l/z)^{1/9}}(Sc.Gr)^{n} \qquad (2.29)$$

$2.1\times10^{5}<Gr<1.1\times10^{7}$	c=0.07	n=1/3
$2.0\times10^{-4}<Gr<2.1\times10^{5}$	c = 0.20	n=1/4

From these equations the heat and mass transfer coefficients can be evaluated for free convection. The heat transfer, in which free convection is the dominating heat transfer mechanism, can be expressed as

$$Q = (h_a + Nc_g)(T_2 - T_4) + N\lambda \qquad (2.30)$$

while the mass transfer is given by

$$N = k_m(c_2 - c_4) \qquad (2.31)$$

where k_m is the mass transfer coefficient and c_2 and c_4 is the concentration at the membrane surface and at the condensate, respectively.

Since the water vapour condenses on the condensing surface, a layer of water will form on the plate and flow downward under the influence of gravity. It is assumed that this layer is of uniform thickness. The temperature of the liquid vapour interface is at the saturation temperature and there is heat transfer through the liquid layer to the metal surface, since the temperature at the surface is lower than the saturation temperature. The following assumptions must be made in order to get useful results:

i) Laminar flow and constant properties for the condensed film;

ii) Negligible shear stress in the liquid-vapour interface;

iii) Negligible momentum and energy transfer by advection in the condensate film, from which it follows that the heat transfer across the film occurs only by conduction, in which the temperature distribution is linear; and

iv) The gas is a pure vapour and at a uniform temperature equal to the saturation temperature (Incropera *et al.*, 1990).

To determine the condensation heat transfer coefficient (h_L,), Kimura *et al.* (1987) used an expression derived by Nusselt, namely

$$h_L = \left[\frac{g k_L^3 \lambda \rho^2}{l \mu (T_4 - T_5)}\right]^{1/4} \qquad (2.32)$$

where g is the gravitational acceleration (9.81 m/s^2), k_L is the conduction heat transfer coefficient, λ is the latent heat of evaporation, ρ is the density of the water layer, l is the length of the condensing plate and μ is the viscosity of the condensed species (Incropera *et al.*, 1990; Kimura *et al.*, 1987).

For the condensation at the surface of the cooling plate, Q is given by

$$Q = h_L (T_4 - T_5) \qquad (2.33)$$

where h_L is the condensation heat transfer coefficient

Since there is no mass transport through the condensing surface and the surface is stationary (no bulk motion), only conduction takes place through the plate. The heat transfer through the plate can be given as

$$Q = \frac{k_a}{d}(T_5 - T_6) \qquad (2.34)$$

where k_a is the conduction heat transfer coefficient and d is the thickness of the condensing plate.

Owing to temperature polarisation, there is a thermal gradient between the condensing surface and the bulk of the cooling water. The fluid is not stationary, so that the heat is transferred by convection. The heat flux is given by (Kimura *et al.*, 1987)

$$Q = h_c(T_6 - T_7) \qquad (2.35)$$

where h_c is the convection heat transfer coefficient.

According to Gostolli *et al.* (1989), the optimum air gap width depends on the salt concentration of the feed, since an increase in salt concentration leads to a wider air gap. Due to the large differences in temperatures between the condensation and evaporation surfaces, the water flux is no longer linear with the transmembrane temperature difference as in direct contact membrane distillation. Heat transfer within the liquid phases has a minor effect when air gaps are large, that is, the resistance due to the air gap is significant. The pressure in the air gap can be controlled, so that a decrease in the air gap pressure will result in an increase in water flux.

2.1.4 Sweeping Gas Membrane Distillation

Sweeping gas membrane distillation (SGMD) is a membrane distillation process with a configuration similar to that of air gap membrane distillation. The only difference between these two processes is that the stagnant gas film in air gap membrane distillation is

replaced by a moving, inert gas stream and the condensing surface is absent (fig. 2.5). Basini *et al.* (1987) studied the influence of the relevant process variables such as the inlet temperatures and the flow rates on the evaporation efficiency by using both tubular and flat porous, hydrophobic membranes. The flat membranes were of polytetrafluoroethylene (PTFE) and polypropylene (PP), and the tubular membranes were polypropylene.

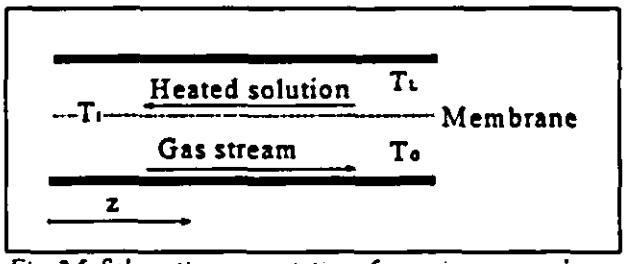

Fig. 2.5 Schematic representation of sweeping gas membrane distillation.

Basini *et al.* (1987) proposed the following model for sweeping gas membrane distillation (SGMD)

The local distillation flux (N) through the membrane is given by

$$N = M_w K_t (c_{w,I} - c_{w,G}) \qquad (2.36)$$

where M_w is the molecular mass of the water, K_t is the overall mass transfer coefficient, $c_{w,I}$ is the concentration of the water at the brine-membrane interface and $c_{w,G}$ is the concentration of the water vapour in the gas stream.

and

$$\frac{1}{K_t} = \frac{1}{k_m} + \frac{1}{k_t} \qquad (2.37)$$

The gas phase mass transfer coefficient (k_t) can be calculated using standard mass transfer correlations, and the mass transfer coefficient through the membrane (k_m) can be calculated as follows

$$k_m = \frac{D_{eff}}{\delta} \qquad (2.38)$$

where D_{eff} is the effective diffusion coefficient and δ is the boundary layer width.

Since the prevailing mechanism for diffusion is not purely convective or diffusive, a combined mechanism should be derived taking into account both convection (D_K) and diffusion (D). Basini *et al.* (1987) suggested an equation of the form

$$\frac{1}{k_m} = \frac{\chi\delta}{\varepsilon}\left(\frac{1}{D} + \frac{1}{D_K}\right) \tag{2.39}$$

where χ is the tortuosity, δ is the membrane thickness and ε is the porosity of the membrane.

The concentration of the water at the evaporative surface (c_{w1}) can be determined from phase equilibrium conditions at the local temperature (T_1). This temperature is related to the temperature of the bulk fluid and can be determined by taking the heat transfer phenomena in the bulk fluid and the temperature polarisation into account.

The overall heat transfer coefficient (U_G) can be calculated by adding the heat transfer coefficients through the membrane (h_m) to those of the heat transfer through the gas phase (h_G).

$$\frac{1}{U_G} = \frac{1}{h_m} + \frac{1}{h_G} \tag{2.40}$$

Basini *et al.* (1987) reported that for a countercurrent configuration the heat and mass transfer can be expressed as

$$\frac{dL}{dz} = NA \tag{2.41}$$

where L is the mass flow of the heated solution, N is the distillation rate and A is the transfer area.

$$\frac{d}{dz}(Lc_{pL}T_L) = Ah_L(T_L - T_1) \tag{2.42}$$

where c_{pL} is the heat capacity of the heated solution

and

$$G\frac{d}{dz}(c_{pG}T_G) = U_G A(T_I - T_G) + NA(T_I - T_G) \qquad (2.43)$$

where G is gas flow rate, c_{pG} is the heat capacity of the gas stream, and c_{pw} is the heat capacity of the water vapour.

The mass transfer resistance mainly depends upon the magnitude of the Reynolds number. For low Reynolds numbers, mass transfer through the gas phase dominates, while the mass transfer through the membrane prevails at high Reynolds numbers. Basini *et al.* (1987) reported that for sweeping gas membrane distillation, the liquid inlet temperature is a very important variable in the distillation rate, while the system is insensitive to the gas inlet temperature. He also found that when comparing sweeping gas membrane distillation to air gap membrane distillation, that the evaporation rate is higher for the former process, although the heat losses are of the same order of magnitude for both processes.

The model predictions are in accord with the experimental values obtained by Basini *et al.* (1987), although there were deviations at higher gas velocities, since the equipment used had a gas inlet distribution system that gave a gas flow regime in the cell for which no standard heat and mass transfer correlations were available.

2.1.5 Vacuum Enhanced Membrane Distillation

When the pressure in air gap membrane distillation is lowered below the equilibrium vapour pressure, a vacuum membrane distillation process is obtained (fig. 2.6), in which there is a net total pressure difference within the gas phase between the region adjacent to the evaporation surface and the bulk gas phase (Gostolli *et al.*, 1989). The operation of this process is very similar to that of pervaporation, although significant differences exist. The transport mechanism through the dense, hydrophilic membrane used in pervaporation is the solution-diffusion process, while the membrane acts only as a physical support for

the liquid phase in vacuum enhanced membrane distillation as with the other membrane distillation processes (Sarti *et al.*, 1993). Because of the low pressure on the permeate side of vacuum enhanced membrane distillation, the pore size of the membrane is smaller than the molecular mean free path of the gaseous phase, resulting in mass transfer through a porous membrane governed primarily by the Knudsen mechanism. A convective transport mechanism is thus the dominating mass transfer mechanism (Dullien, 1979).

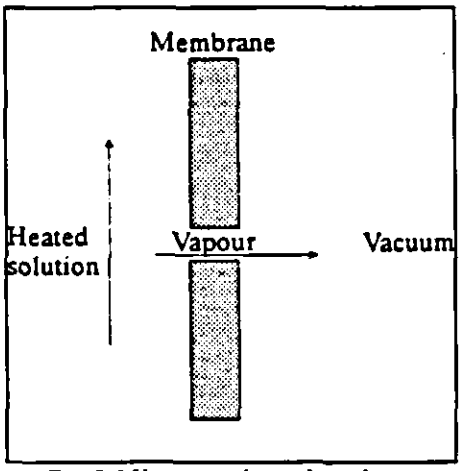

Fig. 2.6 Vacuum enhanced membrane distillation.

The resistance established due to the heat transfer in the liquid phase in vacuum enhanced membrane distillation tends to be the rate determining step, whereas with a membrane with a low permeability the dominating step is the mass transfer through the membrane itself.

Sarti *et al* (1993) proposed a model for the transport phenomena in a vacuum enhanced membrane distillation unit and compared the predicted values to those obtained experimentally. The set-up that was used consisted of hollow fibre polypropylene membranes with a 35 % void fraction, 25 μm thickness, 0.02 μm 0.04 μm nominal pore size and a 0.4 mm inner diameter in a shell-and-tube module. The module consisted of 15 fibres in a plexiglass tube with an effective length of 0.16 m. The different fibres were not closer than 10 capillary diameters from each other, in order to prevent interaction between adjacent fibres. The feed, consisting of volatile organic compounds (VOC), enters the shell side while the tube side is kept under vacuum. As in pervaporation, the permeate phase is collected in a liquid nitrogen condensation trap. The mass flux (N) through the membrane is

$$N = K_m \sqrt{M} \Delta P \qquad (2.44)$$

where K_m is the membrane permeability, M is the molecular mass of the diffusing species and ΔP is the vapour pressure difference across the membrane.

The assumption was made that because of the low pressure on the downstream side, all the temperature, concentration and vapour pressure differences between the membrane surface and the bulk gaseous phase are negligible.

The heat transfer and mass transfer in the bulk fluid and the heat transfer through the membrane was the same as that of direct contact membrane distillation and air gap membrane distillation. The interfacial temperature and concentration were determined by the bulk temperature and bulk concentration, as well as the temperature and concentration polarisation. The same mass transfer and heat transfer correlations can be used as in the abovementioned two processes depending on the configuration thereof.

Sarti *et al.* (1993) found that fairly high transmembrane fluxes were obtained even though the operating temperatures were relatively low and downstream pressures relatively high.

The total pressure difference between the liquid-membrane interface and the gaseous phase gives rise to permeate fluxes much larger than those in any membrane distillation or pervaporation process. This is because the maximum driving force is applied and the membrane used is porous compared with the dense membrane used in pervaporation, resulting into a higher membrane permeability (Sarti *et al.*, 1993).

2.2 Transport Inefficiencies

2.2.1 Temperature Polarisation

Since there is a heat flux in membrane distillation, it is obvious that thermal gradients would exist in the bulk fluids. This leads to the phenomenon that the temperature difference across the diffusion path is smaller than the temperature difference between the bulk liquids (see fig. 2.3). This phenomenon is known as temperature polarisation. The unavoidable presence of temperature polarisation causes the bulk temperatures (T_f and T_c) to have lower effective interface temperatures, which reduce the vapour transport through the membrane.

According to eqn. (2.22), the overall heat transfer coefficient through the membrane (*H*) increases with increase in the average temperature of the membrane (T_m), and consequently the temperature polarisation coefficient (TPC or τ) as indicated by eqn. (2.46) will decrease, having a negative effect on the overall flux. Schofield *et al.* (1987) found that by not taking temperature polarisation into account, the mass transfer driving force was overestimated by 60 %, which in turn led to a 40 % underestimation in experimental transmembrane mass flux.

Ortiz de Zárate *et al.* (1993) investigated the effect of stirring speed on the temperature polarisation of a porous, hydrophobic membrane based on the direct contact membrane distillation principle. It was found that by extrapolating the stirring rate from a low rate to an infinite stirring rate, temperature polarisation could cause a reduction in the mass transport of up to 58 %.

To quantify temperature polarisation, consider the representation of heat flows in fig. 2.3. For the heat transfer in direct contact membrane distillation to and from the membrane surface, we have

$$Q = h_1(T_1 - T_2) = h_o(T_3 - T_c) \qquad (2.45)$$

where h_l and h_o are the heat transfer coefficients of the hot and cold fluids respectively. From (2.21) and (2.45),

$$(T_2 - T_3) = \frac{T_1 - T_c}{1 + \frac{H}{h_1} + \frac{H}{h_o}} = \tau(T_1 - T_c) \qquad (2.46)$$

Temperature polarisation for direct contact membrane distillation can be described by the following equation:

$$\tau = \frac{T_2 - T_3}{T_1 - T_c} \qquad (2.47)$$

where T_1 and T_c are the bulk temperatures of the brine solution and the cooling water respectively, and T_2 and T_3 are the temperatures of membrane surface at the brine side and the coolant side, respectively. Ideally, τ should be as close to unity as possible, but Schofield *et al.* (1987) found that in many cases this value was closer to zero. Since membrane distillation is limited by heat transfer, and temperature polarisation is coupled to heat transfer, the understanding of temperature polarisation is of vital importance, especially in the design of membrane distillation modules and the understanding of membrane distillation data. Temperature polarisation should thus be incorporated in the heat and mass transfer of all membrane distillation processes (Schofield *et al.*, 1987).

Temperature polarisation may be reduced by increasing the film heat transfer coefficients as indicated by eqn. (2.46). This can be done by increasing the velocity of the liquid across the membrane surface. It can also be improved further by including turbulence promoters or by decreasing the flow channel heights (Fane *et al.*, 1987).

2.2.2 Concentration Polarisation

The purpose of any membrane process is the separation of one or more components from a solution. The permeation rate of the solute will be negligible compared with that of the solvent. This will lead to an accumulation of solute at the membrane surface, that is, a concentration increase. A diffusive back flow of solute ($D dc/dz$) towards the bulk solution will occur (fig. 2.7), which eventually will be balanced by the solute build-up (Jc) and the solute which passed through the membrane (Jc_c), that is, steady state conditions will prevail.

$$Jc_c = Jc + D\frac{dc}{dz} \qquad (2.48)$$

$c = c_1$ at $z = 0$

$c = c_2$ at $z = \delta$

Integrating the eqn. (2.48) by using the abovementioned boundary conditions and by assuming that the solute is completely retained by the membrane (i.e. $Jc_p = 0$), the following equation is obtained (Feng *et al.*, 1994; Kurokawa *et al.*, 1990; Mulder, 1991):

$$J = k \ln \frac{c_2}{c_1} \tag{2.49}$$

where c_1 and c_2 are the concentrations of the solute in the bulk and at the membrane surface, respectively, and J is the flux.

This increase in solute concentration will decrease the vapour pressure of the solution, and since the transmembrane vapour pressure difference is the driving force in membrane distillation, this concentration build-up at the membrane surface will decrease the mass flux; this phenomenon is known as concentration polarisation (Mulder, 1991).

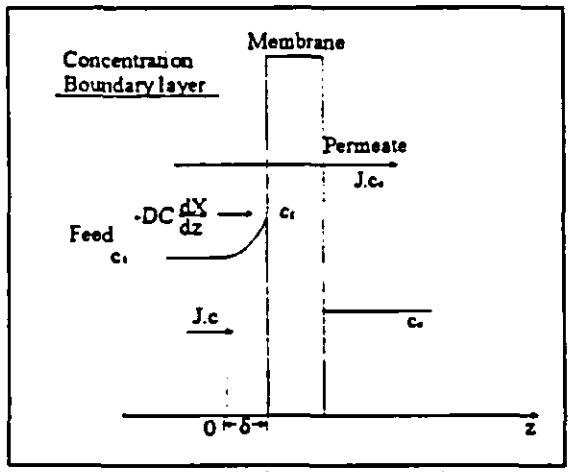

Fig. 2.7 A schematic of concentration polarisation.

Equation (2.49) indicates the importance of the flux (J) and of the mass transfer coefficient (k) on concentration polarisation. This shows that the flux for pure water can be determined for a specific membrane, and that this value is not subject to change. The mass transfer coefficient (k), on the contrary, depends on the hydrodynamics of the system and this value can be varied to optimise the membrane system. The mass transfer coefficient is related to the Sherwood number

$$Sh = \frac{kd_h}{D} = a \, \mathrm{Re}^b \, Sc^c \tag{2.50}$$

where a, b, c are constants, Re is the Reynolds number, and Sc is the Schmidt number.

$$\mathrm{Re} = \frac{\rho u d_h}{\eta} \tag{2.51}$$

where d_h is the characteristic length, ρ is the liquid density, u is the linear flow velocity and η is the dynamic viscosity.

$$Sc = \frac{\eta}{D\rho} \qquad (2.52)$$

where D is the diffusion coefficient.

It can be seen from eqns. (2.50)-(2.52) that for a given module $k=f(u,D)$. Mulder also stated that concentration polarisation can be reduced by manipulating k and the mass flux (N). Since the numerical value for the diffusion coefficient is fixed at a constant temperature, the mass transfer coefficient (k) can be manipulated only by changing the linear velocity of the fluid. As with temperature polarisation, concentration polarisation can be decreased by increasing the flow into the turbulent region by means of turbulence promotors, breaking the boundary layer by using corrugated membranes or by decreasing the flow channel height (Mulder, 1991).

Currently, the resistance-in-series model is used mainly to describe concentration polarisation in membrane separation processes. According to the model, the overall mass transfer resistance is the sum of the mass transfer resistances through the concentration boundary layer, membrane and the air gap. Feng *et al.* (1994) ascertained that the resistance-in-series model is applicable only to the more permeable species, that is, species whose concentration gradient in the boundary layer is in the same direction as the mass transfer. Because the concentration of the less permeable species is higher at the membrane surface than in the bulk, this will lead to a negative resistance, which is unrealistic.

Kurokawa *et al.* (1990) reported that concentration and temperature polarisation increase with an increase in concentration as well as an increase in brine temperature. When Kurokawa *et al.* (1990) neglected concentration polarisation in the modelling of air gap membrane distillation, it was found that the values obtained from the model did not

correlate well with the experimental values, although temperature polarisation had been included.

Weijun *et al.* (1993) studied the models proposed by Jönsson *et al.* (1985), Kimura *et al.* (1987), Schneider *et al.* (1988) and Schofield *et al.* (1987) for direct contact membrane distillation and air gap membrane distillation. Unfortunately, none of these researchers incorporated concentration polarisation into their models, which resulted in incomplete models and, consequently Weijun *et al.* (1993) did intensive studies on the effect of concentration polarisation in membrane distillation. Instead of using a brine solution, he used a $CaCl_2$ solution in a plate-and-frame direct contact membrane distillation module. He found that for a bulk concentration of 5 % (wt.) $CaCl_2$, the concentration at the membrane surface was 19 % (wt.) $CaCl_2$ and for a bulk concentration of 20 % (wt.) $CaCl_2$, the concentration at the membrane surface was 25 % (wt.) $CaCl_2$. In the former case the mass flux was 10.07 $kg/m^2.h$, while in the latter case this mass flux decreased to 6.68 $kg/m^2.h$. In these experiments the temperature of the $CaCl_2$ solution and the cooling water were kept constant at 48° C and 25° C, respectively, while the flow rates of the $CaCl_2$ solution and cooling water were 0.1 m^3/h and 0.09 m^3/h, respectively.

2.3 Heat Efficiency of Membrane Distillation

The heat efficiency in membrane distillation, E, is defined as the ratio of the evaporation heat, Q_{vap}, to the total heat supplied by the hot solutions, Q.

$$E = \frac{Q_{vap}}{Q} \tag{2.54}$$

Moalin *et al.* (1993) reported that the heat efficiency could be increased by enlarging the pore diameter, increasing the porosity and lowering the conductivity of the membrane. It can thus be concluded that the selection of the membrane used in membrane distillation plays a very important role in the heat efficiency. The heat efficiency also increases with increasing average temperature (T_m) in the membrane pores and increasing flow rate. To increase the heat efficiency of the membrane distillation process an air gap can be

introduced between the membrane and the condensing surface. Kubota *et al.* (1988) suggested that the heat efficiency could be increased even more by developing a multi stage membrane distillation process and a suitable membrane module with high heat efficiency to maximise the heat efficiency of the whole system.

Hogan *et al.* (1991) stated that the conduction losses through the membrane increase approximately linearly with increasing brine temperature. This means that although more heat is lost by conduction at higher temperatures difference, it is less as a proportion of the total heat transfer.

In direct contact membrane distillation experiments using a dense, hydrophilic fluoro carbon membrane, it was found that the flow rates of the brine solution and the cooling water had little effect on the thermal efficiency of the membrane (Ohta *et al.*, 1991).

2.4 Solar Radiation as Energy Source

Water is scarcest in those places where sunshine is most abundant. Sunlight has been used for many years in obtaining drinkable water by distillation from contaminated or brackish supplies. Many devices of varying complexity have been used for this purpose; one of the simplest is shown in fig. 2.8.

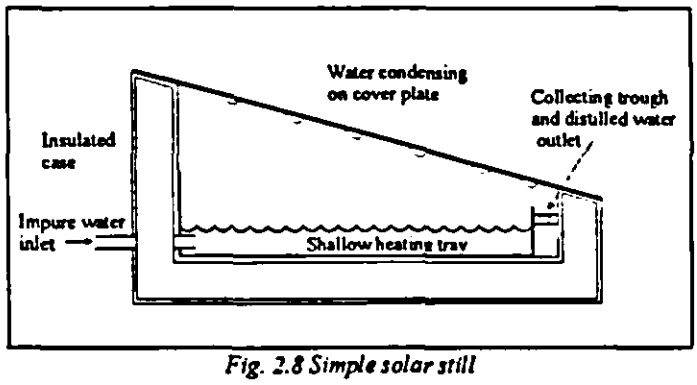

Fig. 2.8 Simple solar still

The unpalatable water is admitted into the tray at the bottom where it is heated by the absorption of solar energy. The base of the tray is usually blackened to facilitate this, since water is substantially transparent to the short wavelength radiation from the sun. As the temperature increases, the motion of the water molecules become more vigorous and they are able to leave the surface in increasing numbers. Convection in the air above the surface carries them away and evaporation thus occurs. The rising air current, laden with moisture, cools on contact with the transparent

cover plate, the water vapour condenses and runs down into the collector channels at the edges.

Solar stills have not lived up to their earlier promise of providing cheap desalinated water, mainly because it has been found to be difficult to produce a cheap enough still of sufficient reliability and life expectancy. Dispite their costs, solar stills should continue to find application in remote, arid regions where small water capacities are required (up to 20 m^3/day (Löf, 1966).

2.5 Summary

In this chapter, the theory and a historical background of membrane distillation was studied. Models for the four types of membrane distillation were also presented. These are i) direct contact membrane distillation, ii) air gap membrane distillation, iii) sweeping gas membrane distillation, and iv) vacuum enhanced membrane distillation. Transport inefficiencies, such as temperature polarisation and concentration polarisation, was discussed. Although they were only discussed for direct contact membrane distillation, they can also be applied to air gap membrane distillation. Heat efficiency, as well as the use of solar radiation for desalination purposes was investigated. In the following chapter, the experimental procedures performed for the purposes of this project will be presented.

CHAPTER 3

EXPERIMENTAL

In this chapter, the experimental procedures that was performed will be presented. The working and manufacturing of the air gap membrane distillation units will be discussed, as well as the experimental set-up and the experimental design. Furthermore, the estimation of the permeability coefficient of the membrane will be determined and the viability of solar radiation as an energy source for membrane distillation will be investigated.

3.1 Air Gap Membrane Distillation Units

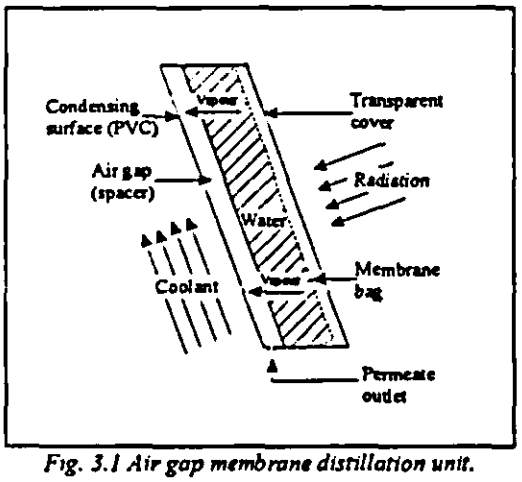

Fig. 3.1 Air gap membrane distillation unit.

The air gap membrane distillation units are presented in fig. 3.1 and fig. B3 in appendix B.

The membrane used was Skin Line 8183 manufactured by Lainière de Picardie.

A clear PVC sheet was supported over a black, radiation absorbent membrane bag, while the membrane bag was made by using a polyurethane-based adhesive (Sikaflex) to seal the sides of the membrane together in the shape of a bag. The membrane was laminated, so that the adhesive was applied to the lamination to prevent the 12 μm thick membrane from ripping. The membrane bag was placed inside a PVC bag with a transparent front and an opaque rear. The PVC bag was made by heat-sealing the PVC sheeting together. A highly porous spacing material was placed between the membrane bag and the rear of the PVC bag to form an air gap. Sunlight entered the PVC bag through the transparent cover and heated the water in the

membrane bag. Since there was a temperature gradient between the water in the bag and the condensing surface, water vapour is transported from the bulk liquid to the rear of the PVC bag (fig. 3.1). The vapour condensed on the rear of the bag and the permeate was collected at the bottom of the system. This unit was tilted at an optimum angle towards the sun. Unfortunately, it was very difficult with this system to control the process variables to obtain useful results, and consequently an alternative set-up was designed.

3.2 Air Gap Membrane Distillation Experimental Set-up

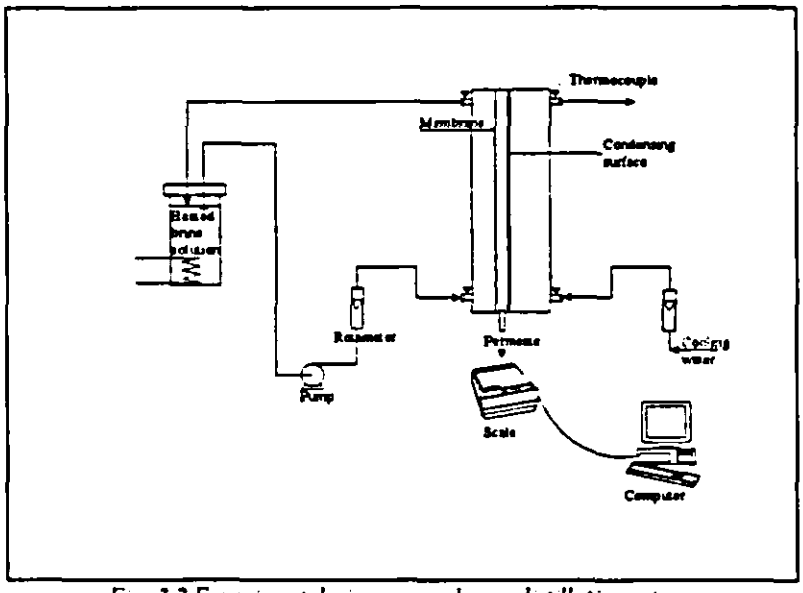

Fig. 3.2 Experimental air gap membrane distillation set-up.

The experimental set-up (fig. 3.2) consisted of an Air Gap Membrane Distillation (Air Gap Membrane Distillation) module in which a heated brine solution and cooling water flowed concurrently from the bottom to the top of the module (fig. B1-B2, appendix B), since this improved the liquid contact with the membrane. To minimise heat losses to the atmosphere, the module was manufactured from polypropylene (PP) sheeting five centimetre (5 cm) thick. Flow channels were machined into the PP sheeting which resulted in an effective transfer area of 320 cm^2. The purpose of these flow channels was to improve the flow patterns and to minimise dead volume. The air gap was situated between the membrane and the condensing surface and in order to support the membrane and vary the width of the air gap, a spacer with a thickness of 1.83 mm was inserted between the membrane and the condensing surface. The width of the air gap was altered by changing the number of spacers used, hence the width of the air gap varied in multiples of 1.83 mm.

Due to the excellent heat transfer properties of the material, the condensing surface, which was in contact with cooling water, was made from 1.6 mm stainless steel sheeting.

Thermocouples were used at the water inlet and outlet of the membrane distillation module and were connected to a Yokogawa multichannel recorder which monitored the inlet and outlet temperatures of the fluids. A waterbath was used to contain the brine solution and to regulate the temperature and concentration of the brine solution. The brine solution was heated and recirculated by means of a pump and the flow rate was measured with a rotameter. Tap water was used as cooling water. The water vapour condensed on the condensing surface and flowed downward to the permeate outlet at the bottom of the module, where it was collected in a glass beaker and weighed continuously. The scale used was a Sartorius B6100 which was connected to a computer with a serial cable, and readings were taken every twenty seconds. Afterwards, the quality of the permeate was determined by measuring the its conductivity.

Before any experiments were done, it was important to determine which variables had a significant effect on the process.

Six variables had to be investigated : i) temperature of the brine solution (T_b), ii) temperature of the cooling water (T_c), iii) width of the air gap (l_2), iv) concentration of the brine solution (c_b), v) flow rate of the brine solution (u_b), and vi) flow rate of the cooling water (u_c). The flow rates were not included as variables in the factorial design, since the flow rates were not an intrinsic property of membrane distillation, but were rather linked to the hydrodynamics of the system. Since a boundary layer was present, the mass flux reached a plateau after certain values in the flow rates were reached, so that the boundary layer would become insignificant.

The next step was to determine which of the remaining four variables had a significant effect on the mass flux.

3.2.1 The factorial design

A preliminary screening test was done to determine the significance of the set of variables by using a two-level, four-factor full factorial design.

Factors	Variables	Levels		Units
		-	+	
A	$T_{cooling\ water}$	297	306	K
B	T_{brine}	318	331	K
C	c_b	3	10	% (wt.)
D	l_2	1.83	9.15	mm

Table 3.1 Factorial design variables and the levels.

Sixteen runs were executed according to the factorial design and after each experiment the mass of the distillate (response) was monitored. The response was used to evaluate the significance of each variable to the process.

A	B	C	D	Response [$g/m^2.h$]
-	+	+	+	501
-	-	+	+	280
+	-	+	+	140
+	+	+	+	414
+	-	-	+	145
+	+	-	+	498
-	+	-	+	555
-	-	-	+	283
-	-	-	-	391
+	-	-	-	311
+	+	-	-	674
-	+	-	-	801
-	+	+	-	756
-	-	+	-	408
+	-	+	-	166
+	+	+	-	621

Table 3.2 Experimental runs with responses of the factorial design.

3.2.2 Statistical Interpretation of the Results

The results of the experimental phase of the factorial design were interpreted by the statistical software program *STATGRAPHICS* version 6.0. The independent variables were defined as the temperature of the brine (T_b), temperature of the cooling water (T_c),

concentration of the brine solution (c_b) and the air gap width (l_2), while the dependent variable was defined as the mass flux (N). It was found that the 1 percent and 5 percent F-values for (1,5) degrees of freedom are 16.26 and 6.61, respectively. This meant that if a factor did not have a significant effect on the response, the probability that its calculated F-statistic would exceed 16.26 was 1 in a 100 (1 %) and the probability that it would be greater than 6.61 was 1 in 20 (5 %).

Variable	F-value
A	366.61
B	51.06
C	6.97
D	86.84
AB	1.89
AD	10.50

Table 3.3 Analysis of variance.

By comparing the F-values from table 3.3 with the tabulated values supplied by Lochner *et al.* (1990), it is concluded that:

- The temperature of the brine, the air gap width and the temperature of the cooling water had the most significant effect on the response variable;
- The interaction between the temperature of the brine and the air gap affects the process on the 5 % level as well as the concentration of the feed; interaction occurred when the effect of one factor was influenced by a variation of another factor (Lochner *et al.*, 1990); and
- The interaction between the temperature of the brine feed and the cooling water had a very small effect on the response.

Consequently, the following experiments were done [see table 3.4 , in which (Δ) indicates a change of the variable and (-) indicates no change in the variable, as well as table A1-A10 in appendix A].

T_b	T_c	l_2	c_b	u_b	u_c
Δ	-	-	-	-	-
-	Δ	-	-	-	-
-	-	Δ	-	-	-
-	-	-	Δ	-	-
Δ	-	Δ	-	-	-
Δ	-	-	Δ	-	-
-	-	Δ	Δ	-	-
Δ	Δ	-	-	-	-
-	-	-	-	-	Δ
-	-	-	-	Δ	-

Table 3.4 Experiments conducted.

3.3 Permeability Coefficient of the Membrane

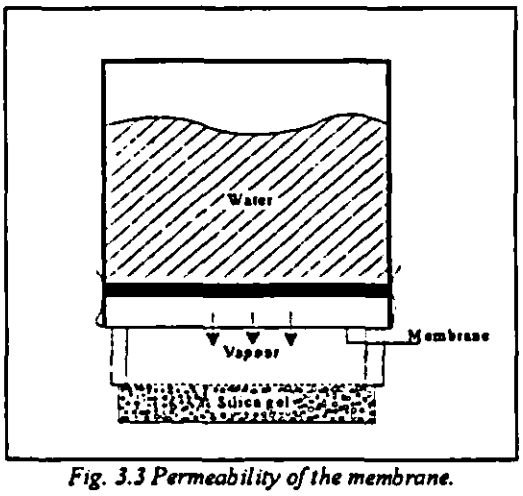

Fig. 3.3 Permeability of the membrane.

The membrane used was a dense, hydrophilic membrane so that transport of the water vapour took place by the solution-diffusion process. According to this mechanism, water vapour dissolves in the membrane, diffusing through the membrane, and then desorbed at the opposite side of the membrane. Equilibrium is reached when the absorption rate is equal to the desorption rate. Each membrane has a unique permeability coefficient for each diffusing species.

The permeability of the membrane was determined as follows (fig. 3.3):

The membrane was tied over of the top a cup filled with tap water and the cup was placed upside down on silica gel in a vacuum oven. This procedure was carried out in a vacuum oven so that the driving force for evaporation was the vapour pressure of the water at the temperature of the oven. After 1 h, the cup was weighed and the difference in weight before and after the experiment indicated the amount of water evaporated. The membrane thickness was 12 μm and it was assumed to be constant throughout the experiment, that is, the swelling

of the membrane has reached equilibrium. The effective transfer area was the circular area of the cup and from all these data, the permeability coefficient [$g.m.m^{-2}.s^{-1}.Pa^{-1}$] for the membrane to water vapour could be determined.

The permeability coefficient could not be determined as a function of concentration due to a lack of apparatus. It is thus assumed that the diffusion coefficient and the solubility is independent of concentration.

3.4 Solar Radiation

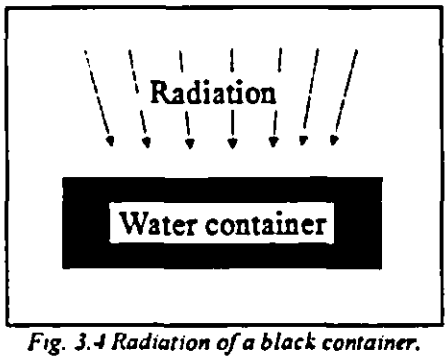

Fig. 3.4 Radiation of a black container.

The following experiment was carried out to determine to what extent sunlight would heat water in contact with a black surface. The distillation units had a black surface which was used to heat the brine solution which had to be desalinated.

This experiment was conducted (fig. 3.4) with a black polyethylene (PE) container with a volume of 16 cm^3 filled with tap water. This relatively small volume of water reached equilibrium rapidly. The bottle was left in direct sunlight in February 1995 and the water and atmospheric temperatures were recorded.

3.5 Summary

The manufacturing and working of the air gap membrane distillation units, that will be used for the purification of contaminated water, was discussed. The experimental set-up was presented and a factorial design was performed to determine which of the process variables had a significant effect on the mass flux. The temperature of the brine, air gap width and the temperature of the cooling water had the most significant effect on the mass flux. Interaction of the temperature of the brine and the air gap affected the process on a 5 % level. The same phenomenon was found for the concentration of the feed.

The effect of solar radiation on the temperature of water, that was in contact with a blackened surface, was also investigated.

The permeability coefficient of the membrane was estimated at various temperatures. Unfortunately it could not be estimated as a function of temperature and concentration. This assumption could lead to deviations in the modelling of the process, which will be discussed in the following chapter.

CHAPTER 4

MODELLING OF THE TRANSPORT PHENOMENA IN AIR GAP MEMBRANE DISTILLATION

In this chapter, the modelling of the transport phenomena in air gap membrane distillation will be performed. A fundamental model, as well as an empirical model will be derived. Apart from the modelling of the transfer phenomena, a sensitivity analysis will be performed, in which different aspects of air gap membrane distillation will be investigated, such as temperature polarisation, concentration polarisation and the heat efficiency of air gap membrane distillation.

The modelling of the transport phenomena in AGMD is a complicated process, since the mass transfer and heat transfer are coupled and must therefore be solved simultaneously. Figure 4.1 illustrates the principle of AGMD. Heat is required to produce a mass flux through the membrane and the energy necessary is obtained by heat transfer from the bulk to the membrane surface.

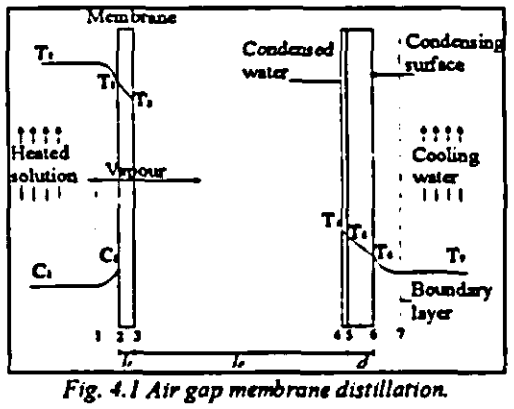

Fig. 4.1 Air gap membrane distillation.

4.1 Physical Properties

4.1.1 Physical Properties of Aqueous NaCl Solution

When a solute (NaCl) is dissolved in water, the density, viscosity and vapour pressure of the brine solution differ from the corresponding properties of pure water. The values obtained from the models presented by Fabuss (1980) tend to deviate from experimental results, especially at high temperatures and concentrations. Since there are data only for concentrations as high as 26 % (wt.) NaCl ,

improved models based on the experimental results supplied by Fabuss were derived using the software program *JANDEL SCIENTIFIC TABLECURVE* version 2.14. In order to obtain physical data for concentrations higher than 26 % (wt.), the data Fabuss supplied for density and vapour pressure were extrapolated.

The density of a NaCl solution can be expressed in terms of concentration and temperature (fig. 4.2) as follows:

$$\rho = a_1 + b_1 c + c_1 c \tag{4.1}$$

$$a_1 = a_2 + b_2 T + \frac{c_2}{T^2} \tag{4.2}$$

$$b_1 = a_3 + b_3 T + c_3 T^3 + d_3 e^{-T} \tag{4.3}$$

$$c_1 = a_4 + b_4 T + c_4 T^2 + d_4 T^3 + e_4 T^4 + f_4 T^5 \tag{4.4}$$

where ρ = density of the brine solution [kg/m^3]

T = temperature [K],

c = molality,

a_n, b_n = constants for density correlations ,

c_n, d_n = constants for density correlations,

e_n, f_n = constants for density correlations.

n	a	b	c	d	e	f
2	1.478	-1.162×10^{-3}	-11942.93	-	-	-
3	0.0986	-2.64×10^{-4}	7.53×10^{-10}	3.99×10^{123}	-	-
4	-9.486	1.44×10^{-1}	-8.77×10^{-4}	2.666×10^{-6}	-4.05×10^{-9}	2.45×10^{-12}

Table 4.1 Constants for density correlations.

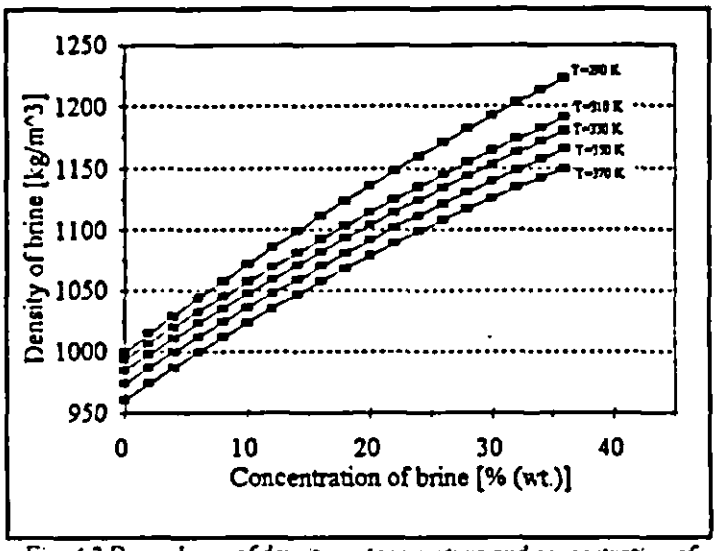

Fig. 4.2 Dependency of density on temperature and concentration of brine.

The vapour pressure can be expressed in terms of concentration and temperature (fig. 4.3) as follows:

$$p = a_1 + b_1 c$$

$$a_1 = \exp(a_2 + b_2 T + c_2 T^2) \tag{4.6}$$

$$b_1 = a_3 + b_3 T + \frac{c_3}{T} + d_3 T^3 \tag{4.7}$$

where p = vapour pressure of the salt solution [Pa],

a_n, b_n = constants for vapour pressure correlation,

c = concentration of the NaCl [kg/m^3],

T = temperature [K].

n	a_n	b_n	c_n	d_n
2	-29.248	0.159	-1.69×10^{-4}	-
3	-3349.03	8.395	376967	-1.58×10^{-3}

Table 4.2 Constants for vapour pressure correlations.

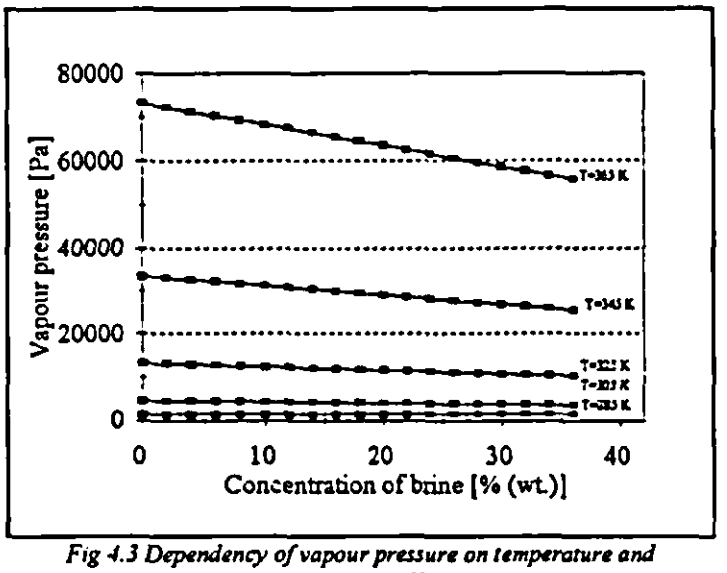

Fig 4.3 Dependency of vapour pressure on temperature and concentration of brine.

The viscosity is determined from the correlation supplied by Fabuss (fig. 4.4) as follows:

$$\mu_{brine} = \mu_{water} 10^{A'_{0i} + B'_{0i} \log \mu_{water}} \qquad (4.8)$$

where μ = dynamic viscosity [cP]

$$A'_{0i} = A'_{1i} + A'_{2i} I + A'_{3i} I^2 \qquad (4.9)$$

$$B'_{0i} = B'_{1i} + B'_{2i} I + B'_{3i} I^2 \qquad (4.10)$$

and

$$\log \mu_{water} = -1.64779 + \frac{262.37}{139.18 + (T - 273)} \qquad (4.11)$$

where T = temperature [K].

The ionic strength can be calculated as follows

$$I = \frac{1}{2} \sum_{0}^{i} n_i v_i^2 \qquad (4.12)$$

where n = ionic concentration of the ionic species [g-ion/kg water],

v = valence of the ion.

	1	2	3
A	3.55×10^{-2}	2.31×10^{-3}	-3×10^{-5}
B	-4.75×10^{-2}	1.6×10^{-2}	-1.94×10^{-3}

Table 4.3 Constants for viscosity correlations.

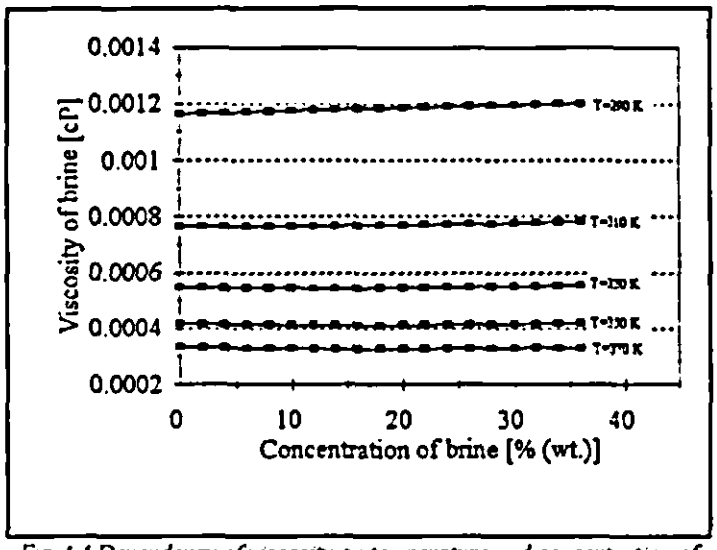

Fig 4.4 Dependency of viscosity on temperature and concentration of brine (Fabuss et al., 1980).

4.1.2 Physical Properties of Water

Physical data supplied by Incropera *et al.* (1990) were used to derive equations for the physical properties of water using the software program *JANDEL SCIENTIFIC TABLECURVE* version 2.14.

The latent heat of evaporation (λ) of water can be expressed as

$$\lambda = a_1 + b_1 T \tag{4.13}$$

where T = temperature [K].

Specific heat capacity of water

$$c_{p,f} = a_2 + b_2 T + c_2 T^2 + d_2 T^3 + e_2 T^4 \tag{4.14}$$

Specific heat capacity of water vapour

$$c_{p,g} = a_3 + b_3 T^2 + c_3 T^3 \tag{4.15}$$

Thermal conductivity of water

$$k = a_4 + b_4 (T - 273) + c_4 (T - 273)^2 \tag{4.16}$$

n	a	b	c	d	e
1	3168.28	-2.44	-	-	-
2	45.36	-0.4916	2.21×10^{-3}	-4.38	3.276
3	2.13	-1.18	2.953	-	-
4	0.577	1.52×10^{-3}	5.81×10^{-6}	-	-

Table 4.4 Constants for physical properties correlations.

(Fabuss, 1980)

4.1.3 Physical Properties of Air

The physical properties of air were supplied by Incropera *et al.* (1990) and the equation was also derived using *JANDEL SCIENTIFIC TABLECURVE* version 2.14.

Thermal conductivity of air (k_{air})

$$k_{air} = 3.27\times10^{-3} + 7.64\times10^{-5}T \qquad (4.17)$$

4.2 Transport Phenomena

4.2.1 Mass Transfer in Air Gap Membrane Distillation

Concentration polarisation is an intrinsic part of any membrane separation process. Concentration polarisation causes a concentration gradient to develop in the boundary layer because of the retention of NaCl at the membrane surface. Consequently, the concentration of the water is lower at the membrane surface than in the bulk because the NaCl concentration increases across the boundary layer. This phenomenon leads to a decrease in the mass flux, since an increase in NaCl concentration leads to a decrease in vapour pressure, which decreases the driving force. The resistance-in-series model is used to determine the mass transfer (Feng *et al.*, 1990).

Mass transfer is analogous to the heat transfer which permits one to derive the mass transfer correlations from the heat transfer correlations in equivalent boundary conditions, and this is done by simply substituting the Nusselt number (Nu) by the Sherwood number

(*Sh*) and the Prandl number (*Pr*) by the Schmidt number (*Sc*). For this to be applicable, the following assumptions must be made:

i) Constant physical properties;

ii) No chemical reactions in the fluid;

iii) No viscous dissipation;

iv) A small rate of mass transfer;

v) No emission or adsorption of radiant energy; and

vi) No pressure, thermal or forced diffusion (Bird *et al.*, 1960).

The Sherwood number (*Sh*) is equal to the dimensionless concentration gradient at the membrane surface, and provides a measure of the mass transfer coefficient at the surface. The Sherwood number is to the concentration boundary layer what the Nusselt number is to the thermal boundary layer. The flow of the fluid across the membrane surface can be regarded as parallel flow over a flat plate, so that the average Sherwood number ($\overline{Sh}$) is

$$\overline{Sh} = \frac{\bar{h}_m L}{D_{AB}} \tag{4.18}$$

where $\bar{h}_m$ = average mass transfer coefficient [m/s],

L = length of the membrane parallel to the flow direction [m],

D_{AB} = diffusion coefficient [m^2/s].

The average Sherwood number for laminar flow can also be expressed as

$$\overline{Sh} = 0.664\, Re_x^{1/2}\, Sc^{1/3} \tag{4.19}$$

for $0.6 \leq Sc \leq 50$

where the Reynolds number

$$\mathrm{Re} = \frac{\rho u L}{\mu} \tag{4.20}$$

and the Schmidt number

$$Sc = \frac{\nu}{D_{AB}} \tag{4.21}$$

where ρ = density of the aqueous NaCl [kg/m^3],

u = linear velocity of the brine solution [m/s],

ν = kinematic viscosity of the brine solution [m^2/s],

μ = dynamic viscosity of the brine solution [Pa.s],

D_{AB} = diffusion coefficient of NaCl through water [m^2/s],

L = length of the membrane parallel to the flow direction [m].

The diffusion coefficient for sodium chloride through water is temperature dependent and this leads to

$$\frac{D_{AB}}{D_{AB_{298K}}} = \frac{\mu_{298K}}{\mu}\frac{T}{T_{298K}} \tag{4.22}$$

where $D_{\mathrm{NaCl\text{-}H2O,\,298K}} = 1.9\times10^{-9}$ m^2/s (Incropera *et al.*, 1990)

For turbulent flow across the membrane surface, the average Sherwood number is

$$\overline{Sh} = 0.0296\,\mathrm{Re}_x^{4/5}\,Sc^{1/3} \tag{4.23}$$

for $0.6 \le Sc \le 60$.

In order to develop a model for a module with a different geometry, different correlations have to be used to determine the Sherwood number (Sh).

The mass transfer coefficient, h_m, can be calculated from eqns. (4.18)-(4.23) (Incropera *et al.*, 1990).

The mass transfer through the concentration boundary layer can be determined from (Karlsson *et al.*, 1993)

$$N = \bar{h}_m M_r A(c_1 - c_2) \tag{4.24}$$

where N = water vapour flux [g/s],

c_1, c_2 = concentration of the water at 1 and 2 (fig. 4.1), respectively [mol/m^3],

$\bar{h}_m$ = average mass transfer coefficient [m/s],

M_r = molecular mass of water [g/mol],

A = transfer area [m^2].

The membrane used was a hydrophilic, non porous membrane which swells by absorbing water. The term non porous is relatively ambiguous, because pores are present, but only at molecular level and it can be adequately described by free and swollen volume theory. The transport of a liquid, gas or vapour can be described by the so-called solution-diffusion mechanism (Mulder, 1991). The transport mechanism through a dense membrane, that is, a membrane not possessing microporosity, can be described by the following steps:

i) Sorption in the active layer from the upstream side;

ii) Molecular diffusion through the swollen membrane;

iii) Desorption from the membrane to the permeate side (Heintz *et al.*, 1994).

Mulder (1991) reported that the resistance induced by the mass transfer by desorption is negligible compared with that of sorption or diffusion.

$$P_{av} = D_{av} S \tag{4.25}$$

where P_{av} = Average permeability coefficient [g.m.m^{-2}.s^{-1}.Pa^{-1}],

S = Solubility [g.m.m^{-4}.Pa^{-1}],

D_{av} = Average diffusivity [m^2/s].

The solubility is a thermodynamic parameter and gives a measure of the amount of penetrant absorbed into the membrane under equilibrium conditions, whereas the diffusivity is a kinetic parameter which indicates how fast the penetrant is transported through the membrane. The permeability coefficient is defined as the amount of vapour permeating 1 m^2 of a membrane of 1 m thickness in 1 s with a pressure difference of 1 Pa across the membrane. In concentration dependent systems, the membrane may swell considerably leading to a change in the diffusive media, so that this in turn will lead to a change in the concentration in the polymer and a subsequent increase in the diffusion coefficient (Mulder, 1991). Since the diffusion coefficient is dependent on the concentration of the water in the membrane, the symbols P_{av} and D_{av} are used as averages across the membrane (Sherwood *et al.*, 1975). Matsuura (1995) suggested that the permeate evaporates somewhere between the upstream and downstream side of the membrane, that is, unlike membrane distillation, the water does not evaporate at the membrane surface. Since the driving force for pervaporation, like membrane distillation, is the vapour pressure gradient, Matsuura (1995) suggested an imaginary vapour phase adjacent to the membrane as a thermodynamic tool. The feed is in equilibrium with the vapour phase which, in turn, is in equilibrium with the feed side of the membrane. This assumption is satisfactory, since sorption from a liquid phase and that from a vapour phase are the same as long as the activity of the sorbate is the same in both cases (Barrie, 1968; Deng *et al.*, 1990). Matsuura (1995) also suggested that the vapour pressure across the membrane is constant from the upstream side to the border of the downstream side, where the vapour pressure falls discontinuously to the vapour pressure of the permeate. Conversely, Sheng *et al.* (1993) proposed that for a hydrophilic membrane used in pervaporation experiments, the water evaporates at the membrane surface and only vapour penetrates the membrane, that is, no liquid is present in the membrane. The argument supporting this phenomenon is that if evaporation occurs in the membrane pore channels, they would soon be blocked by salt crystals. As a result, the salt concentration in the permeate would increase steadily and the experiment would only last a few hours. This phenomenon was not observed.

By conducting permeability experiments, the average permeability coefficient of the membrane for water was determined as a function of temperature (see table 5.2 for results).

$$P_{av} = \frac{10^{-10}}{(a + bf_1)} \tag{4.26}$$

where

$$f_1 = e^{\frac{-(T-317)^2}{2(67.2872925)^2}} \tag{4.27}$$

and

a = 1.197,

b = -1.084.

The flux through the membrane can be expressed as

$$N = \frac{P_{av}}{l_1} A(p_2 - p_3) \tag{4.28}$$

where P_{av} = average permeability coefficient of water through membrane [g.m.m^{-2}s^{-1}Pa^{-1}],

p = vapour pressure [Pa],

A = mass transfer area [m^2],

l_1 = thickness of the membrane [m] (Mulder, 1991).

The diffusion of the water vapour through the air gap can be approximated as diffusion through a stagnant layer of air under atmospheric conditions. Furthermore it is also assumed that the water vapour and air in the air gap are ideal gases, since the operating pressure and temperature are close to those of atmospheric conditions (Jönsson *et al.*, 1985; Kimura *et al.*, 1987; Kurokawa *et al.*, 1990). The diffusion coefficient of water vapour through air can be regarded as concentration independent, since it can be approximated as a dilute gas system (Sherwood *et al.*, 1975)

Equations for the steady state diffusion of only one of the two species in binary mixtures of ideal gases are supplied by Sherwood *et al.* (1975).

$$N = \frac{D_{AB} PA}{RTl_2 p_{BM}} (p_3 - p_4) \qquad (4.29)$$

where P = total pressure in the air gap [Pa],

D_{AB} = diffusion coefficient of water vapour through air [m^2/s],

R = universal gas constant [J/mol.K],

T = average temperature in the air gap [K],

l_2 = air gap thickness [m],

p_{BM} = logarithmic mean pressure of the air in the air gap [Pa],

p_2, p_3 = vapour pressure of the at 2 and 3 fig. (4.1), respectively [Pa],

A = mass transfer area [m^2].

Since the above equation is applied to diffusion at a constant temperature and pressure, the average temperature and pressure between the two surfaces of the air gap were used (Sherwood *et al.*, 1975). The water vapour in the air gap is in contact with the condensed water, so the assumption is made that the vapour is in equilibrium with the adjacent condensed water layer. To calculate the vapour pressure of this vapour, the Antoine equation was used

$$\ln p = A - \frac{B}{C+T} \qquad (4.30)$$

where p = vapour pressure [mm Hg],

T = temperature [K],

A = 18.3036,

B = 3816.44,

C = -46.13 (Coulson *et al.*, 1983).

The temperature dependency of the diffusion coefficient of water vapour through air can be described by the expression (Banat *et al.*, 1994)

$$D = D_{298K}\left[\frac{T_{av}}{298}\right]^{2.334} \qquad (4.31)$$

where T_{av} = average temperature of the air gap [K] (Banat *et al.*, 1994),

D_{298K} = diffusion coefficient of water vapour though air (0.26×10^{-4} m^2/s) (Incropera *et al.*, 1990).

Assuming ideal gas properties for the vapour in the air gap and the vapour adjacent to the membrane on the upstream side, the vapour pressure and the concentration are related by

$$c = \frac{p}{RT} \qquad (4.32)$$

where p = vapour pressure of the water [Pa],

R = universal gas constant [J/mol.K],

T = temperature [K] (Coulson *et al.*, 1990).

By using eqn. (4.32) together with eqn. (4.28) and eqn. (4.29), the driving force can be re-written in terms of the concentration difference so that the mass transfer through the boundary layer, membrane and the air gap can be calculated by using the resistance-in-series model.

4.2.2 Heat Transfer in Air Gap Membrane Distillation

It is assumed that the air gap membrane distillation module is adiabatic, that is, there are no heat losses to the environment.

The motion of the brine solution over the membrane results in convective heat transfer and consequently a temperature boundary layer forms. Since the temperature of the bulk differs from that at the membrane surface, there is a change in the enthalpy of the water that diffuses through the boundary layer. This leads to the following expression:

$$Q = (\bar{h}_1 + Nc_{p,f})A(T_1 - T_2) \qquad (4.33)$$

where Q = heat flux [W],

N = mass flux [g/s],

A = transfer area [m^2],

c_{pf}= specific heat capacity of the brine solution [J/g.K],

$\bar{h}_1$ = average heat transfer coefficient [$W/m^2.K$],

T_1, T_2= temperatures of 1 and 2, respectively (fig. 4.1) [K] (Kimura *et al.*, 1987).

The convection heat transfer coefficient (h_f) depends on the fluid properties (k, μ, ρ and c_p), the fluid velocity, the length scale and the surface velocity. The Nusselt number, which is equal to the dimensionless temperature gradient at the surface, provides a measure of the convection heat transfer at the surface.

$$\overline{Nu} = \frac{\bar{h}L}{k_f} \tag{4.34}$$

where $\bar{h}$ = convection heat transfer coefficient [$W/m^2.K$],

L = length of the membrane parallel to the flow [m],

k_f= conduction heat transfer coefficient [W/m.K].

The motion of the brine solution over the membrane surface can be simplified to that of parallel flow over a flat plate. Consequently, the average Nusselt number can be expressed as

$$\overline{Nu} = 0.332\,Re_x^{1/2}\,Pr^{1/3} \tag{4.35}$$

where Re_x is the Reynolds number and Pr is the Prandl number. This equation is applicable if steady, incompressible, laminar flow with constant fluid properties and negligible viscous dissipation are assumed. Equations (4.34)-(4.35) can be used to determine the convection heat transfer coefficient ($\bar{h}_1$).

For turbulent flow, the average Nusselt number can be expressed as follows:

$$\overline{Nu} = 0.0296\,Re_x^{4/5}\,Pr^{1/3} \tag{4.36}$$

(Incropera *et al.*, 1990).

Since the transport mechanism through the membrane is that of solution-diffusion, water is absorbed into the membrane. Although the existence of an imaginary layer of vapour adjacent to the membrane is assumed as Matsuura (1995) suggested to determine the driving force, water is still absorbed into the membrane and all this water is evaporated before it is desorped from the membrane. In order to simplify the transport, it is assumed that only water is absorbed (i.e. no solute) and, furthermore, it is also assumed that evaporation occurs at the average membrane temperature (T_m) of the membrane. For heat transfer purposes, the process is simplified by taking the diffusion path (x) as a whole and not the membrane and the air gap separately.

The temperature gradient across the diffusion path results in conduction losses (membrane and air gap is stagnant) as well as a change in the vapour's enthalpy due to the thermal gradient. This leads to the following expression for the heat flux through the diffusion path.

$$Q = \left(\left(\frac{l_1}{k_m} + \frac{l_2}{k_{air}} \right)^{-1} + N c_{p,g} \right) A (T_2 - T_3) + N\lambda \qquad (4.37)$$

where l_1 = thickness of the membrane [m],

l_2 = width of air gap [m],

$c_{p,g}$ = specific heat of the water vapour in the membrane [J/g.K],

T_2, T_3 = temperatures at 2 and 3 (fig. 4.1), respectively [K],

λ = latent heat of evaporation [J/g],

A = transfer area [m^2],

k_{air} = thermal conductivity of air [W/m.K] (Kimura *et al.*, 1987),

k_m = thermal conductivity (0.06 W/m.K) (Kimura *et al.*, 1987, Schofield *et al.*, 1987).

The temperature at the surface of the condensate is equal to the saturation temperature of water vapour at the operating pressure in the air gap. The thickness of the condensate is assumed to be uniform. Since a temperature gradient is present in the condensate, heat

will be transferred towards the condensing plate. In order to obtain useful results, the same assumptions have to be made as those made in section 2.1.3 (Incropera *et al.*, 1990).

The heat transfer coefficient of the condensed water layer can be determined with an expression derived by Nusselt

$$\overline{Nu} = \frac{\overline{h_L} L}{k_l} = 0.943 \left[\frac{\rho_l g (\rho_l - \rho_v) h_{fg}' L^3}{\mu_l k_l (T_4 - T_5)} \right]^{1/4} \qquad (4.38)$$

where $\overline{h}_L$ = average convection heat transfer coefficient [W/m^2.K],

L = length of the membrane parallel to the flow direction [m],

k_l = conduction heat transfer coefficient [W/m.K],

ρ_l, ρ_v = density of water in liquid and vapour phases, respectively [kg/m^3],

h_{fg}' = modified latent heat [J/g],

μ_l = dynamic viscosity of water [Pa.s],

T_4, T_5 = temperatures at 4 and 5 (fig. 4.1), respectively [K].

The modified latent heat can be expressed as follows in terms of the Jacob number (Ja)

$$h_{fg}' = h_{fg}(1 + 0.68Ja) \qquad (4.39)$$

The Jacob number (Ja), which is the ratio of the sensible heat to the latent energy absorbed during liquid-vapour phase change, can be expressed as

$$Ja = \frac{c_p (T_s - T_{sat})}{h_{fg}} \qquad (4.40)$$

where c_p = specific heat capacity of vapour [J/g.K],

T_s = temperatures at the surface of the plate [K],

T_{sat} = saturation temperature [K],

h_{fg} = latent heat of evaporation [J/g].

All the liquid properties are evaluated at the film temperature $T_f = (T_4+T_5)/2$ and h_{fg} at the saturation temperature (T_4).

The heat flux through the condensed liquid layer on the surface of the condensing surface can be expressed as follows

$$Q = \bar{h}_L A(T_4 - T_5) \qquad (4.41)$$

where $\bar{h}_L$ = average heat transfer coefficient [W/m^2.K],

A = transfer area [m^2],

T_4, T_5 = temperatures at 4 and 5 (fig. 4.1), respectively [K] (Incropera *et al.*, 1990; Kimura *et al.*, 1987).

A sheet of stainless steel was used as a condensing surface and the thermal conductivity was taken as that of AISI 304 (Incropera *et al.*, 1990). There was once more a thermal gradient across the condensing surface and since there was no bulk motion, conduction was the only way by which heat was transported across the stainless steel plate.

$$Q = \frac{k_{ss}}{d}(T_5 - T_6) \qquad (4.42)$$

where k_{ss} = thermal conductivity of the stainless steel [W/m.K],

d = thickness of the condensing plate [m],

T_5, T_6 = temperatures of 5 and 6, respectively [K].

The data for the thermal conductivity of AISI 304 Stainless Steel were supplied by Incropera *et al.* (1990) and the equation was derived by means of *JANDEL SCIENTIFIC TABLECURVE* version 2.14.

$$k_{ss} = 3.27\text{x}10^{-3} + 7.64\text{x}10^{-5}T \qquad (4.43)$$

The motion of the cooling water with respect to the condensing plate leads to convective heat transfer from the condensing surface to the bulk fluid. The heat transfer can be expressed as

$$Q = h_{cw} A(T_6 - T_7) \qquad (4.44)$$

where h_{cw} = convection heat transfer coefficient [W/m^2.K],

T_6, T_7 = temperatures at 6 and 7 (fig. 4.1), respectively [K].

The convection heat transfer coefficient in the boundary layer of the cooling water can be determined in the same way as the coefficient in the brine solution by using eqns. (4.18)-(4.23) (Kimura *et al.*, 1987).

4.3 Solving the Model Equations

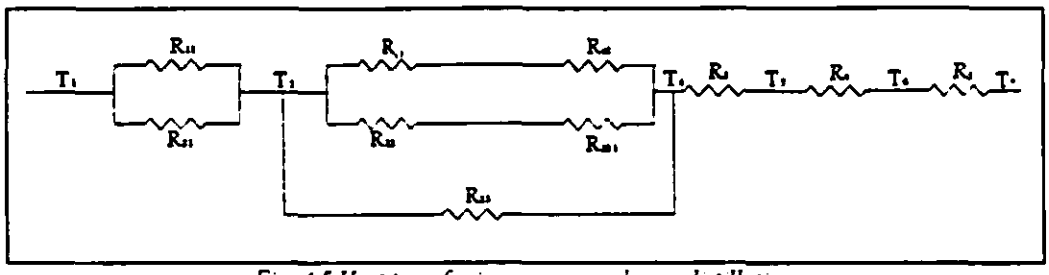

Fig. 4.5 Heat transfer in air gap membrane distillation.

As mentioned previously, the heat and mass transfer is coupled in air gap membrane distillation, so that the equations in section 4.2 and 4.3 have to be solved simultaneously. This was done by compiling a computer program in *TURBO PASCAL* version 7 (Appendix C). To simplify the solution of the equations, the heat and mass transfer are seen as resistances in series and in parallel (fig. 4.5 and fig. 4.6), due to the analogy between heat and mass transfer and electricity.

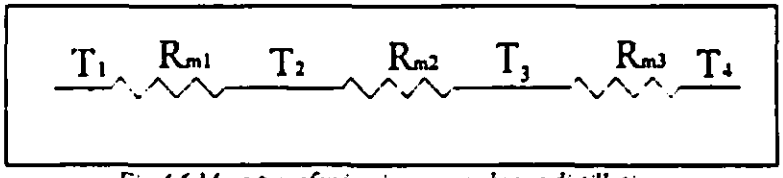

Fig 4.6 Mass transfer in air gap membrane distillation.

To solve the equations, initial conditions were specified and an iterative process was used to solve the equations for the resistances. These initial conditions were used to determine the magnitude of the resistances as well as the heat and mass fluxes. By using these results the temperatures were determined, and this iteration process was repeated until the different temperatures converged.

As mentioned before, the resistance-in-series model was used to solve the mass transfer phenomena (fig. 4.6). Since two phases were present, that is, liquid and vapour, the mass transfer driving force was expressed as a concentration difference, instead of a vapour pressure difference. The water vapour was regarded as an ideal gas, so that the ideal gas

law could be used to convert the vapour pressure to concentration. To determine the concentration of the water at the membrane surface, the two-film theory (Coulson *et al.*, 1990, Sherwood *et al.*, 1975) was used. This theory is based on the fact that the resistances adjacent to the interface can be added together and the interface induces no additional resistance to mass transfer. According to this theory, material is transferred in the bulk of the phases by convection currents and it also assumes that the phases are in equilibrium at the interface.

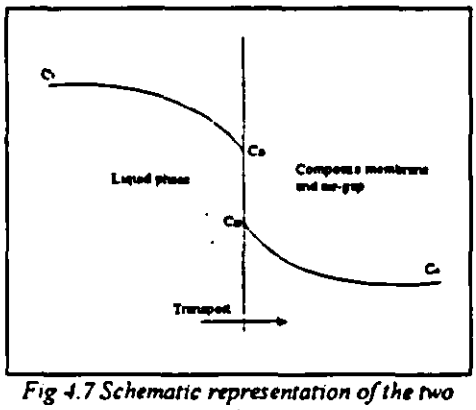

Fig 4.7 Schematic representation of the two film theory.

From fig. 4.7 the following equations can be derived for the mass flux (N).

$$N = \frac{1}{R_{m1}}(c_1 - c_{21}) = \frac{1}{R_{m2} + R_{m3}}(c_{22} - c_4) \qquad (4.45)$$

where R_{m1}, R_{m2}, R_{m3} are the mass transfer resistances for the concentration boundary layer, membrane and the air gap, respectively, while c_1 and c_{21} are the concentrations of the water in the bulk, and at the interface, respectively. The vapour concentrations c_{22} and c_4 are the concentrations at the interface and at the condensing surface, respectively. The two phases considered are the liquid and the air gap/membrane composite. The concentration at the membrane surface can be determined from eqn. (4.45). Although there are two unknown variables, c_{21} and c_{22}, it is known that the vapour pressure at the interface is a function of the concentration of the water at the interface. With this in mind, the vapour pressure, the concentration of the vapour, and consequently the concentration of the water at the interface can be determined.

4.3.1 Correlation between Predicted and Experimental Results

If two sets of data change in a related way, they are said to be correlated. The correlation coefficient (r), used to determine the degree of correlation, can be expressed as

$$r = \frac{n\sum xy - \sum x \sum y}{\sqrt{[n\sum x^2 - (\sum x)^2][n\sum y^2 - (\sum y)^2]}} \qquad (4.46)$$

This correlation coefficient is the ratio of the covariance of x and y to the square root of the product of the variance of x and the variance of y (Johnson *et al.*, 1964).

4.4 Empirical Modelling

Empirical modelling was performed by linear regression on the experimental results by using the software program *QUATTRO PRO for WINDOWS* version 5. Not all of the experimental data were used for this purpose, since some of the data had to be set aside to test the validity of the model. The empirical modelling was executed on a trial-and-error basis until the best fit was obtained.

$$f_1 = aT_c + bT_b + cl_2 + dc_b + eu_b + fu_c \qquad (4.47)$$

$$f_2 = gT_c^2 + hT_b^2 + iu_b^2 + ju_c^2 + kl_2^2 + lc_b^2 \qquad (4.48)$$

$$f_3 = mT_bT_c + nT_bc_b \qquad (4.49)$$

$$N = f_1 + f_2 + f_3 - 1925.02 \qquad (4.50)$$

a	198.65	h	0.198
b	-194.34	i	-107453
c	469.03	j	-4380535
d	-23.10	k	-0.330
e	12535	l	0.666
f	45019	m	0.333
g	-0.528	n	-1.512

Table 4.5 Empirical modelling constants.

4.4 Sensitivity Analysis

4.4.1 Temperature Polarisation

Figure 4.8 shows that temperature polarisation becomes more significant as the temperature of the brine solution increases. Furthermore, the temperature polarisation coefficient tends to become constant at higher temperatures. Since the mass and heat transfer in air gap membrane distillation is represented as resistances in series and parallel (fig. 4.5-4.6), table A32 indicates that the heat transfer resistance induced by the evaporation process (R_{23}) is the most important resistance in determining the effective heat transfer resistance across the diffusion path. The heat transfer resistances induced by the diffusion path (R_{2t}) is the rate determining resistance in heat transfer. When the temperature of the brine solution increases, the magnitude of the heat transfer resistance (fig. 4.36) through the diffusion path (R_{2t}) tends to a plateau, which leads to the same phenomena in the temperature polarisation coefficient.

The temperature polarisation coefficient decreases as the temperature of the cooling water increases (fig. 4.9). Once again, as in the case of a variation in the temperature of the brine solution, the dominating heat transfer resistance is the resistance induced by the diffusion path (R_{2t}) (fig. 4.37).

Figure 4.10 shows that the concentration of the brine feed has a negligible effect on the temperature polarisation coefficient. A variation in the concentration of the brine solution has a negligible effect on the heat transfer resistances (fig. 4.38).

The presence of the air gap leads to an improved temperature polarisation coefficient (fig. 4.11). Once again, the heat transfer resistance induced by the diffusion path is the rate determining step in the heat transfer (fig. 4.39). Although the heat transfer resistance induced by the evaporation process determines the effective resistance, there is a large increase in the resistance due to conduction through the air gap (table A35).

When the membrane thickness increases, there is an increase in the temperature polarisation coefficient (fig. 4.12). A change in membrane thickness mainly affects the resistance induced by the diffusion path, since the diffusion path consists of the air gap as well as the membrane (fig. 4.40).

Increase in the linear velocity of the brine feed leads to an improved temperature polarisation coefficient (fig. 4.13). The flow rate mainly affects the heat transfer resistance across the boundary layer at the upstream side of the membrane (R_{fl}) (fig. 4.41). Although there is also variation in the heat transfer resistance of the diffusion path, the former has a more significant effect on the total heat transfer resistance. At a Reynolds number of about 2400 there is a radical change in the magnitude of the temperature polarisation coefficient due to the transition from laminar to turbulent flow.

Similar trends are observed for a variation in the linear velocity of the cooling water (fig. 4.14). The variation of the linear velocity of the cooling water affects mainly heat transfer resistance across the boundary layer in the cooling water (R_5) (fig. 4.42).

The heat transfer resistances are presented in tables A31-A40.

4.4.2 Concentration Polarisation

As can be expected from the theory of concentration polarisation, the concentration of the salt at the membrane surface increases as the bulk concentration increases (fig. 4.17), which leads to a loss in driving force and hence a reduction in mass flux (fig. 4.31). Figure 4.15 shows that the concentration at the surface of the membrane is further affected by the temperature of the brine solution, although the concentration in the bulk is constant. This emphasises the coupling between the heat and mass transfer in membrane distillation. When the temperature of the cooling water is decreased, there is an increase in concentration at the membrane surface (fig. 4.16).

An increase in the air gap width causes a drop in the concentration of the salt at the membrane surface (fig. 4.18). Although the driving force will increase as the salt concentration at the surface decreases, the mass transfer resistance (table A25) induced by

the air gap will have such a large effect on the mass flux that the increase in driving force will be completely dominated, which will lead to a decrease in mass flux as the air gap width increases (fig. 4.32).

Similar trends were observed when the membrane thickness was changed (fig. 4.19). The same arguments can be used to explain this phenomenon that was also used to explain a variation in air gap width.

As is to be expected, the concentration at the surface of the membrane will decrease significantly if the linear velocity of the brine solution is increased (fig. 4.20), while an increase in velocity of the cooling water will increase the concentration at the membrane surface (fig. 4.21).

4.4.3 Heat Flux in Air Gap Membrane Distillation

Figures 4.29, 4.30, 4.32 and 4.33 show that when the temperature of the brine solution, temperature of the cooling water, air gap width or membrane thickness is varied, the heat and mass fluxes show the same trends, that is an increase in the heat flux will produce a larger mass flux. As the concentration of the brine feed changes from 0 % (wt.) to 26 % (wt.), the heat flux decreases from 33.9 W to 33.4 W (fig. 4.31). This decrease is negligible and the heat flux can therefore be regarded as constant.

The heat transfer resistances decrease with an increasing brine temperature (fig. 4.36), that is, the overall heat transfer coefficient increases. When the temperature of the cooling water is varied, both the heat transfer resistances induced by diffusion path (R_{2i}), as well the heat transfer resistance induced by the boundary layer at the cooling water side (R_5) play an important role in the heat transfer (fig. 4.37).

The decrease in the heat flux as the air gap width increases can be attributed to the increasing heat transfer resistance across the diffusion path (R_{2i}) (fig. 4.39). When the concentration of the brine solution is varied, the change of the heat flux is negligible (fig. 4.31). There is a change in the heat transfer resistance of the boundary layer at the

upstream side (table A34), but this change has a negligible effect on the overall heat transfer resistance.

When the flow rates of the brine solution and the cooling water are varied (fig. 4.34-4.35), the heat transfer resistance in the relevant boundary and the diffusion path change (fig. 4.41-4.42), which leads to the corresponding change in the heat flux.

4.4.4. Heat Efficiency in Air Gap Membrane Distillation

An increase in the temperature of the brine solution leads to improved heat efficiency (fig. 4.22), since the increase in the heat of evaporation is greater than the conduction losses. As in the case of temperature polarisation, the heat efficiency tends to a constant value at high temperatures. This can also be attributed to the heat transfer resistance induced by the diffusion path (R_{21}) which tends to a constant value at high temperatures (fig. 4.36).

On the other hand, the heat efficiency decreases as the temperature of the cooling water decreases (fig. 4.23), that is for an increasing temperature difference between the feed and cooling water. The heat efficiency increases for an increasing temperature difference if the brine temperature is varied, while the opposite occurs if the cooling water temperature is changed.

For an increase in feed concentration there is negligible change in the heat efficiency (fig. 4.24). As the concentration increases, there is negligible change in the heat transfer resistances (fig. 4.38), which produces the constant heat efficiency.

Although the air gap produces a lower mass flux, the heat efficiency improves with an increasing air gap width (fig. 4.25). The air gap reduces the ratio of conduction losses to total heat flux. A similar trend is observed for a change in the membrane thickness (fig. 4.26).

The heat efficiency increases as the flow rate of the brine solution increases (fig. 4.27). Although the heat efficiency increases, the conduction heat losses also increase with higher

flow rates (table A18). At a Reynolds number of 2400 there is a sudden change in heat efficiency, which can be attributed to the transition from laminar flow to turbulent flow.

The heat efficiency decreases as the linear velocity of the cooling water increases (fig. 4.28). As with the brine solution, the heat losses due to conduction increase with flow rate, but unfortunately the evaporative heat transfer does not change at the same rate (table A19).

4.5 Summary

A fundamental model and empirical model was derived for the transport phenomena in air gap membrane distillation. Due to a lack of apparatus, the assumption had to be made that the permeability coefficient was independent of the concentration of water in the membrane. The diffusion coefficient (D) and the solubility (S) was thus assumed to be independent of the concentration of the permeating species. The permeability coefficient was evaluated when the solubility (S) had reached equilibrium. Due to a lack of physical data, the density and vapour pressure of the brine solution had to be extrapolated for values above 26 % (wt.) NaCl. These assumptions could have a negative affect on the accuracy of the fundamental model. Furthermore, the presence of NaCl could also affect the solubility of water in the membrane. Apart from determining the mass flux, the fundamental model also estimated the heat flux through air gap membrane distillation. The sensitivity analysis did an in-depth study on aspects such as temperature polarisation, concentration polarisation and heat efficiency.

The model can be extended to modules of different geometries, although changes will have to be made to the fundamental model. One of the most important changes will be the correlations used to determine the transfer coefficients through the bulk fluids.

In the following chapter, the results obtained from the experimental procedures will be discussed.

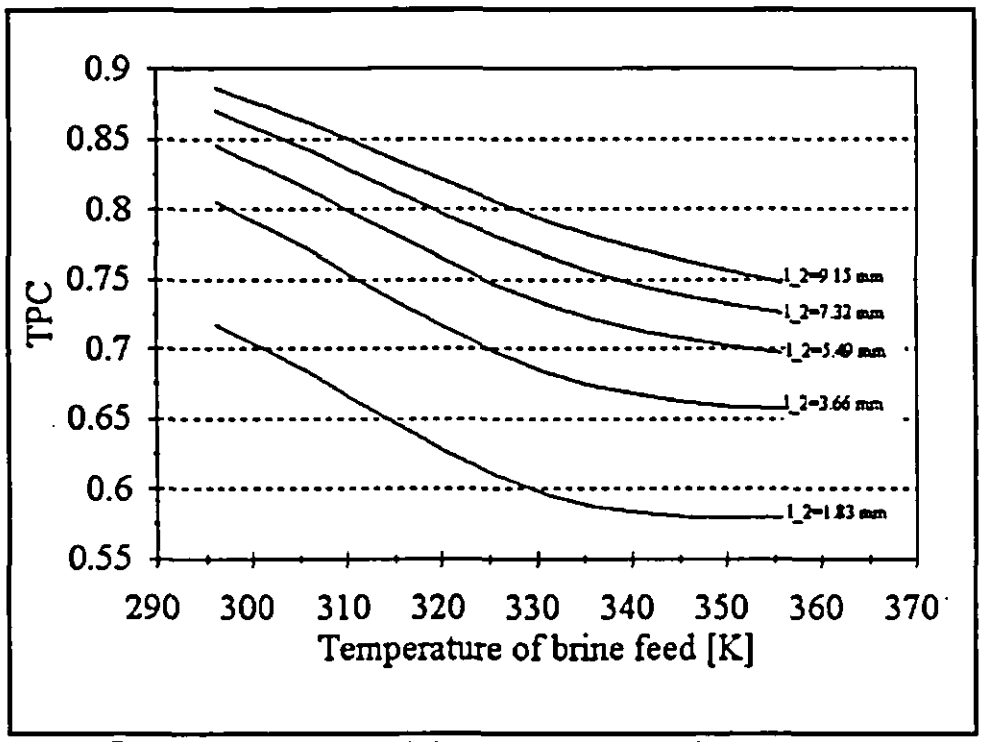

Fig. 4.8 Temperature polarisation as the brine temperature is varied at various air gap widths.
(T_c = 291 K, c_b = 3 % (wt.), l_1 = 24 μm, u_b = 0.03 m/s, u_c = 0.0026 m/s)

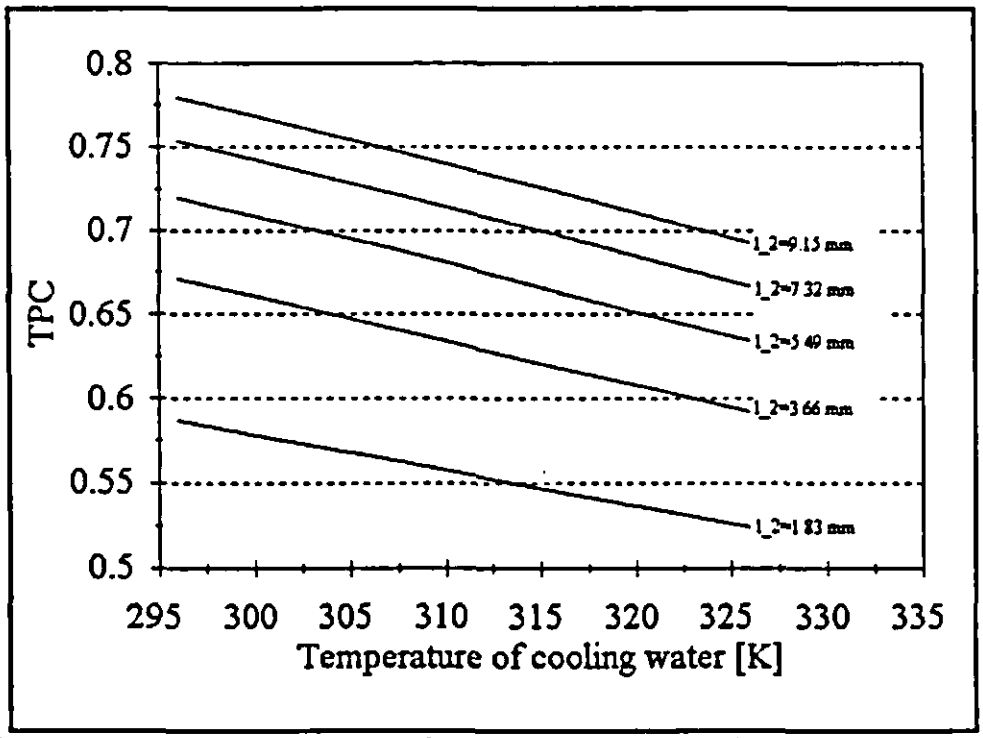

Fig 4.9 Temperature polarisation as the cooling water temperature is varied at various air gap widths.
(T_b = 331 K, c_b = 3 % (wt.), l_1 = 24 μm, u_b = 0.03 m/s, u_c = 0.0026 m/s)

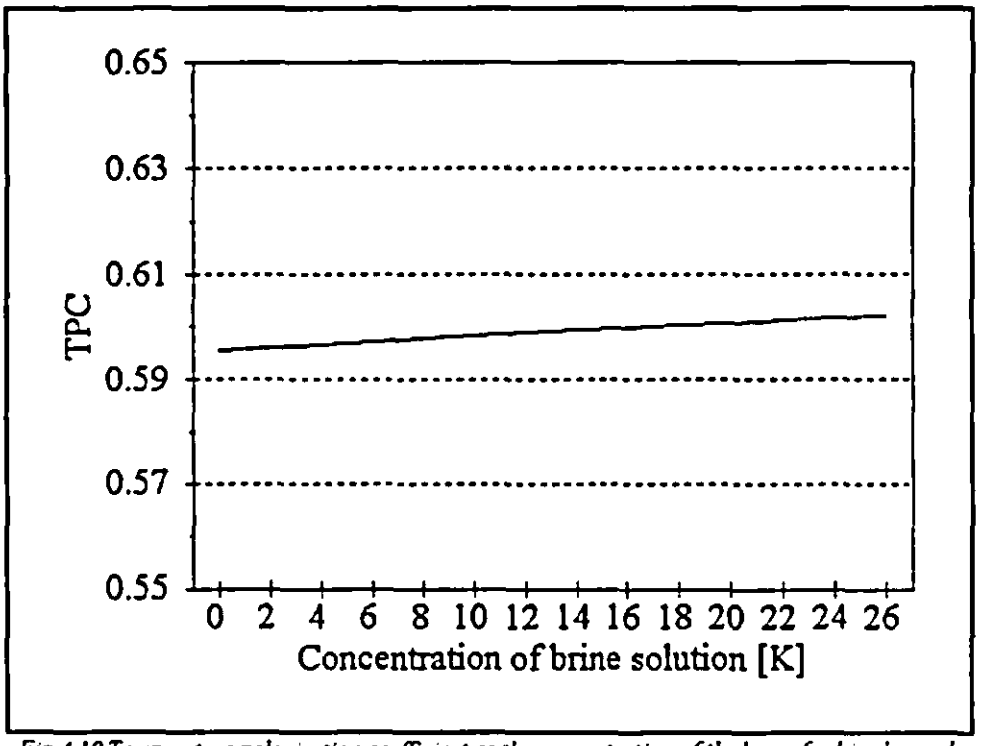

Fig 4.10 Temperature polarisation coefficient as the concentration of the brine feed is changed.
(T_b = 331 K, T_c = 291 K, l_1 = 24 μm, l_2 = 1.83 mm, u_b = 0.03 m/s, u_c = 0.0026 m/s)

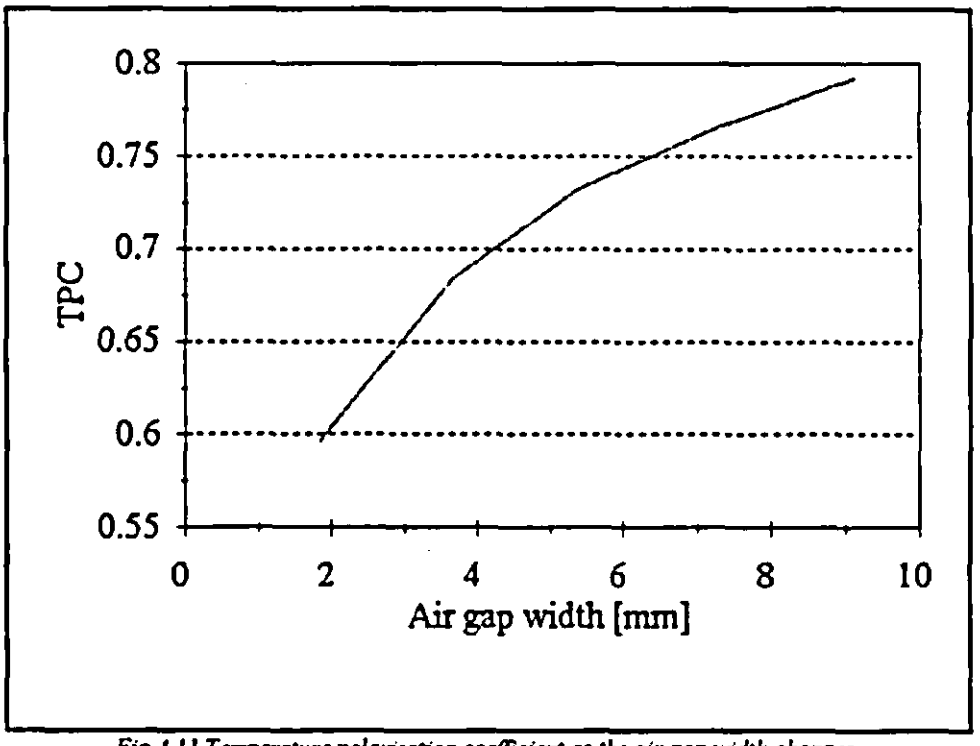

Fig 4.11 Temperature polarisation coefficient as the air gap width changes.
(T_b = 331 K, T_c = 291 K, l_1 = 24 μm, c_b = 3 % (wt.), u_b = 0.03 m/s, u_c = 0.0026 m/s)

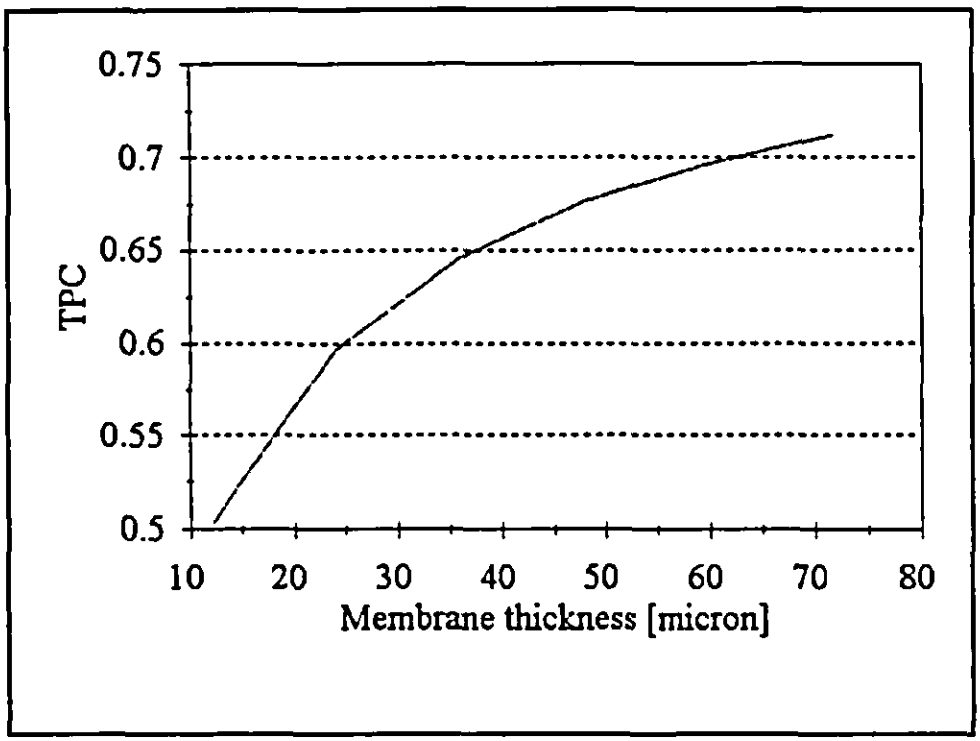

Fig 4.12 Temperature polarisation coefficient as the membrane thickness is changed.
(T_b = 331 K, T_c = 291 K, l_2 = 1.83 mm, c_b = 3 % (wt.), u_b = 0.03 m/s, u_c = 0.0026 m/s)

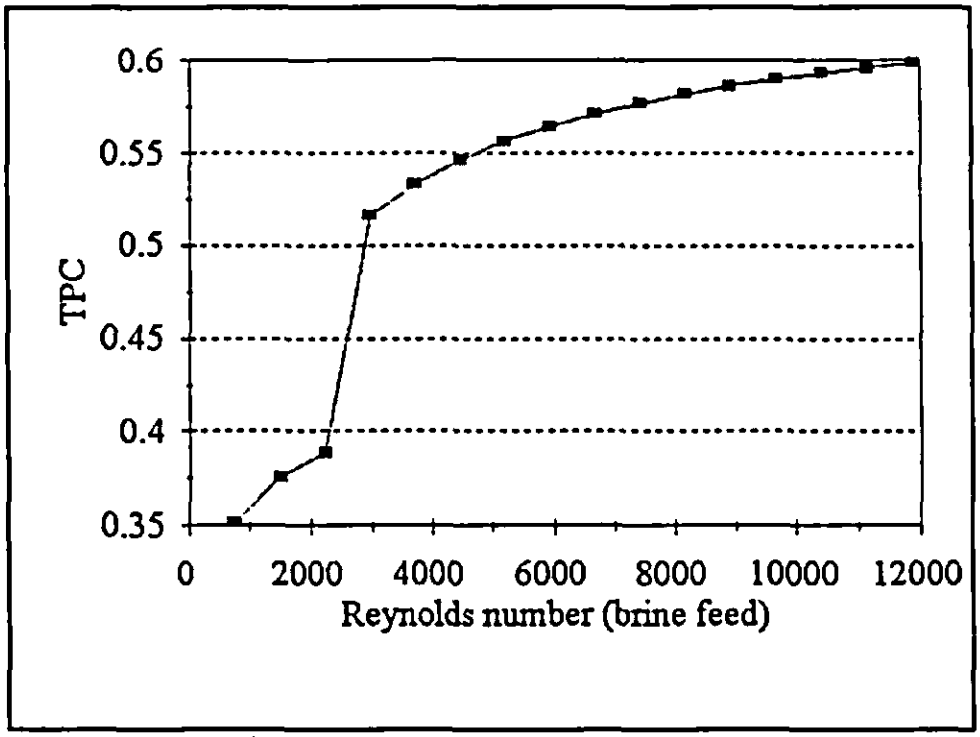

Fig 4.13 Temperature polarisation coefficient as the Reynolds number of the brine feed is changed.
(T_b = 331, T_c = 291 K, l_1 = 24 micron, l_2 = 1.83 mm, c_b = 3 % (wt.), u_c = 0.0026 m/s)

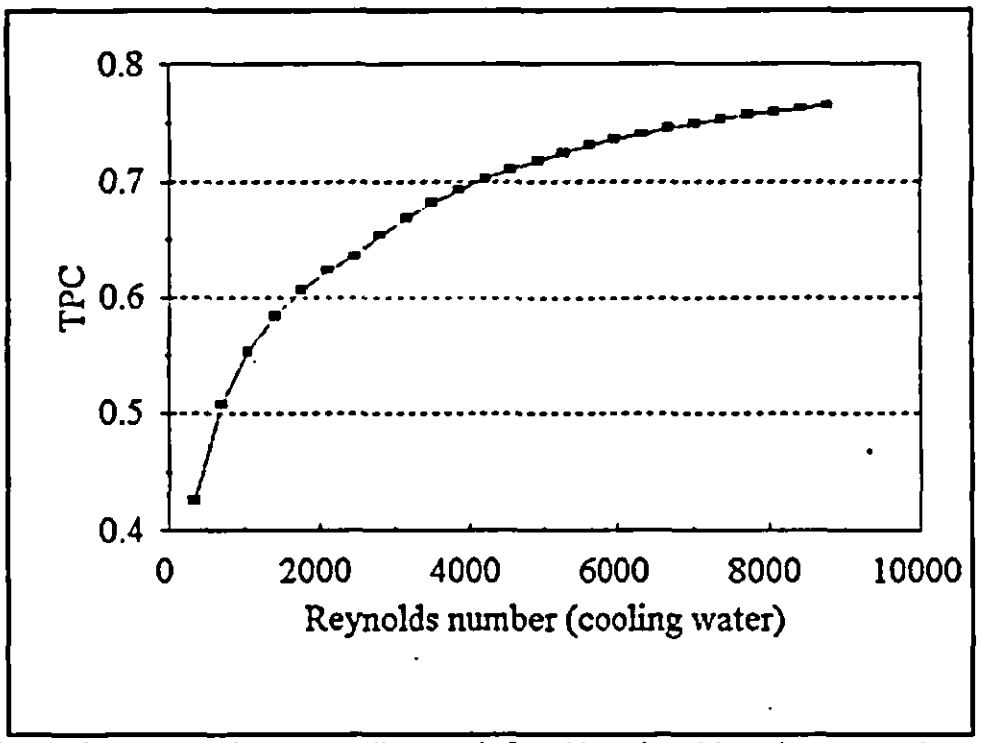

Fig 4.14 Temperature polarisation coefficient as the Reynolds number of the cooling water is changed. (T_b = 331, T_c = 291 K, l_1 = 24 micron, l_2 = 1.83 mm, c_b = 3 % (wt.), u_b = 0.03 m/s)

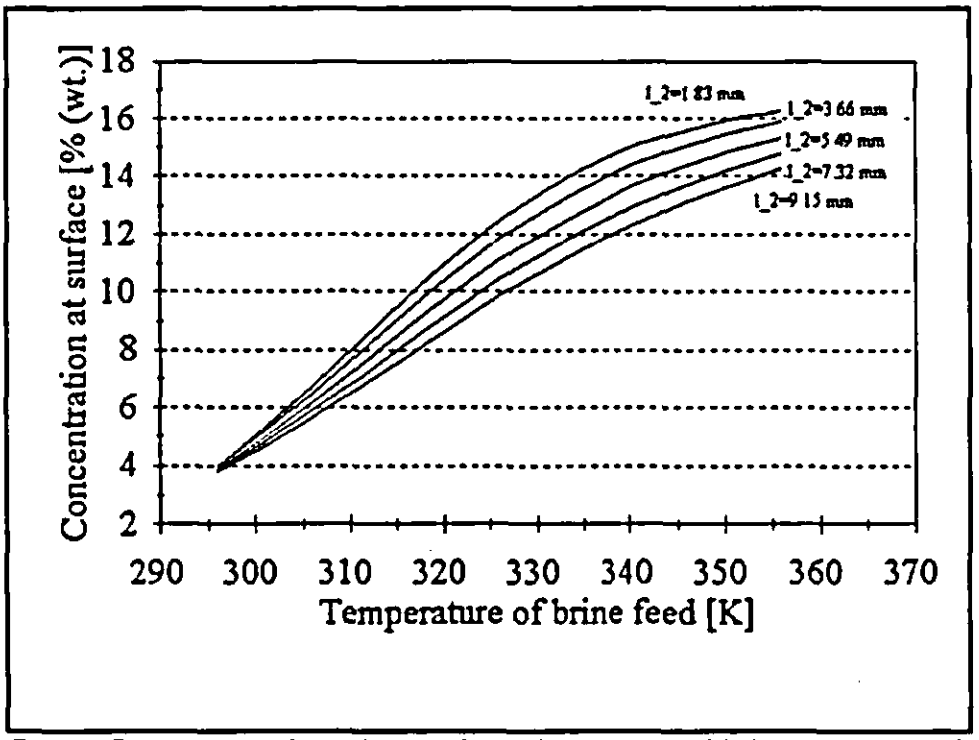

Fig. 4.15 Concentration at the membrane surface as the temperature of the brine feed is changed. (T_c = 291 K, c_b = 3 % (wt.), l_1 = 24μm, u_b = 0.03 m/s, u_c = 0.0026 m/s)

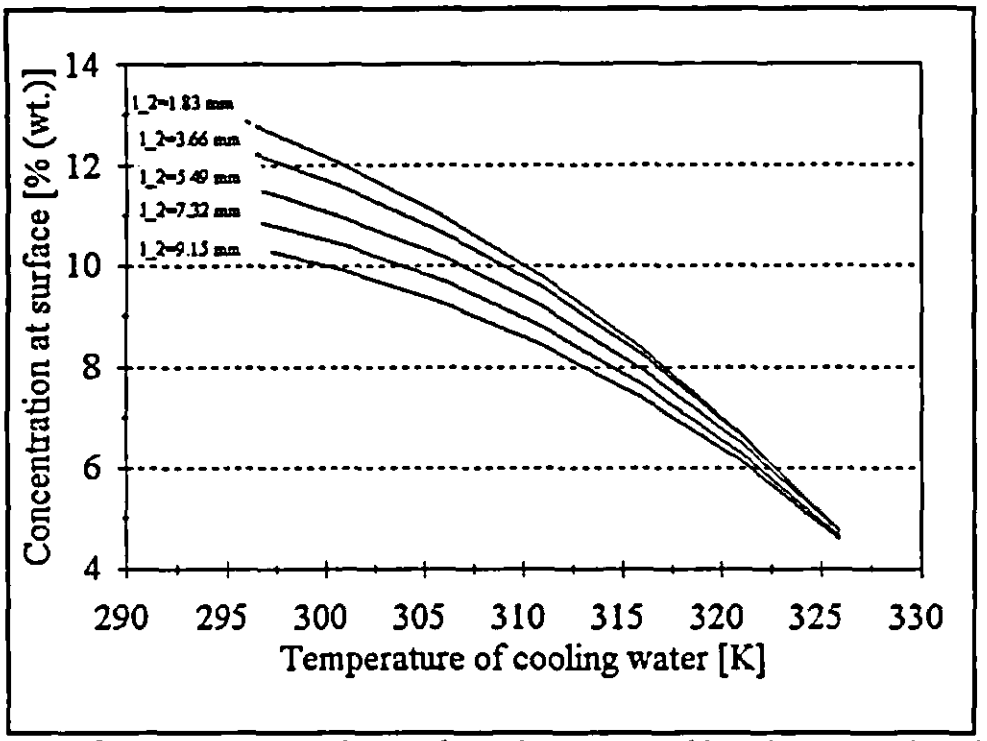

Fig 4.16 Concentration at the membrane surface as the temperature of the cooling water is changed. (T_b = 331 K, c_b = 3 %(wt.), l_1 = 24 μm, u_b = 0.03 m/s, u_e = 0.00226 m/s)

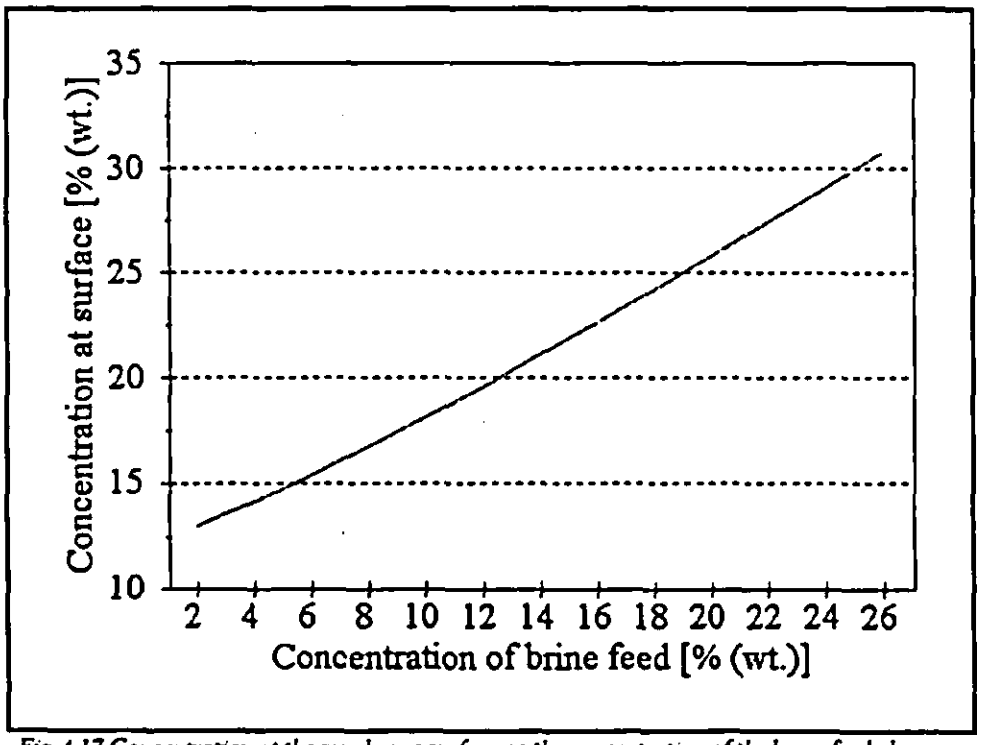

Fig 4.17 Concentration at the membrane surface as the concentration of the brine feed changes. (T_b = 331 K, T_c = 291, l_1 = 24 μm, l_2 = 1.83 mm, u_b = 0.03 m/s, u_e = 0.00226 m/s)

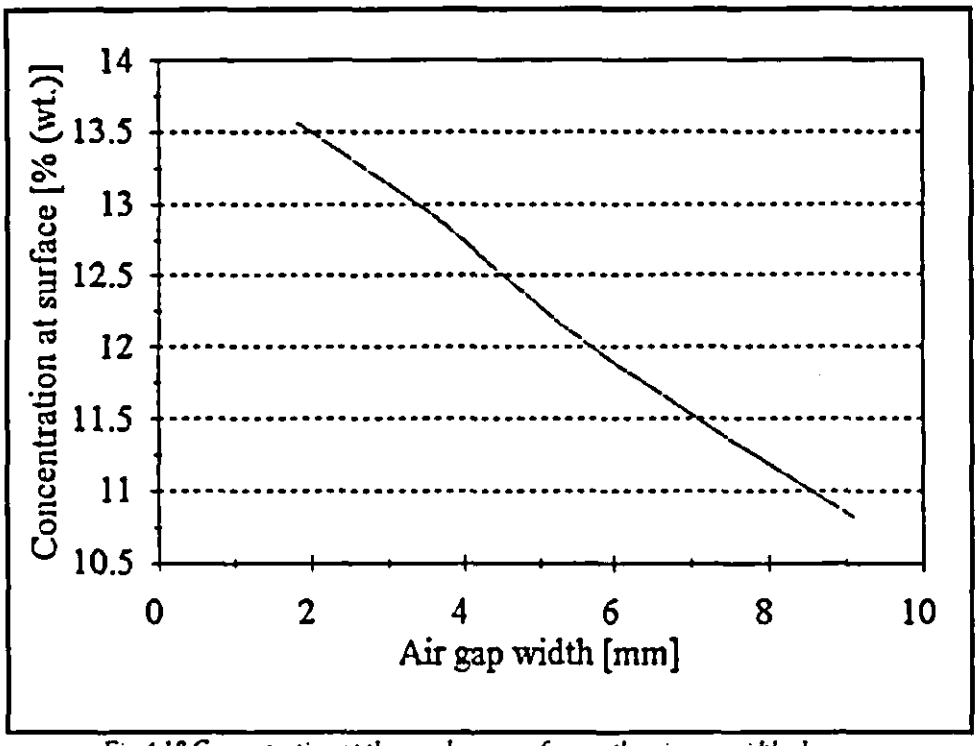

Fig 4.18 Concentration at the membrane surface as the air gap width changes.
(T_b = 331 K, T_c = 291, l_1 = 24 μm, c_b = 3 % (wt.), u_b = 0.03 m/s, u_c = 0.00226 m/s)

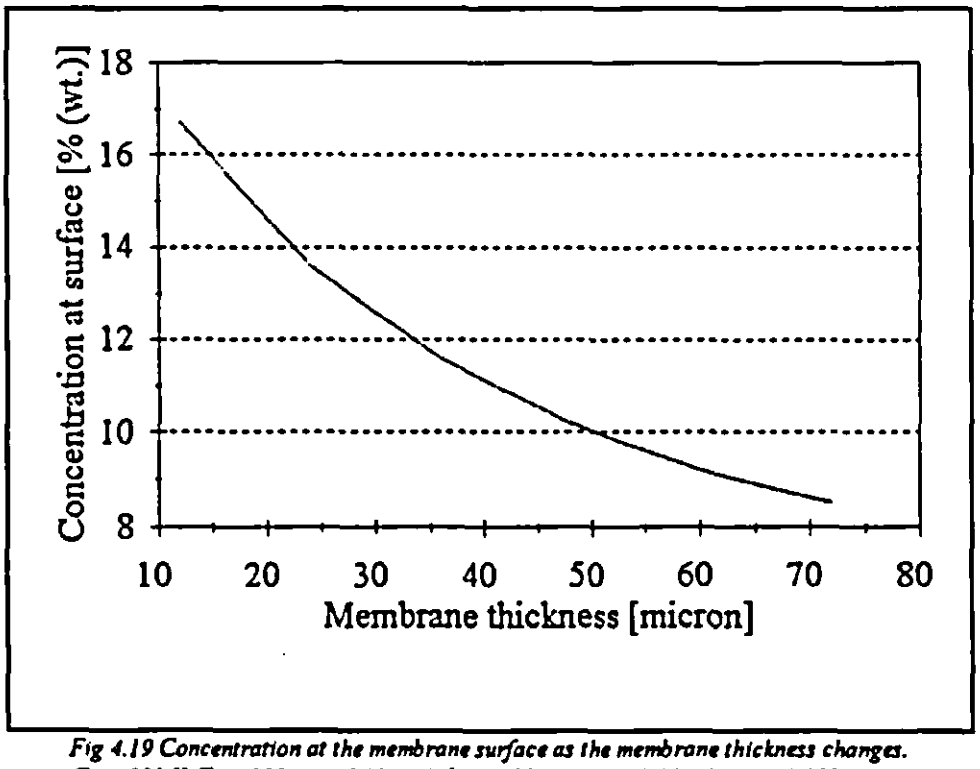

Fig 4.19 Concentration at the membrane surface as the membrane thickness changes.
(T_b = 331 K, T_c = 291, c_b = 3 % (wt.), l_2 = 1.83 mm, u_b = 0.03 m/s, u_c = 0.00226 m/s)

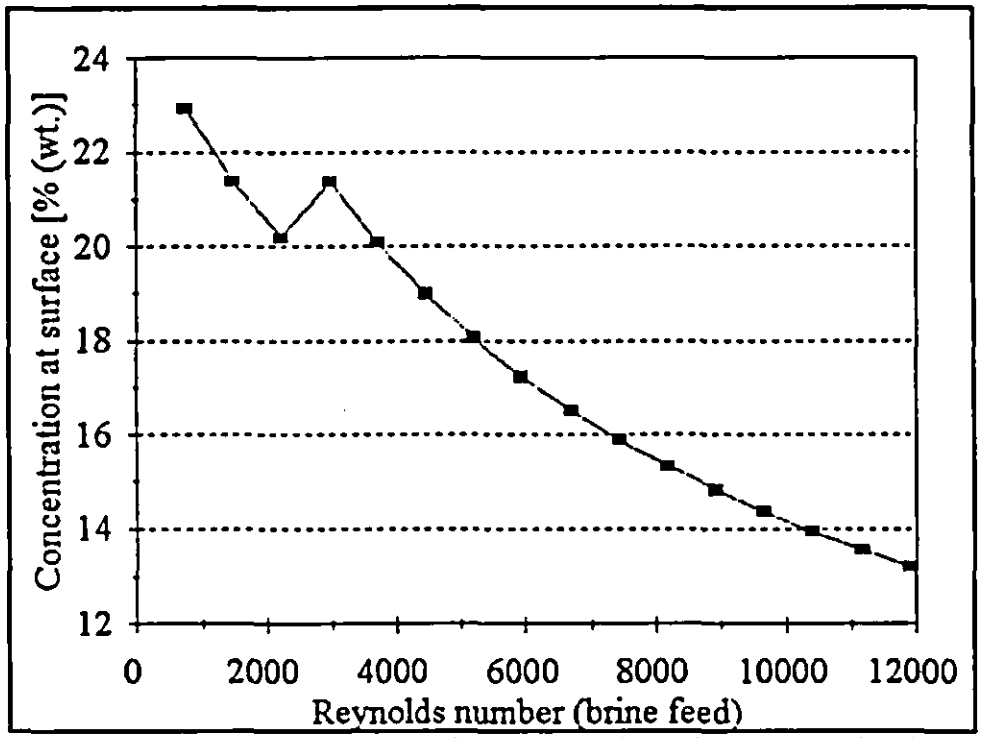

Fig. 4.20 Concentration at the membrane surface as the Reynolds number of the brine feed changes. (T_b = 331 K, T_c = 291, c_b = 3 % (wt.), l_1 = 24 μm, l_2 = 1.83 mm, u_c = 0.00226 m/s)

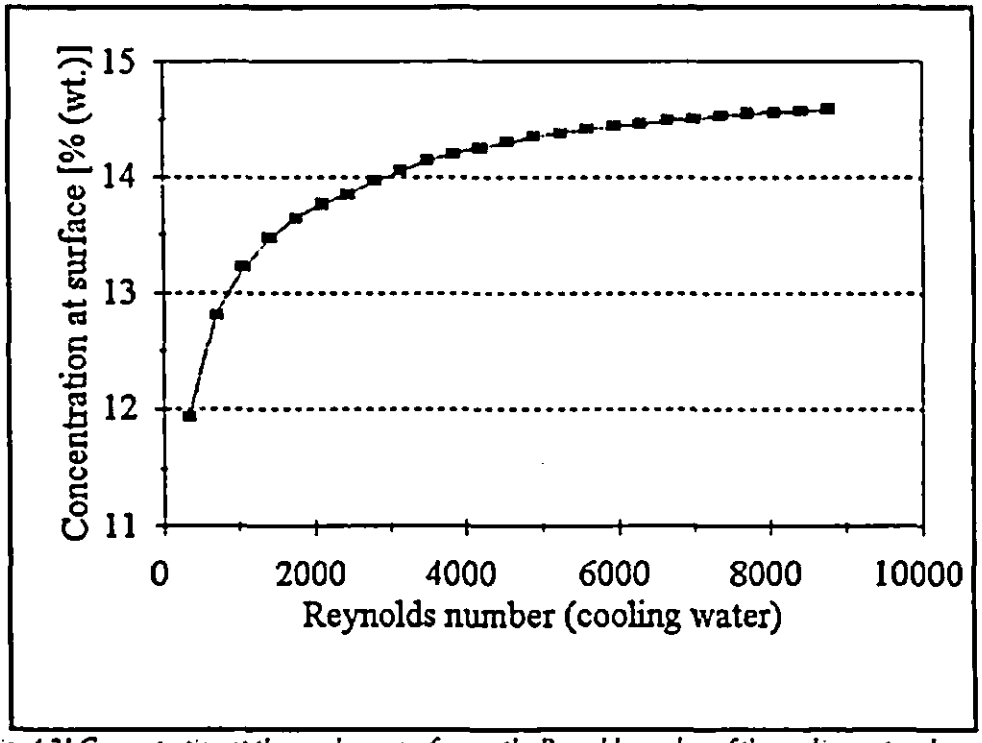

Fig. 4.21 Concentration at the membrane surface as the Reynolds number of the cooling water changes. (T_b = 331 K, T_c = 291, c_b = 3 % (wt.), l_1 = 24 μm, l_2 = 1.83 mm, u_b = 0.03 m/s)

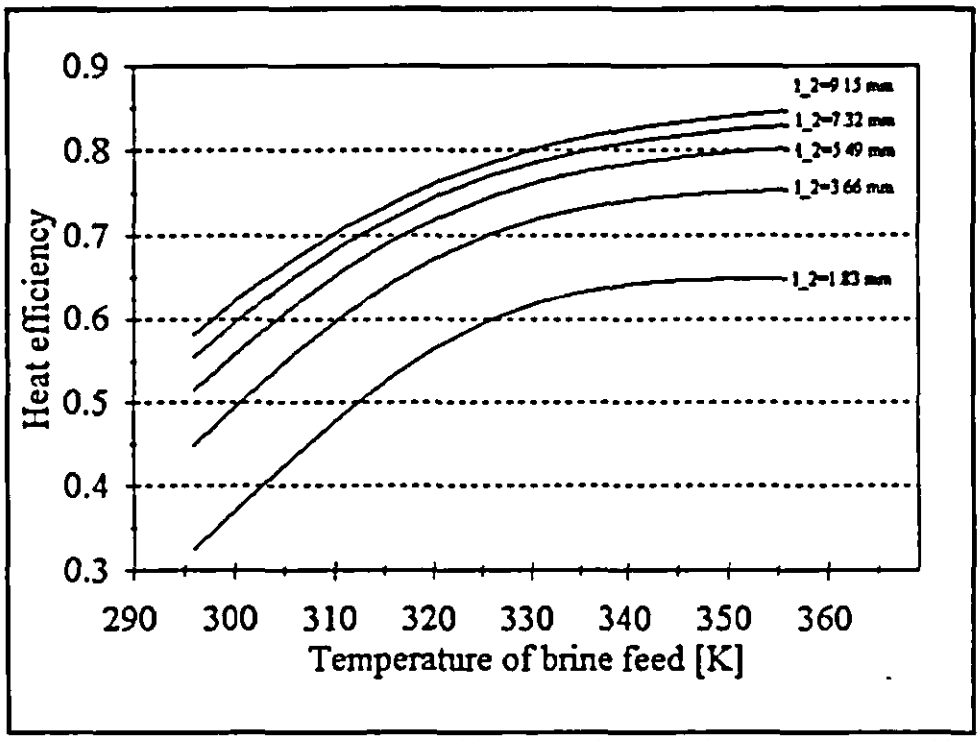

Fig 4.22 Heat efficiency as the temperature of the brine feed is changed at various air gap widths. (T_c = 291 K, c_b = 3 % (wt.), l_1 = 24 μm, u_b = 0.03 m/s, u_c = 0.00226 m/s)

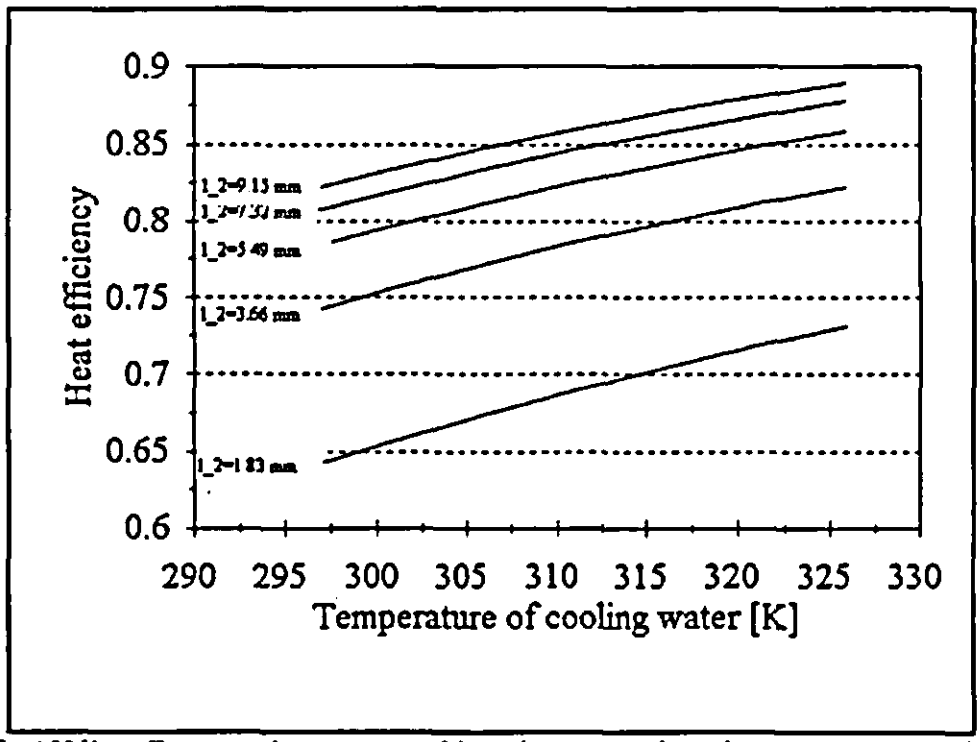

Fig 4.23 Heat efficiency as the temperature of the cooling water is changed at various air gap widths. (T_d = 331 K, c_b = 3 % (wt.), l_1 = 24 μm, u_b = 0.03 m/s, u_c = 0.00226 m/s)

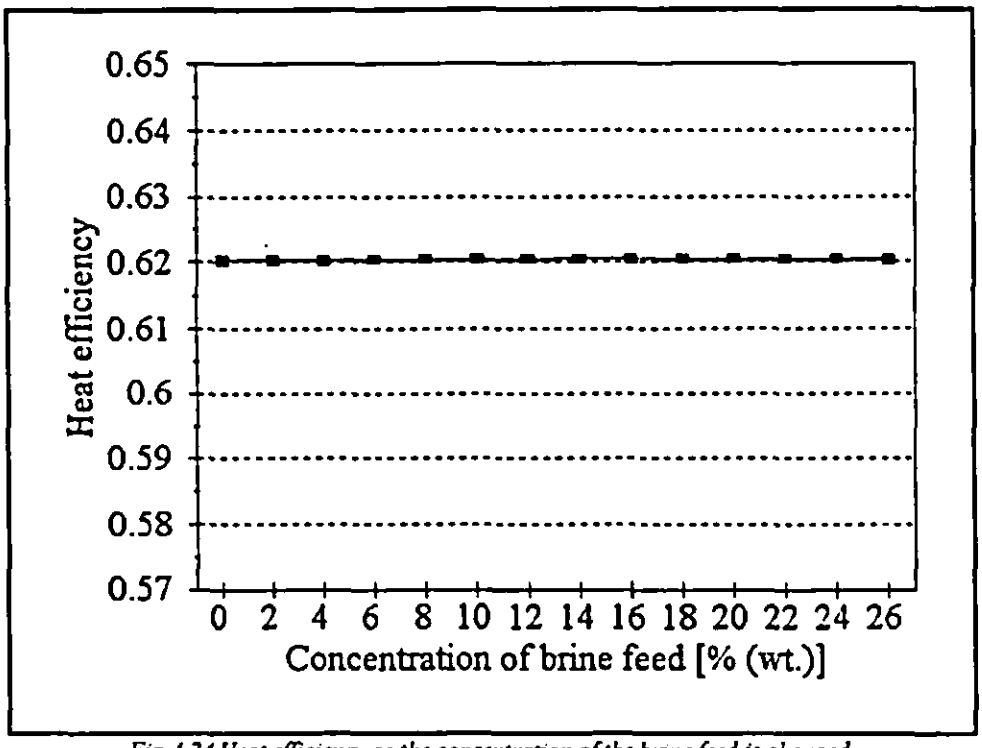

Fig 4.24 Heat efficiency as the concentration of the brine feed is changed.
(T_b = 331 K, Tc = 291 K, l_1 = 24 μm, l_2 = 1.83 mm, u_b = 0.03 m/s, u_c = 0.00226 m/s)

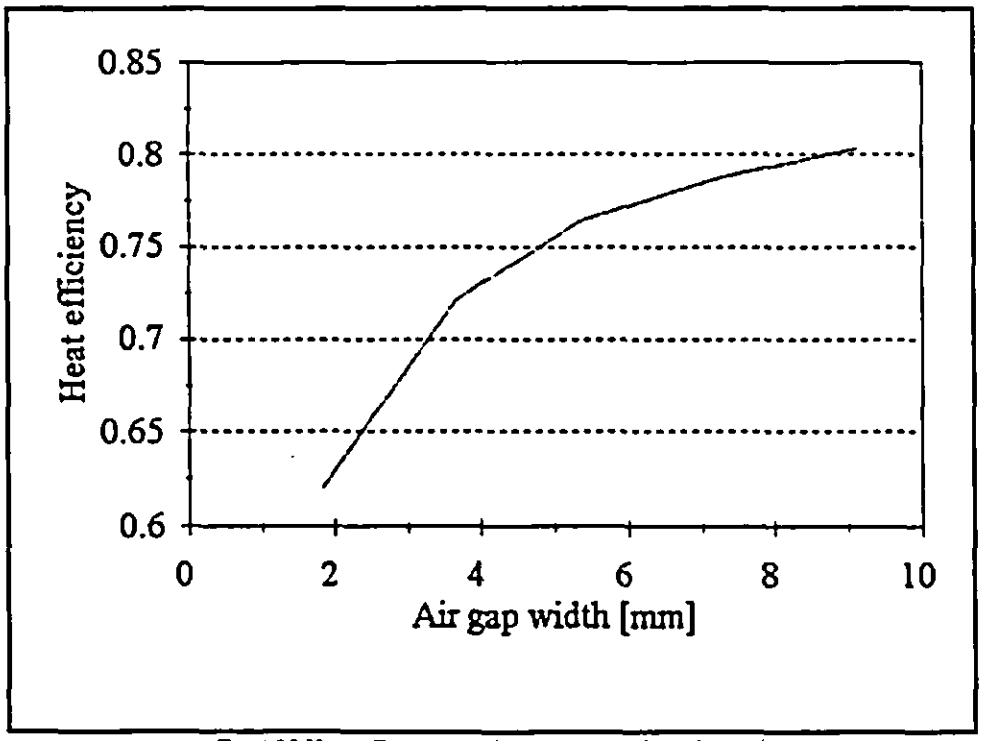

Fig 4.25 Heat efficiency as the air gap width is changed.
(T_b = 331 K, T_c = 291 K, l_1 = 24 μm, c_b = 3 % (wt.), u_b = 0.03 m/s, u_c = 0.00226 m/s)

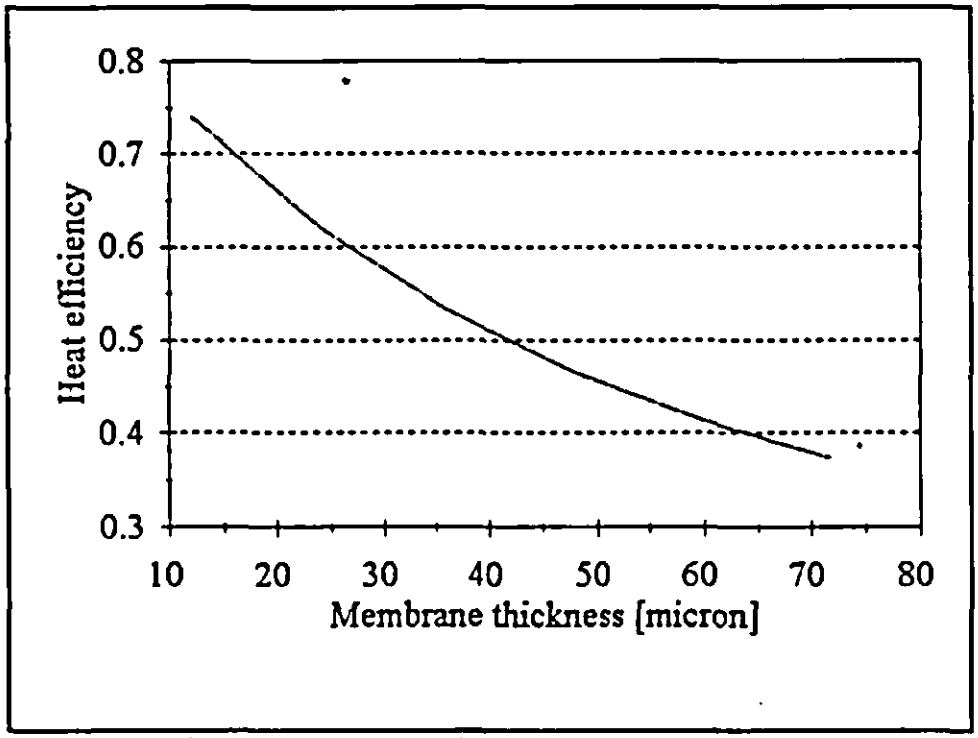

Fig 4.26 Heat efficiency as the membrane thickness is changed.
(T_b = 331 K, T_c = 291 K, c_b = 3 % (wt.), l_2 = 1.83 mm, u_b = 0.03 m/s, u_c = 0.00226 m/s)

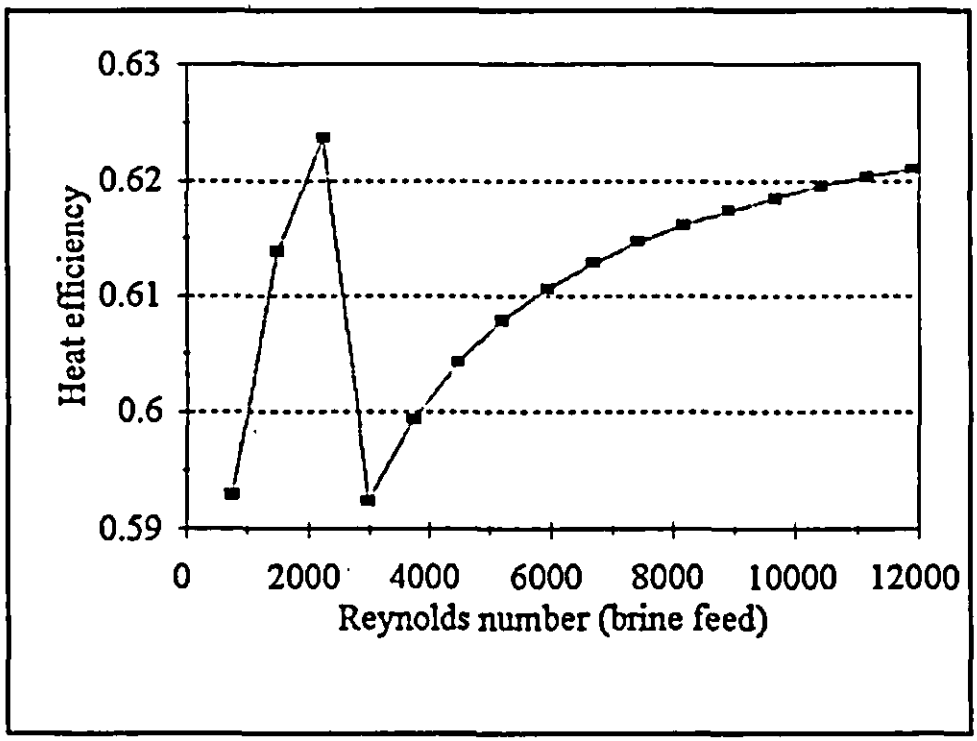

Fig 4.27 Heat efficiency as the Reynolds number of the brine feed is changed.
(T_b = 331 K, T_c = 291 K, l_1 = 24 μm, c_b = 3 % (wt.), l_2 = 1.83 mm, u_c = 0.00226 m/s)

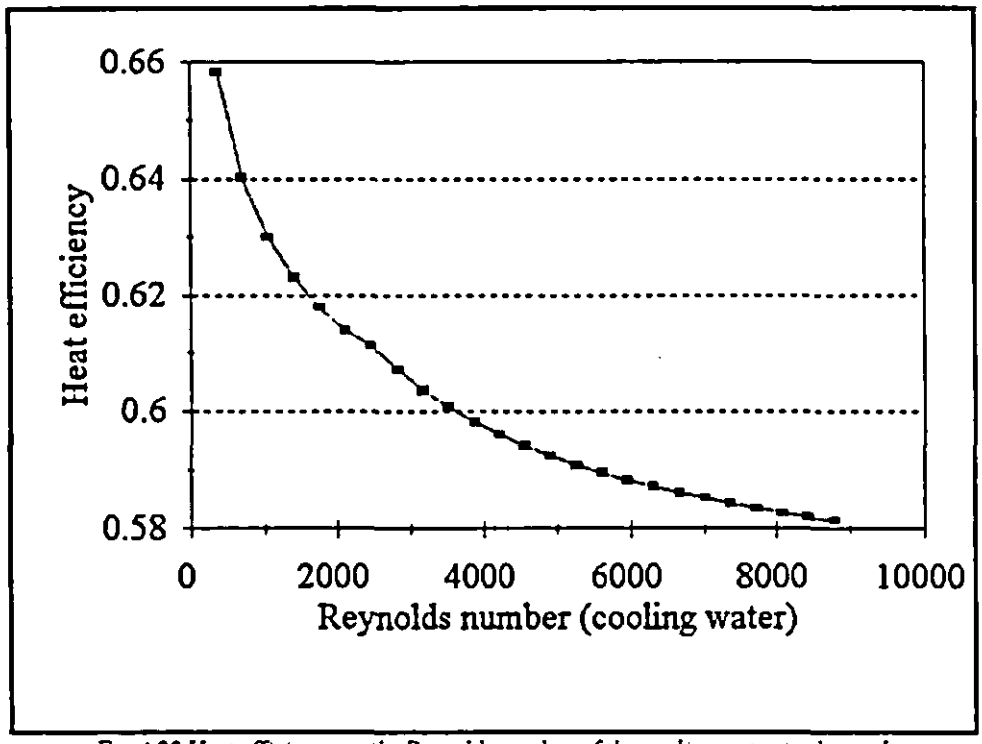

Fig 4.28 Heat efficiency as the Reynolds number of the cooling water is changed.
(T_b = 331 K, T_c = 291 K, l_1 = 24 μm, c_b = 3 % (wt.), l_2 = 1.83 mm, u_b = 0.03 m/s)

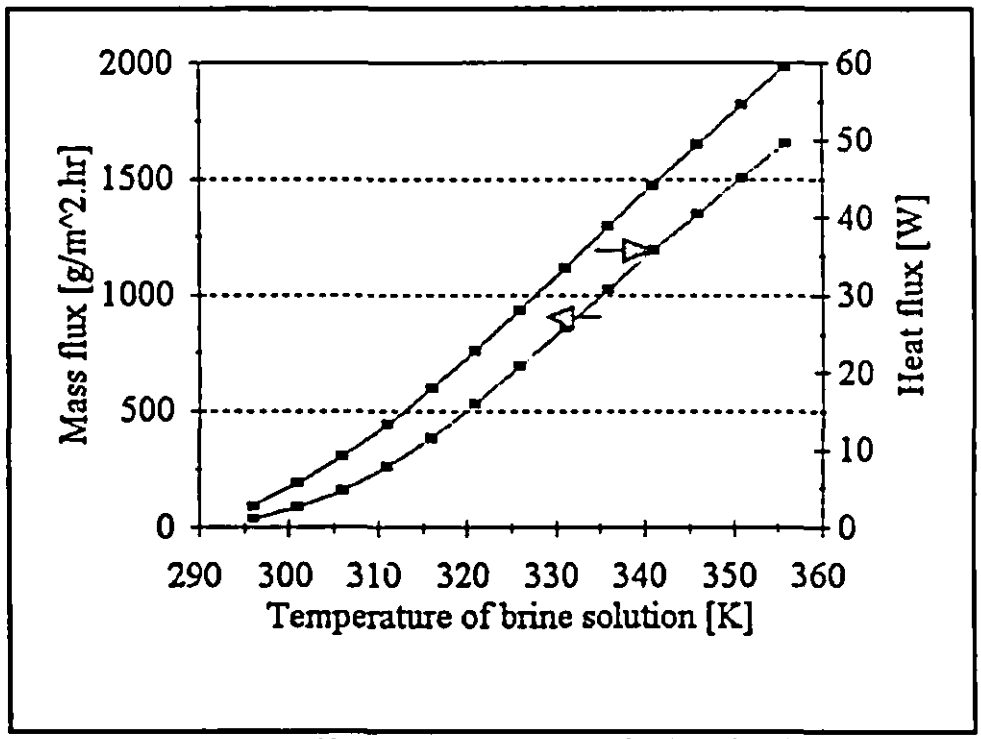

Fig. 4.29 Mass and heat flux as the temperature of the brine feed changes.
(T_c = 291 K, c_b = 3 % (wt.), l_1 = 24 μm, l_2 = 1.83 mm, u_b = 0.03 m/s, u_c = 0.00226 m/s)

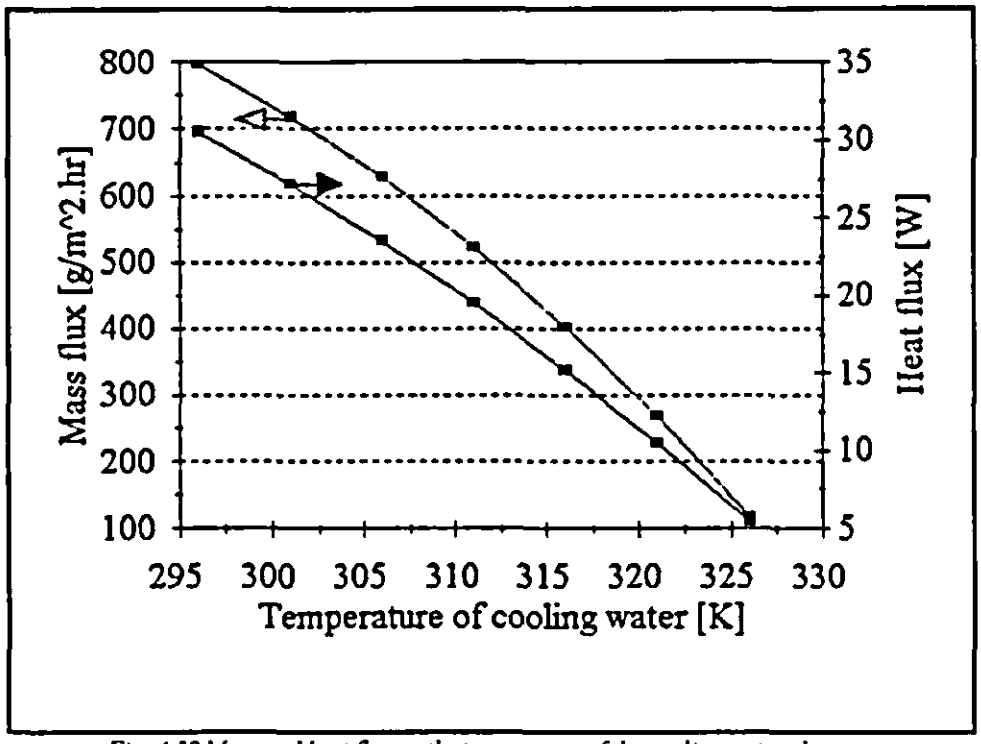

Fig. 4.30 Mass and heat flux as the temperature of the cooling water changes.
(T_b = 331 K, c_b = 3 % (wt.), l_1 = 24 μm, l_2 = 1.83 mm, u_b = 0.03 m/s, u_c = 0.00226 m/s)

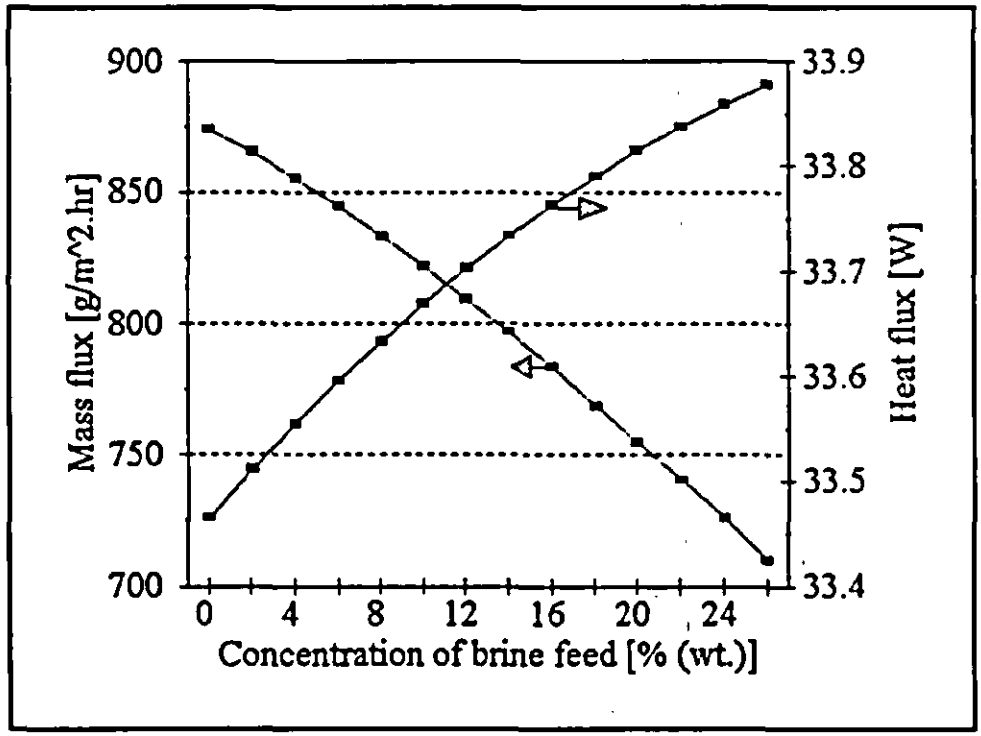

Fig. 4.31 Mass and heat flux as the concentration of the feed changes.
(T_b = 331K, T_c = 291 K, c_b = 3 % (wt.), l_1 = 24 μm, l_2 = 1.83 mm, u_b = 0.03 m/s, u_c = 0.00226 m/s)

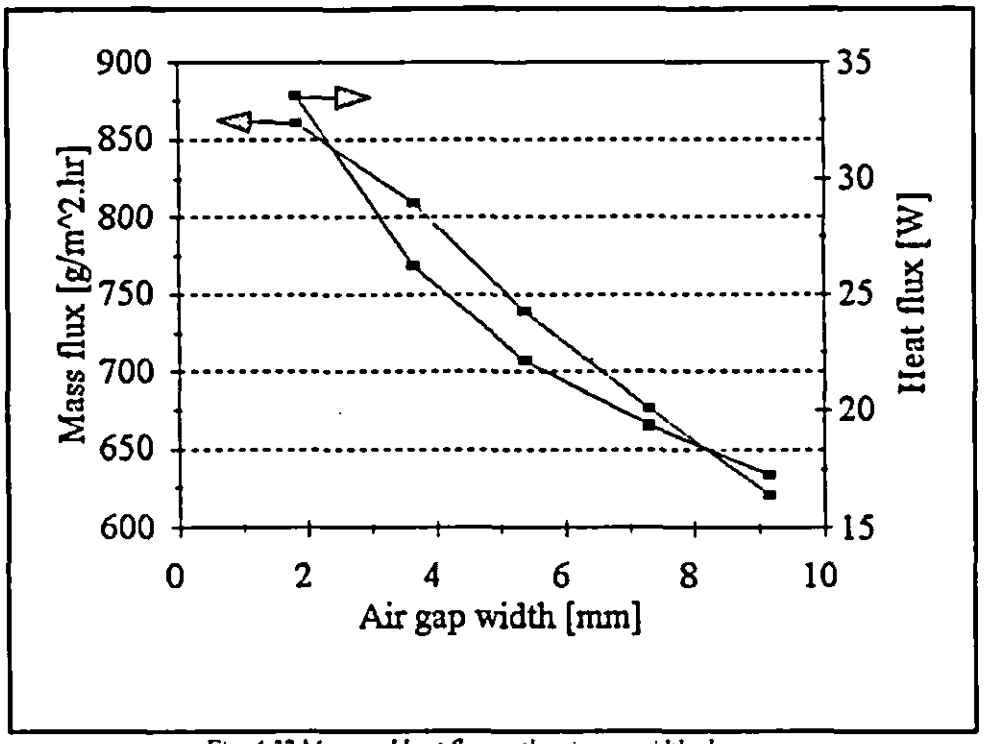

Fig. 4.32 Mass and heat flux as the air gap width changes.
(T_b = 331 K, T_c = 291 K, l_1 = 24 μm, c_b = 3 % (wt.), u_b = 0.03 m/s, u_c = 0.00226 m/s)

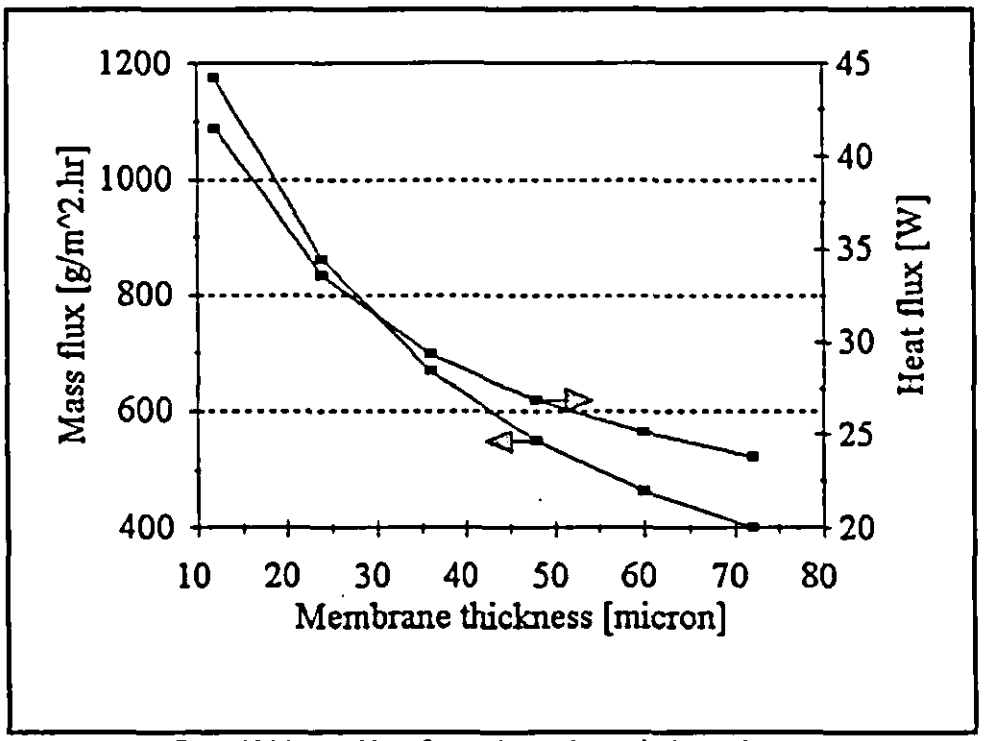

Fig. 4.33 Mass and heat flux as the membrane thickness changes.
(T_b = 331 K, T_c = 291 K, c_b = 3 % (wt.), l_2 = 1.83 mm, u_b = 0.03 m/s, u_c = 0.00226 m/s)

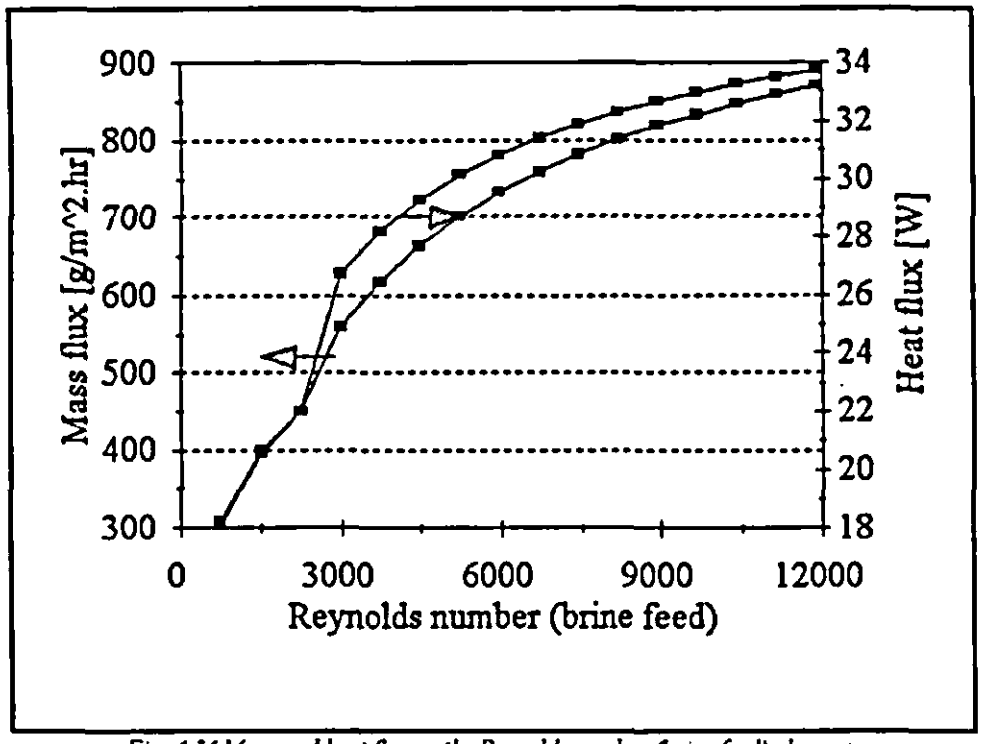

Fig. 4.34 Mass and heat flux as the Reynolds number (brine feed) changes.
(T_b = 331 K, T_c = 291 K, l_1 = 24 μm, c_b = 3 % (wt.), l_2 = 1.83 mm, u_c = 0.00226 m/s)

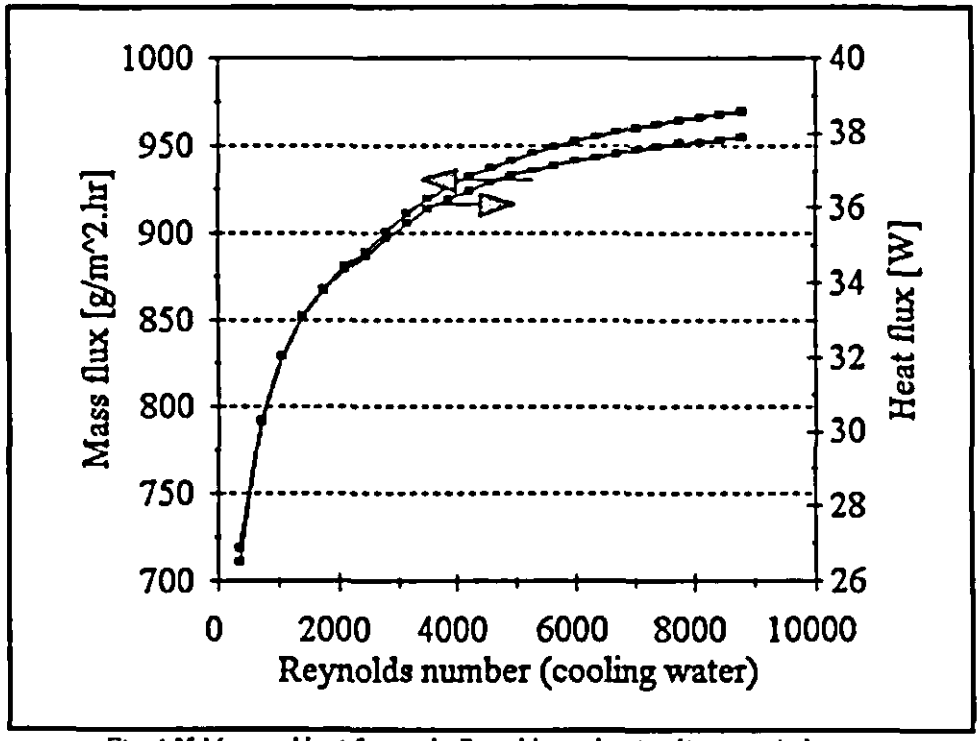

Fig. 4.35 Mass and heat flux as the Reynolds number (cooling water) changes.
(T_b = 331 K, T_c = 291 K, l_1 = 24 micron, c_b = 3 % (wt.), l_2 = 1.83 mm, u_b = 0.03 m/s)

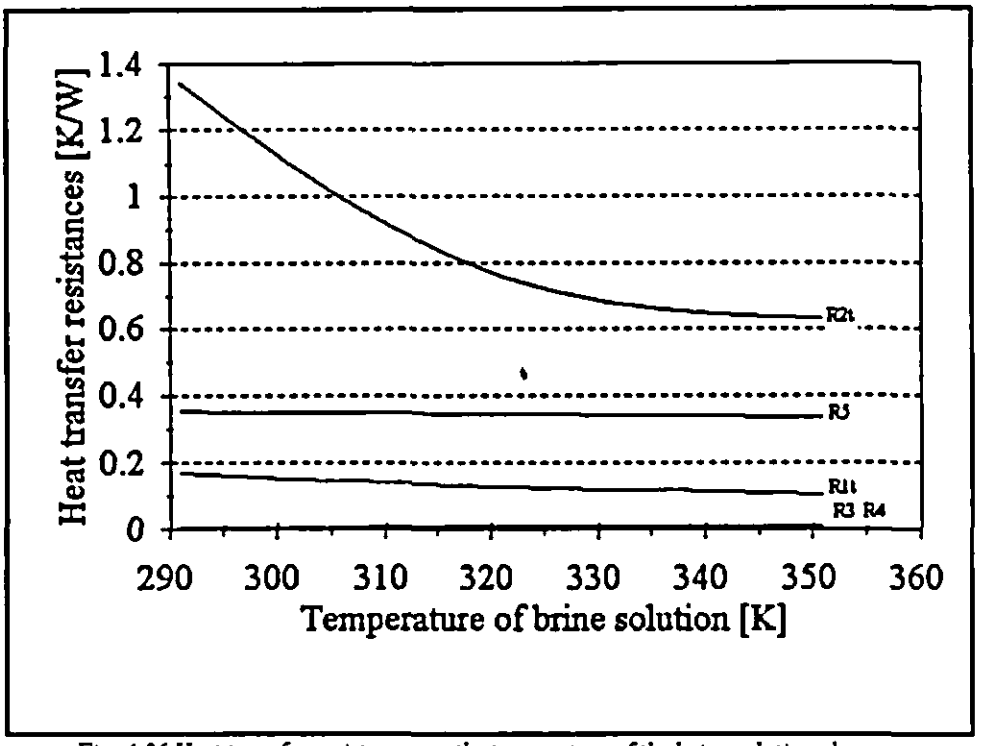

Fig. 4.36 Heat transfer resistances as the temperature of the brine solution changes.
(T_c = 291 K, c_b = 3 % (wt.), l_1 = 24 μm, l_2 = 1.83 mm, u_b = 0.03 m/s, u_c = 0.00226 m/s)

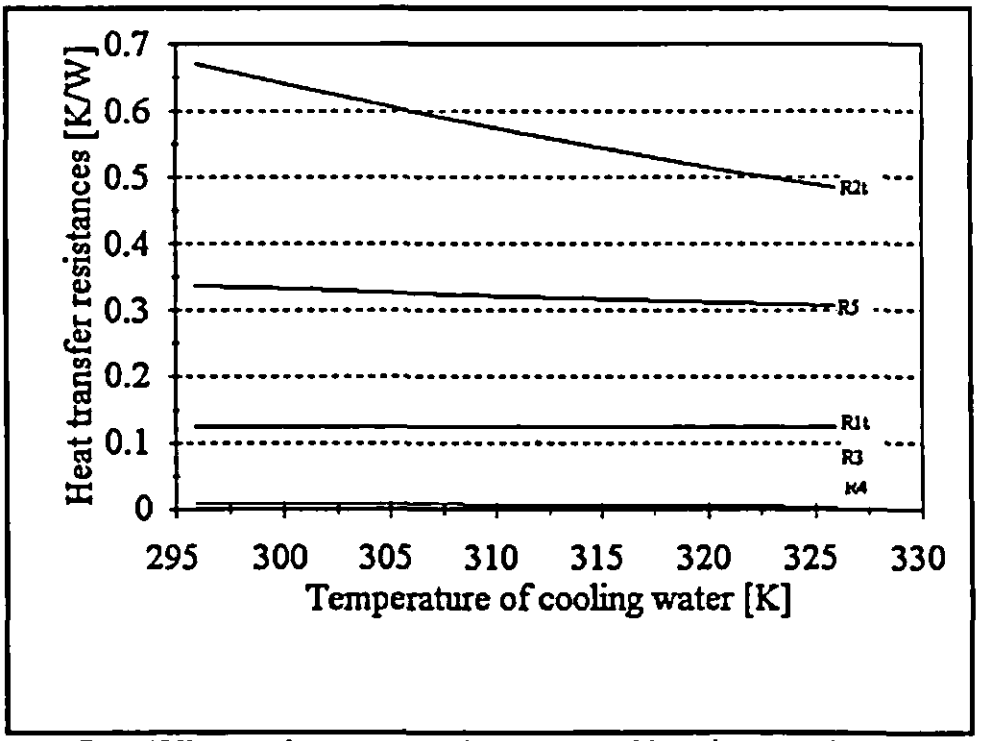

Fig. 4.37 Heat transfer resistances as the temperature of the cooling water changes.
(T_b = 331 K, c_b = 3 % (wt.), l_1 = 24 μm, l_2 = 1.83 mm, u_b = 0.03 m/s, u_c = 0.00226 m/s)

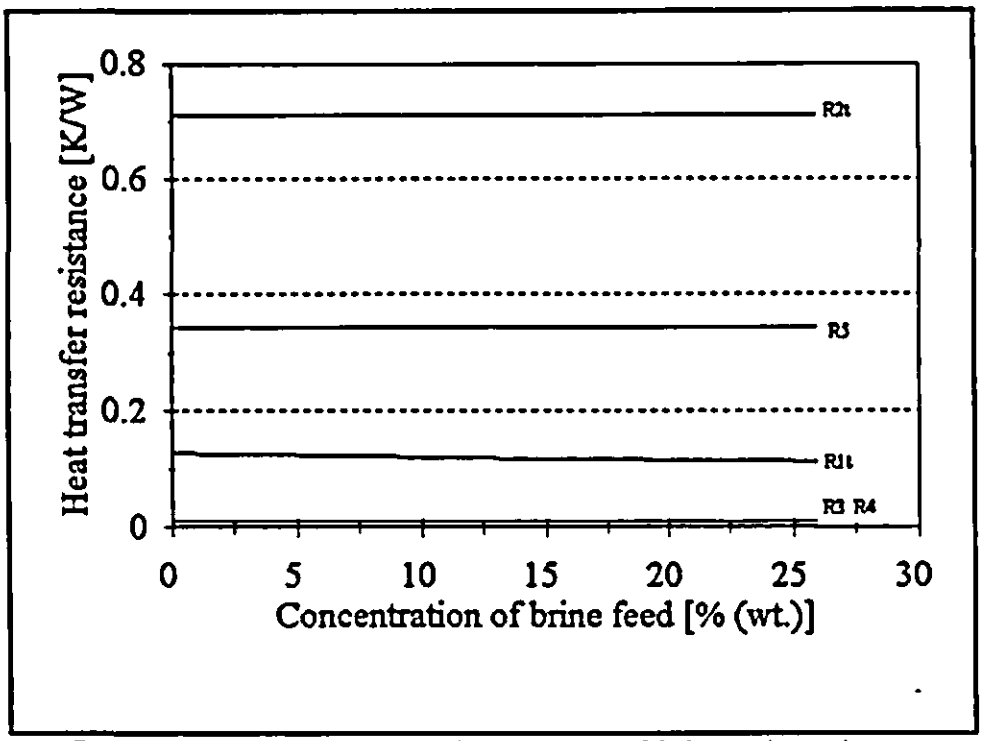

Fig. 4.38 Heat transfer resistances as the concentration of the brine solution changes.
(T_b = 331 K, T_c = 291 K, c_b = 3 % (wt.), l_1 = 24 μm, l_2 = 1.83 mm, u_b = 0.03 m/s, u_c = 0.00226 m/s)

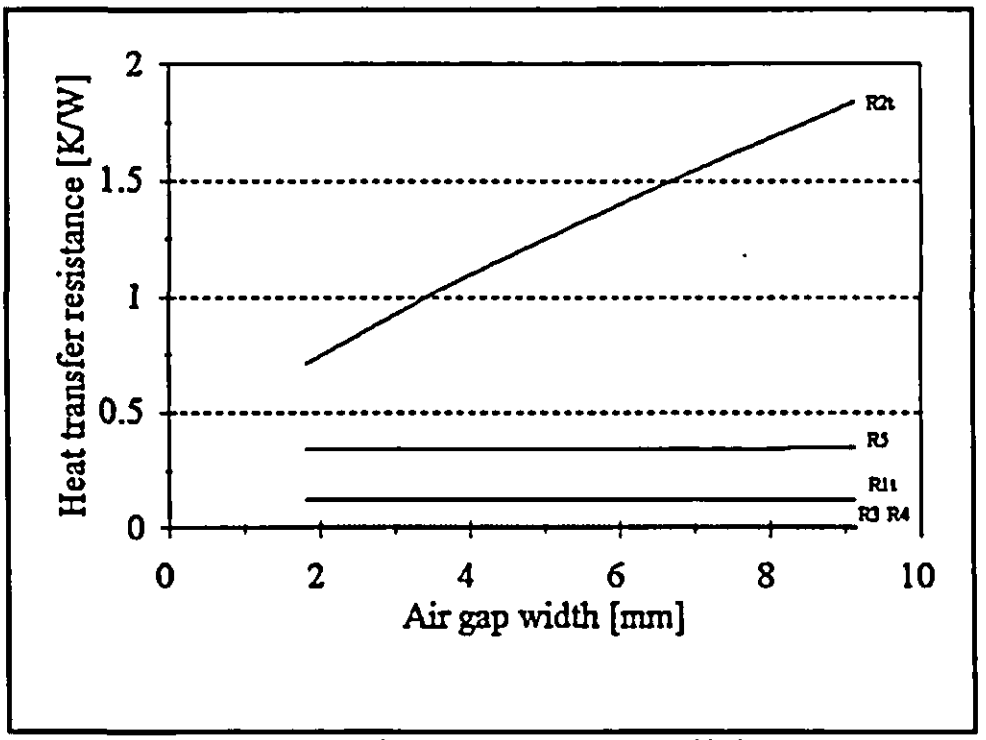

Fig. 4.39 Heat transfer resistances as the air gap width changes.
(T_b = 331 K, T_c = 291 K, c_b = 3 % (wt.), l_1 = 24 μm, u_b = 0.03 m/s, u_c = 0.00226 m/s)

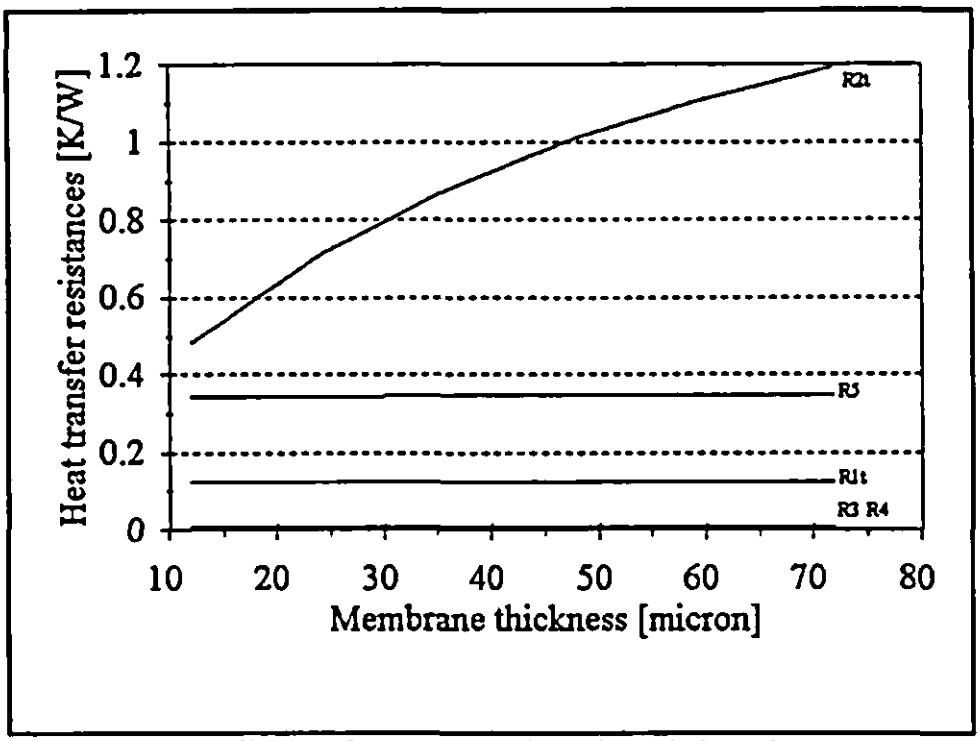

Fig. 4.40 Heat transfer resistances as the membrane thickness changes.
(T_b = 331 K, T_c = 291 K, c_b = 3 % (wt.), l_2 = 1.83 mm, u_b = 0.03 m/s, u_c = 0.00226 m/s)

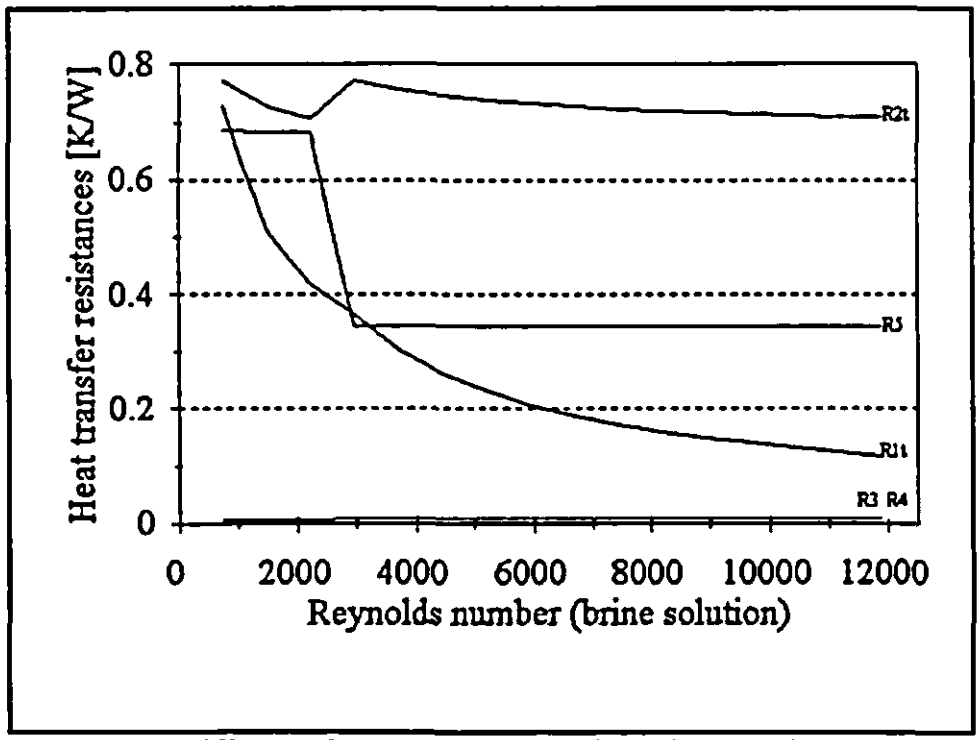

Fig. 4.41 Heat transfer resistances as the Reynolds number(brine) changes.
(T_b = 331 K, T_c = 291 K, c_b = 3 % (wt.), l_1 = 24 μm, l_2 = 1.83 mm, u_c = 0.00226 m/s)

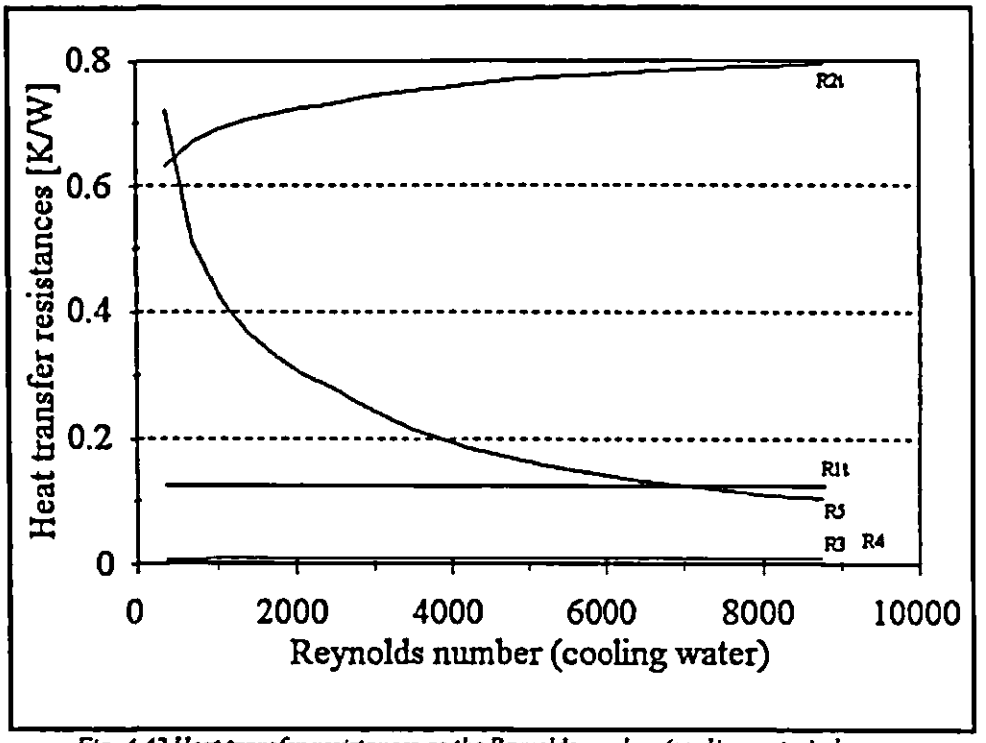

Fig. 4.42 Heat transfer resistances as the Reynolds number (cooling water) changes. (T_b = 331 K, T_e = 291 K, c_b = 3 % (wt.), l_1 = 24 μm, l_2 = 1.83 mm, u_b = 0.03 m/s)

CHAPTER 5

DISCUSSION OF RESULTS

In this chapter the results obtained from the experimental procedures will be discussed. The fundamental model and the empirical model will also be evaluated.

The results of the experiments and the figures used for the subsequent discussion are presented in figs. 5.1-5.27.

5.1 Temperature Variation Experiments

There is an exponential relationship between the mass flux and the temperature of the brine feed (fig. 5.5-5.7). The driving force in membrane distillation is the vapour pressure difference across the diffusion path and since there is an exponential relationship between vapour pressure and temperature of a brine solution (Fabuss, 1980), a approximately linear relation should exist between the vapour pressure and the mass flux (fig. 5.4). This means that the mass flux (N) is proportional to the vapour pressure difference (ΔP)

$$N = K\Delta P \qquad (5.1)$$

where K is a proportionality coefficient which expresses the permeation rate. According to the mass transfer theory in membrane distillation, the magnitude of K is a function of the physical nature of the permeating species, the turbulence conditions of the feed flow, the operating temperature and pressure of the feed side of the membrane, the membrane structure properties and the width of the air gap. The gradient of fig. 5.4 is the combined mass transfer resistances of the membrane and the air gap, since the driving force is the vapour pressure difference across the diffusion path. Figure 5.4 shows that the relationship is not perfectly linear, since the proportionality coefficient is not constant for a variation in the temperature of the brine feed. Table A22 and A23 elucidate this

phenomenon, since the mass transfer resistance induced by the membrane and air gap is temperature dependent.

The exponential trend is still dominant for the mass flux as the temperature of the brine solution changes, even though feeds at various concentrations are used (fig. 5.5-5.7).

For a variation in the cooling water temperature (fig. 5.8), the mass flux follows the same trend as for a variation in the brine temperature, that is, an exponential increase, but the magnitude of the mass flux does not change as rapidly when the temperature of the cooling water is varied as when the temperature of the brine solution is changed by the same increment. Once again, the change in the mass flux can be attributed to the vapour pressure difference across the diffusion path. A 5°C increase in an aqueous solution at 50°C produces a larger increase in vapour pressure than a 5°C increase at 20°C. The rate of evaporation increases if the temperature of the brine feed is increased, even if the temperature difference between the brine solution and the cooling water is constant (fig. 5.9).

5.2 Feed Concentration Experiments

The mass flux decreases with an increase in feed concentration (fig. 5.14-5.19) and, as mentioned previously, this decrease is caused by concentration polarisation. Banat *et al.* (1994) suggested that this reduction in mass flux can also be attributed partially to the salt effects (precipitation on the membrane), and a variation of the concentration of the feed also influences the temperature polarisation coefficient (TPC) (fig. 4.10). Because of the concentration gradient across the boundary layer, the concentration of the Na^+ and the Cl^- in the bulk is lower than that at the membrane surface (fig. 4.17). Since the vapour pressure of the aqueous brine solution depends on the temperature as well as on the concentration of the solution (Fabuss, 1980), the vapour pressure at the membrane surface is lower than the maximum vapour pressure and there is a loss in the driving force if the concentration of the feed rises. The mass flux decay at higher concentrations can also

possibly be attributed to the increase in solution viscosity. The rise in the solution viscosity can also affect the linear velocity of the brine, which can decrease the mass flux.

The concentration at the membrane surface depends mainly on the concentration of the feed (fig. 4.17), the temperature of the feed (fig. 4.15) and on the hydrodynamic conditions of the feed (fig. 4.20). Ideally, the concentration of the salt at the membrane surface should be as close as possible to the concentration of the bulk so that the driving force will be maximised for a higher permeation rate.

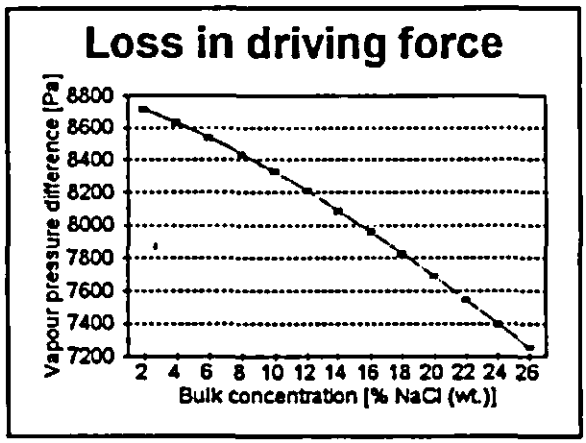

Fig 5.1 Loss in driving force by concentration polarisation (T_b = 331 K, T_c = 291 K, l_f = 1.83 mm, u_b = 0.03 m/s, u_c = 0.0026 m/s).

If the salt content is increased from 2 % to 10 %, the vapour pressure difference across the diffusion path will decrease by 4.4 % and a change from 2 % to 20 % will lead to a loss of 11.8 % (fig. 5.1). The effect of concentration polarisation on the mass flux is not as significant as that of temperature polarisation (fig. 4.8-4.14). The trend for the change in mass flux as the concentration changes stays the same even at different air gap widths (fig. 5.15-5.19).

5.3 Experiments on the Diffusion Path

5.3.1 Air Gap Experiments

As mentioned previously, the air gap was introduced to membrane distillation to minimise the conduction heat losses. By enlarging the air gap width, the mass flux decreases (fig. 5.10-5.13), since the water vapour has to diffuse through a thicker layer of air, increasing the resistance against mass transfer (table A25). This is why sweeping gas membrane

distillation gives a higher flux than air gap membrane distillation, since the vapour is removed as soon as it leaves the membrane, so that it does not have to diffuse through a layer of air.

5.3.2 Membrane Thickness

The membrane used had a thickness of only 12 micron, and imperfections occurred because of membrane handling, which produced a product of poor quality. Unfortunately thicker membranes were unobtainable, so the membrane thickness was increased by doubling the membrane. This had the disadvantage that air pockets could be present between the membranes, which could affect the mass flux. The thicker membranes improved the permeate quality considerably (table 5.1), since it was difficult for impurities to pass through the membranes as the probability that two holes would be aligned was low.

l_1	Mass flux (Experimental) [$g.m^{-2}.h^{-1}$]	Mass flux (Fundamental) [$g.m^{-2}.h^{-1}$]	Permeate quality µS/cm
12 µm	826.7	821.5	12430
24 µm	620.8	625.8	30

Table 5.1 Effect of membrane width on the permeation flux and the product quality. (T_b = 325 K, T_c = 289 K, c = 3% (wt.), l_2 = 3.2 mm, u_b = 0.024 m/s, u_c = 0.0026 m/s).

According to the solution-diffusion theory, the flux is inversely proportional to the thickness of the membrane ($N \alpha 1/x$), so that it is expected that the flux will increase by the same factor as that by which the membrane thickness is reduced. This, however, is not the case, since the mass transfer resistance induced by the membrane is only part of the total resistance against mass transfer. The total mass transfer resistance consists of the mass transfer resistances induced by the membrane, air gap and the concentration boundary layer (see eqn. (4.23), (4.27) and (4.28)), so that by changing the membrane thickness the total resistance is affected, but it is not affected proportionally to the variation in the thickness of the membrane.

From the fundamental model it was found that the mass transfer resistance induced by the membrane had a local minimum at a brine temperature of approximately 320 K.

Furthermore it was observed that the mass transfer resistance induced by the membrane was larger than the resistance induced by the air gap (fig. 5.23).

From fig. 5.24 it is seen that the permeation of water through the membrane increased as the temperature of the water increased, as the water had a higher enthalpy, so that more heat was available for the evaporation process. The permeation rate is defined as the mass (g) of water that permeates a membrane of $1m^2$ in 1s. The permeability coefficient is defined as the mass (g) of water that permeates a membrane of 1 m^2 and width of 1 m in 1s and the pressure drop across the membrane is 1 Pa.

Time [s]	Mass/time [g/s]	Temperature of water [K]	Vapour pressure [Pa]	Permeability coefficients [$g.m.m^{-2}.s^{-1}.Pa^{-1}$]
2711	$1.39x10^{-4}$	307.5	5403	$8.12x10^{-10}$
181	$2.23x10^{-4}$	315	8119	$8.67x10^{-10}$
6059	$3.27x10^{-4}$	320	10521	$9.81x10^{-10}$
6500	$6.27x10^{-4}$	331	18020	$1.10x10^{-10}$
5714	$7.92x10^{-4}$	337	23756	$1.05x10^{-10}$

Table 5.2 Results for the permeation experiments on the membrane.

By using the software program *JANDEL SCIENTIFIC TABLECURVE* version 2.14, eqns. (4.25)-(4.26) could be derived from the results in table 5.2.

Because of the exponential relationship between vapour pressure and temperature, a local maximum was expected for the permeability coefficient (fig. 5.24). The behaviour of the permeability coefficient explained the trend of the membrane resistance, since the resistance was inversely proportional to the permeability coefficient, so that that the local maximum of the permeability coefficient caused the local minimum of the resistance.

5.4 Velocity Experiments

The boundary layer adjacent to the membrane leads to temperature and concentration gradients between the bulk liquid and the membrane surface so that heat and mass transfer occurs between these two regions. The heat and mass transfer coefficient is dependent on the Reynolds number, which depends on the linear velocity of the fluid. According to

Incropera *et al.* (1990), turbulent flow is advantageous as far as mass and heat transfer is concerned, since this enhances both of these transfer phenomena.

This trend of a rising mass flux with a higher flow rate was observed for both the brine feed and the cooling water (figs. 5.21-5.22).

According to Incropera *et al.* (1990), the heat transfer coefficient is dependent on the fluid properties (k, c_p, μ, ρ), the fluid velocity u, the length scale L and the surface geometry. The easiest way to increase the heat transfer coefficient to enhance heat transfer is to change the linear velocity of the feed (fig. 5.26) rather than try to change the fluid properties or the geometry of the module. This argument will be the same for the mass transfer because of the analogy between heat and mass transfer.

5.5 Model Evaluation

5.5.1 Fundamental Model

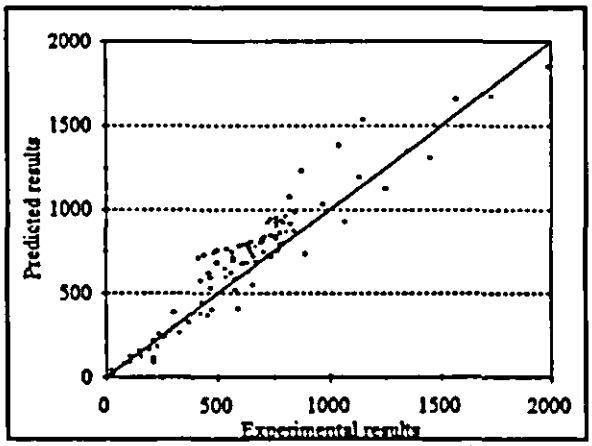

Fig 5.2 Comparison between the experimental and predicted results (fundamental model) R^2 = 0.9156.

There is a good relationship between the experimental results and those predicted by the fundamental model (fig. 5.2). This model had an overall correlation coefficient (R^2) of 0.9156.

When the temperature of the brine feed was changed at low feed concentrations, the predicted values were very close to the experimental results (fig. 5.5-5.6). The predicted values deviated as the concentration became larger (fig. 5.7, 5.15-5.19). As the concentration increased from 3 % (wt.) to 10 % (wt.), the correlation coefficient decreased from 0.9955 to 0.9315 (fig. 5.5-5.6).

The deviation became larger at higher concentrations and it was further aggravated by high temperatures (fig. 5.7). This deviation could possibly be attributed to the fact that the vapour pressure and density of the brine solution were extrapolated for concentrations above 26 % (wt.), since physical data were available only for a salt concentration below 26 % (wt.). There was also a lack of data for the thermal conductivity of a brine solution, so that the thermal conductivity of pure water was used instead.

Since concentration polarisation has already been accounted for in the fundamental model, the precipitation of salt crystals on the membrane surface can also lead to deviations from the predicted values. The deviation can also be observed in fig. 5.14 which gives data from a study of the relationship between the concentration of the brine solution and the mass flux at a fixed temperature. The deviation increased considerably at very high salt concentrations.

Figures 5.10-5.13 shows the relationship between the mass flux as the air gap width changed at different concentrations. As the air gap width increased at a fixed concentration the deviation of the experimental results from the fundamental model decreased. This could be attributed to the fact that the concentration at the membrane surface decreased with an increasing air gap width (fig. 4.18).

5.5.2 Empirical Model

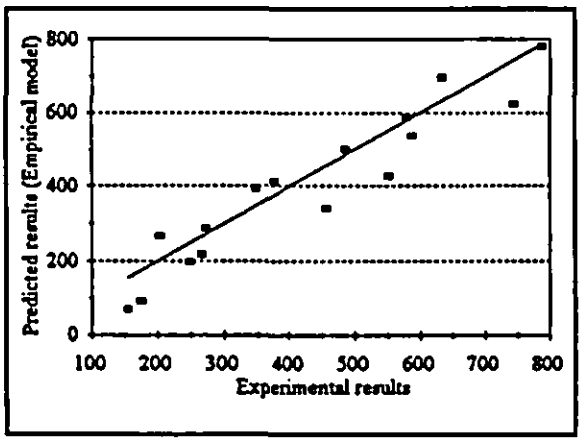

Fig 5.3 Comparison between the experimental and predicted results (empirical model) R^2 = 0.90258.

The empirical model was fitted to a set of data that was not accounted for in the linear regression in order to cross-validate the process. This resulted in a correlation coefficient (R^2) of 0.9026. A correlation coefficient (R^2) of 0.9702 was obtained for the regression on the experimental data. When fig. 5.5-5.7 is investigated, it is noted that the empirical

model is not inclined to deviate at high brine concentrations as the fundamental model does. As for the empirical model, a good correlation exists between the experimental and predicted values when a variety of cooling water temperatures are used (fig. 5.10). A better correlation exists between the experimental and predicted values for the empirical model than for the fundamental model when the air gap width is changed (fig. 5.10-5.13). For low brine concentrations, that is, below 8 % (wt.) NaCl, the empirical model predicts the experimental data well. At very high concentrations, this model tends to reach a plateau (fig. 5.14). The fact that the empirical model is not as inclined to deviate from experimental results at high brine concentrations as the fundamental model does, is further emphasised by fig. 5.14-5.19.

When the linear velocity of the feed is varied, a better correlation exists for the fundamental model than for the empirical model (fig. 5.21). Although the empirical model correlates the experimental data better than the fundamental model, the trend of the data obtained from the empirical model is different to that of the experimental data, whilst the fundamental model does not have such a good correlation, but the trend is similar to the experimental data (fig. 5.22).

5.6 Product Quality

Since only water vapour permeated the membrane, it was expected that the salt rejection would be 100%.

From fig. 5.25 and table A1-A9 in appendix A, it appears as if there is no proportional change between the feed concentration and the concentration of the product. There are fluctuations in the product quality, and the passage of salt through the membrane could be attributed to imperfections in the membrane (table A1-A9). The salt rejection varied from 99.69 % to 99.94 %.

5.7 Time Dependency of the Flux

Although steady state conditions set in quickly, fluctuations were still present at first, but as time passed these fluctuations became smaller (fig. 5.27). The magnitude of the mass flux did not change with time, so that for short periods of time no fouling occurred. Since a dense membrane was used, ideally no salt should have passed through the membrane. The only fouling that could have occurred was that precipitated on the membrane surface.

5.8 Effect of Other Salts on the Mass Flux

Although there are considerable differences in the salt concentration of sea water from different sources, the relative abundance of major components is about the same everywhere. According to Fabuss (1980), the two main constituents are 78 % NaCl and 10.5 % $MgCl_2$, so that these two salts total 88.5 % of the entire salt content.

	Mass flux $[g.m^{-2}.h^{-1}]$	
Species	$T_{b,low}$	$T_{b,high}$
$H_2O_{Distilled}$	276.6	862.5
NaCl	262.5	768.8
$MgCl_2.6H_2O$	267.2	839
Sea water	239.1	675

Table 5.3 Effect of different salts on the mass flux ($T_{b,high}$ = 325 K, $T_{b,low}$ = 305 K, T_c = 289 K, l_1 = 24 μm, l_2 = 1.6 mm, c = 3 % (wt.), u_b = 0.03 m/s, u_c = 0.0026 m/s).

From the theory of membrane distillation (see chapter 2) it is known that the driving force in membrane distillation is the vapour pressure difference across the diffusion path and further it is also known that the vapour pressure of an aqueous solution differs for different dissolved species and concentrations. The driving force and consequently the mass flux is the highest for pure water since there are no dissolved species present to lower the vapour pressure. From table 5.3, it is observed that the mass flux of a 3 % (wt.) $MgCl_2.6H_2O$ and NaCl is very much the same as that as that of sea water. This can be attributed to the fact that the physical properatires of both these solutions are similar to that of sea water (Fabuss, 1980).

5.9 Solar Radiation as Energy Source for Membrane Distillation

According to Löf (1966), a daily average of 17 MJ/m^2 solar radiation is received on the ground in the United States of America. Most of the inhabited parts of the world experience average daily radiation of up to 28 MJ/m^2.

Theoretically, solar energy can be used for any process which requires heat or motive power. Solar energy may be used to generate heat or power which can then be used for operating any desalination process, or it may be employed directly for distillation of saline water in equipment which serves both as a solar energy absorber and as a distiller.

Since the air gap membrane distillation unit has to be used outdoors, solar radiation will be used as an energy source. Because of the high levels of radiation in South Africa, it was found that for a typical summers day in South Africa water could be heated to a temperature of 52 °C (Table 5.4).

Time of day	Atmospheric Temperature [K]	Water temperature [K]
8:40	299	302
9:30	302	310
10:30	306	317
11:30	306	325
12:30	306	325
13:30	306	325
14:40	306	325
15:30	305	325
16:30	305	325

Table 5.4 Radiation of sunlight on water in a black container.

5.10 Distillation Units

The distillation units had the disadvantage of uncontrollable process variables. If a light source was used to heat the brine solution, it was very difficult to regulate the temperature of the brine solution and the radiation from the sun was totally unreliable to use for experimental purposes. It was furthermore also very difficult to regulate the temperature

of the cooling water as well as the linear velocities of the brine solution and the cooling water.

Brine temperature [K]	Experimental mass flux [$g.m^{-2}.h^{-1}$]
318	272
323	312
328	348

Table 5.5 Results from distillation unit.

Since the temperature of the condensing surface could not be measured, these results could not be compared with the predicted results. The experiments performed on the distillation unit were batch experiments, while the results obtained from the alternative set-up was that of continuous experiments. Due to the configuration of the alternative set-up, it was impossible to obtain results for batch experiments. The disadvantage of a batch type configuration is that the salt tends to precipitate on the membrane, leading to a decreasing mass flux. To prevent this phenomenon in the distillation units, the brine solution can be agitated regularly.

5.11 Summary

In this chapter, the results obtained from the experimental procedures were discussed. It was discovered that an exponential relationship exists between the mass flux and the temperature of the brine feed. The effect on the magnitude of the mass flux is smaller when the temperature of the cooling water is decreased as when the temperature of the brine solution increases. When the concentration of the feed and the air gap width is increased, there is a decrease in mass flux. An increase in mass flux was noted when the linear velocity of the cooling water and the brine solution was increased.

The fundamental model was inclined to deviate from the experimental results, especially at high concentrations, which was further aggravated by high temperatures. These deviations can possibly be attributed to the fact that the permeability coefficient was assumed to be concentration independent, and the vapour pressure that was extrapolated for salt concentrations above 26 % (wt.).

By using solar radiation as energy source, it was discovered that water can reach temperatures of as high as 52° C on a typical summers day in South Africa. The salt rejection of this process varied between 99.69 %-99.94 % and for a continuous system no fouling occurred over short periods of time.

In the next chapter, the conclusions and recommendations for this project will be made, as well as future developments.

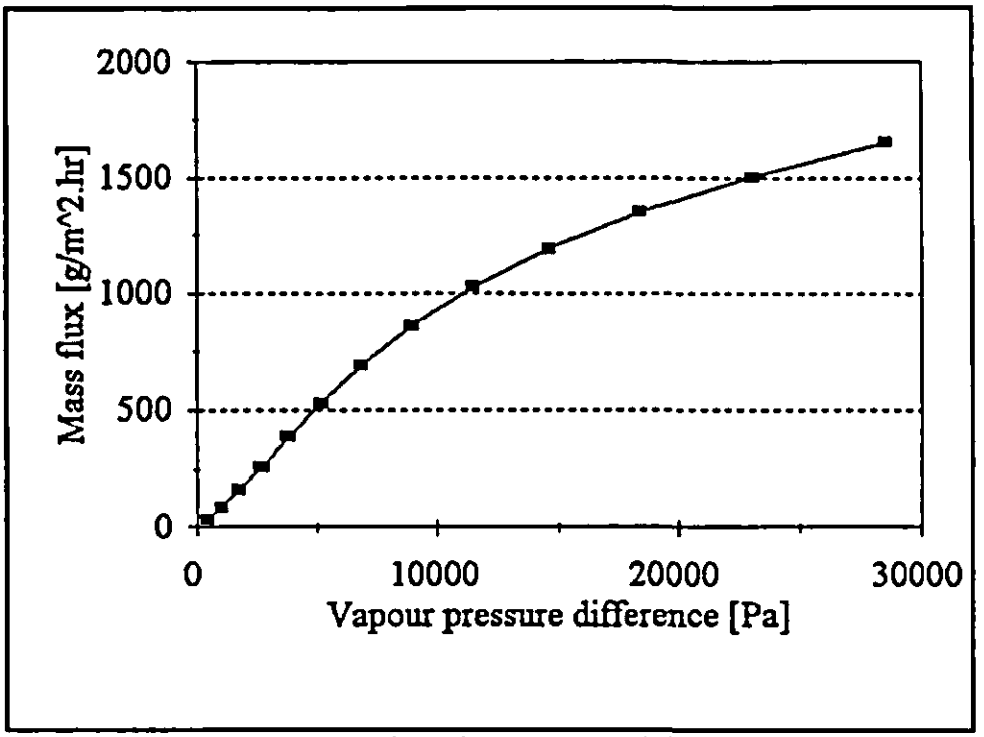

Fig. 5.4 Relationship between the mass flux and vapour pressure difference across the diffusion path.
(T_e = 291 K, c_b = 3 % (wt.), l_1 = 24 μm, l_2 = 1.83 mm, u_b = 0.03 m/s, u_e = 0.00226 m/s)

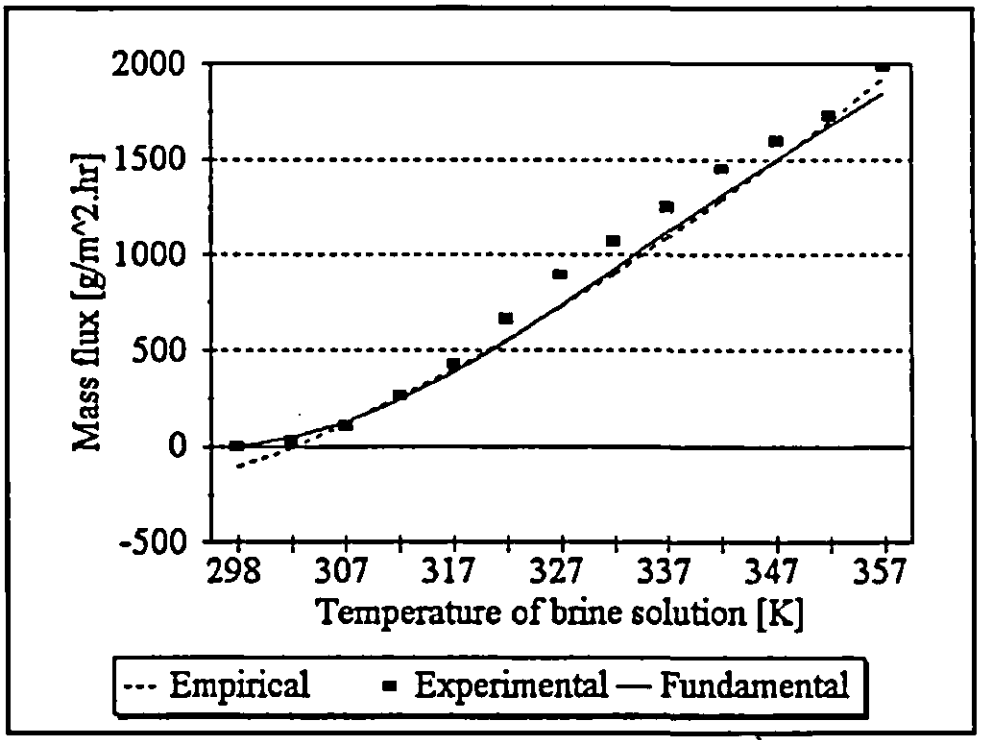

Fig 5.5 Mass flux as the temperature of the brine feed changes (R^2 = 0.9951).
(T_e = 291 K, c_b = 0 %, l_1 = 24 μm, l_2 = 1.83 mm, u_b = 0.03 m/s, u_e = 0.00226 m/s)

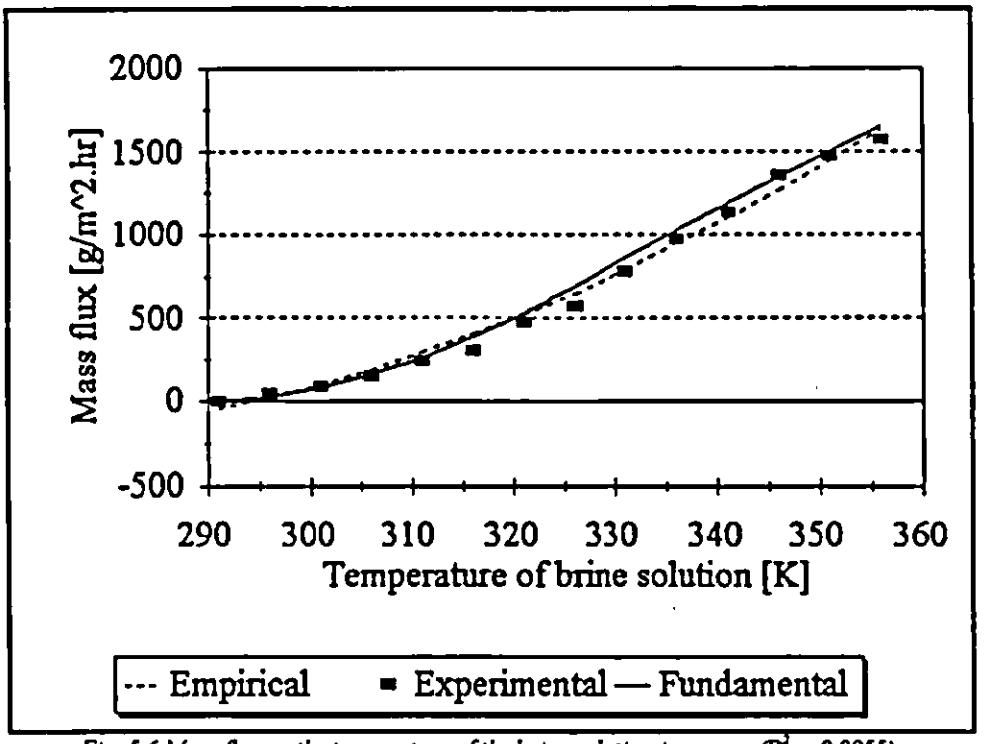

Fig. 5.6 Mass flux as the temperature of the brine solution increases (R^2 = 0.9955).
(T_e = 291 K, c_b = 3 % (wt.), l_1 = 24 μm, l_2 = 1.83 mm, u_b = 0.03 m/s, u_e = 0.00226 m/s)

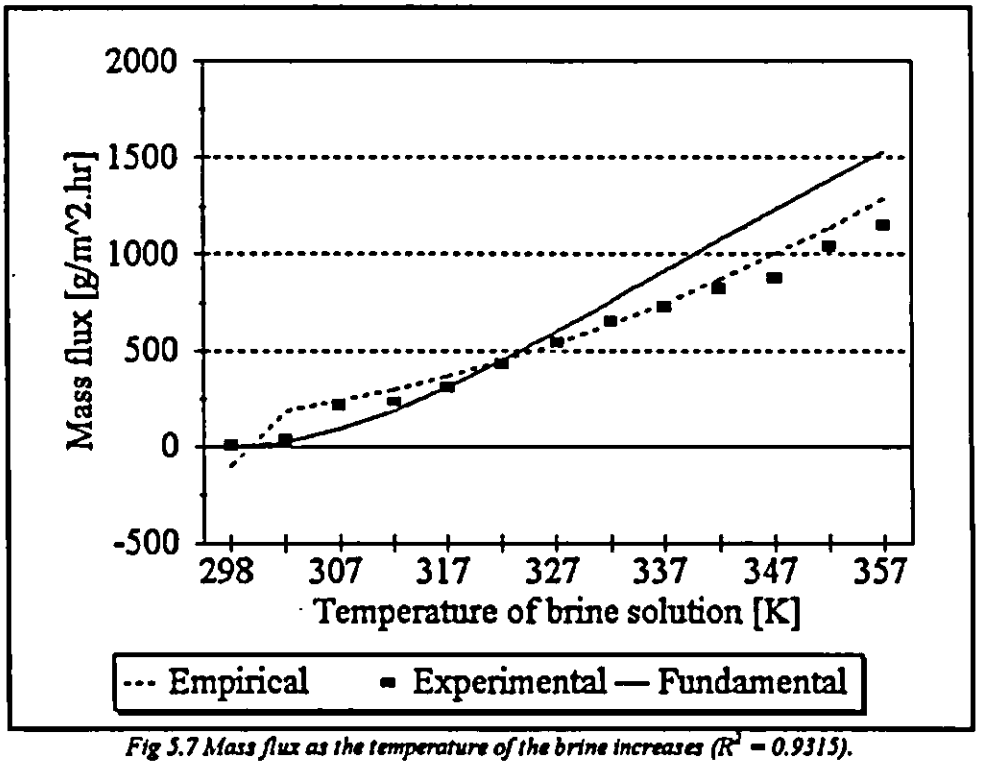

Fig 5.7 Mass flux as the temperature of the brine increases (R^2 = 0.9315).
(T_e = 291 K, c_b = 15 % (wt.), l_1 = 24 μm, l_2 = 1.83 mm, u_b = 0.03 m/s, u_e = 0.00226 m/s)

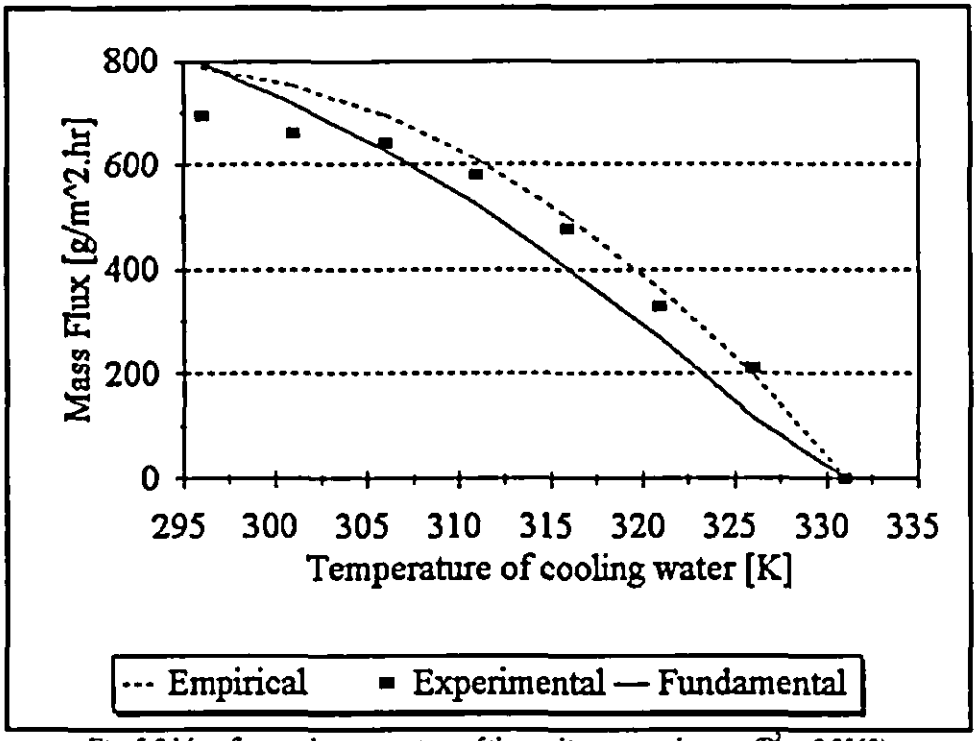

Fig. 5.8 Mass flux as the temperature of the cooling water changes (R^2 = 0.9560).
(T_b = 331 K, c_b = 3 % (wt.), l_1 = 24 μm, l_2 = 1.83 mm, u_b = 0.03 m/s, u_e = 0.00226 m/s)

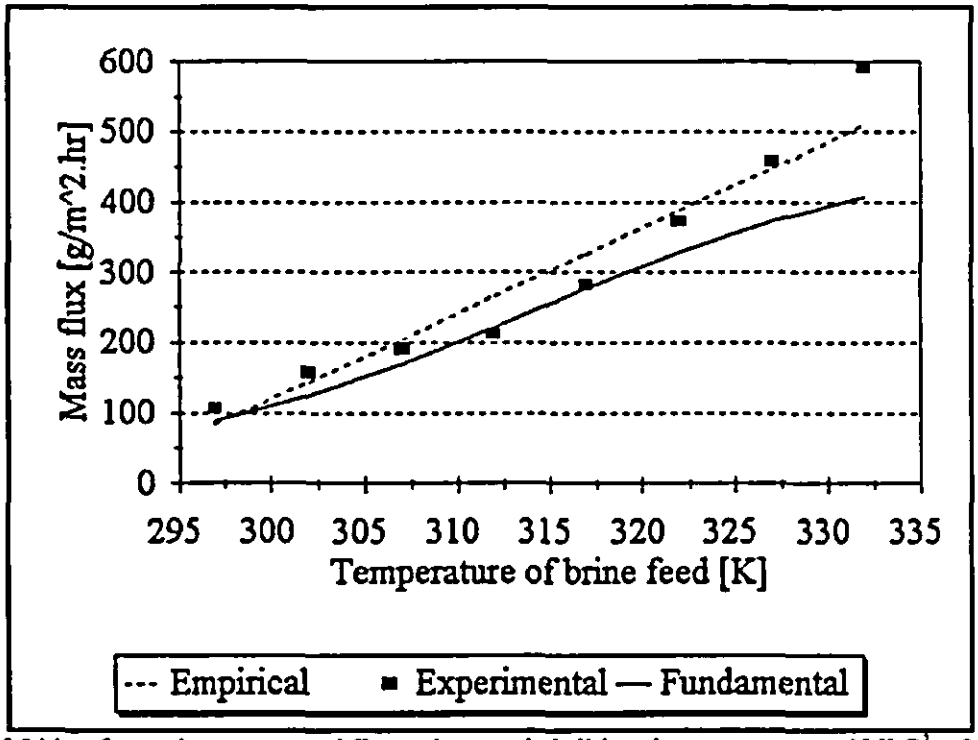

Fig. 5.9 Mass flux as the temperature difference between the bulk liquids stays constant at 15 K (R^2 = 0.982).
(ΔT = 15 K, c_b = 3 % (wt.), l_1 = 24 μm, l_2 = 1.83 mm, u_b = 0.03 m/s, u_e = 0.00226 m/s)

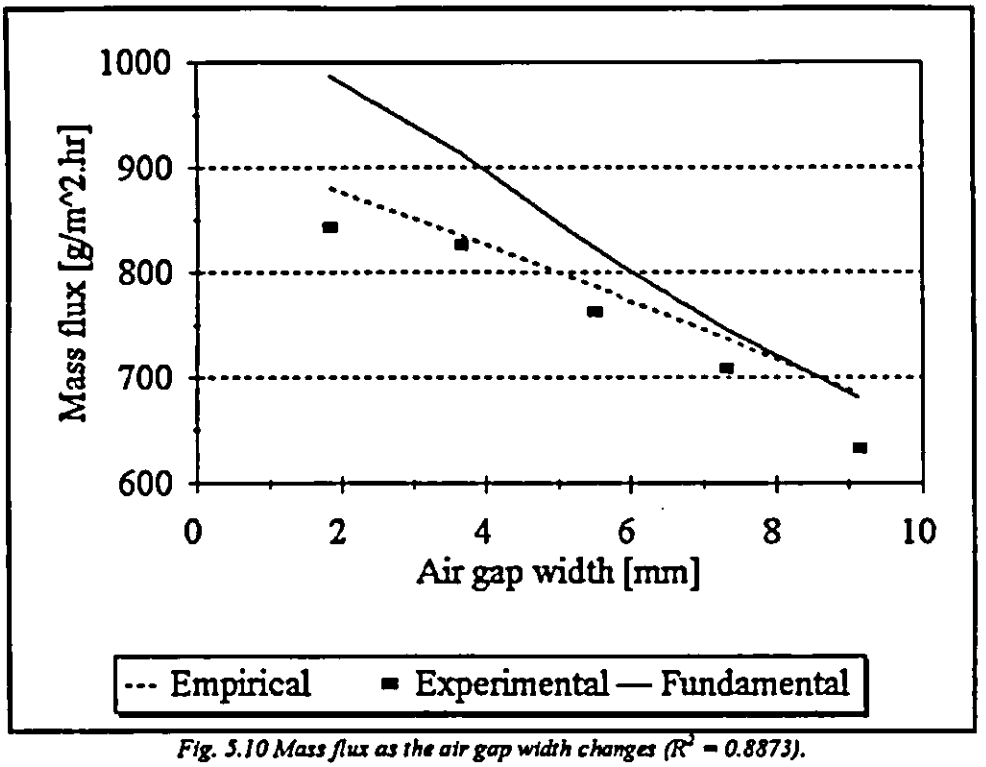

Fig. 5.10 Mass flux as the air gap width changes (R^2 = 0.8873).
(T_b = 331 K, T_e = 291 K, c_b = 0 % (wt.), l_1 = 24 μm, u_b = 0.03 m/s, u_e = 0.00226 m/s)

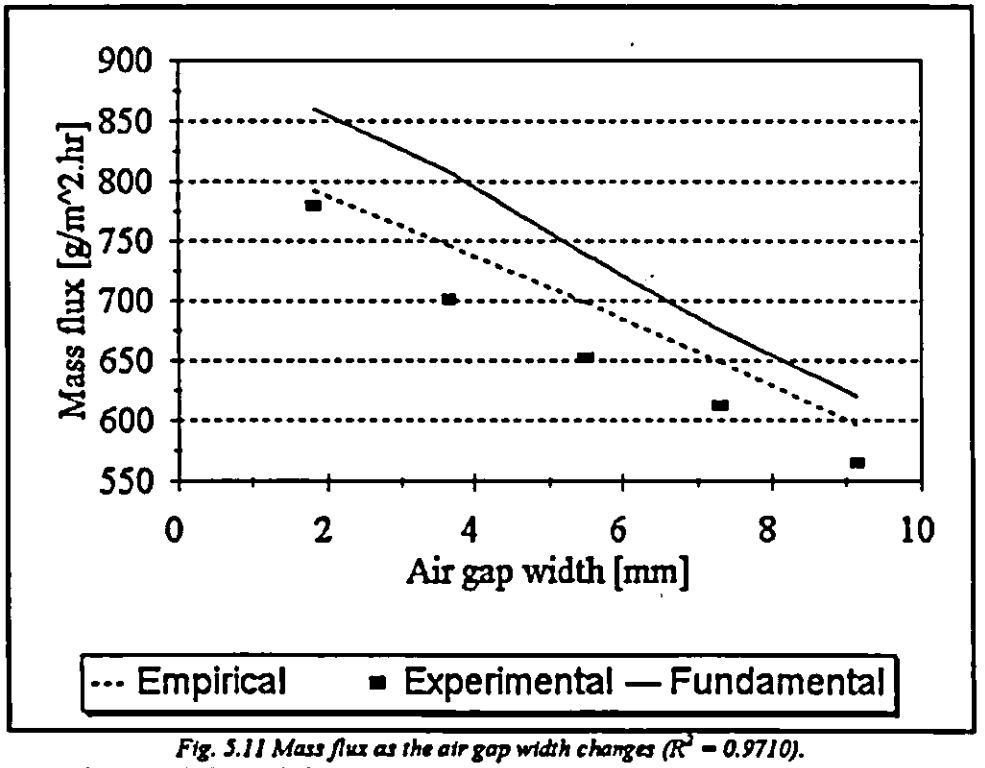

Fig. 5.11 Mass flux as the air gap width changes (R^2 = 0.9710).
(T_b = 331 K, T_e = 291 K, c_b = 3 % (wt.), l_1 = 24 μm, u_b = 0.03 m/s, u_e = 0.00226 m/s)

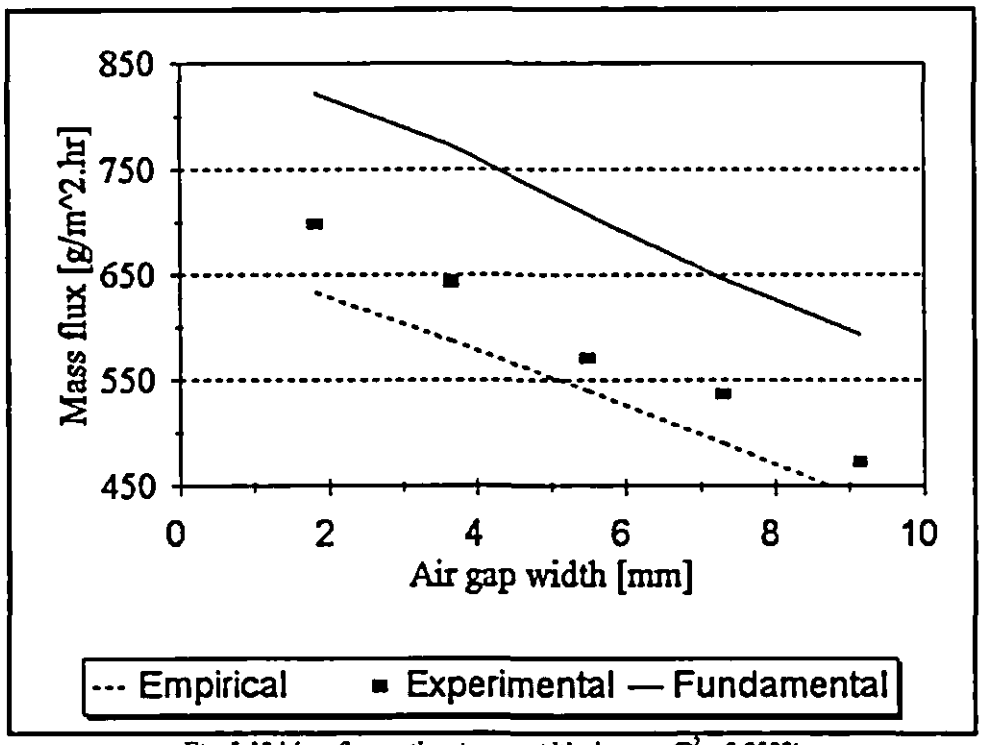

Fig. 5.12 Mass flux as the air gap width changes (R^2 =0.9582).
(T_b = 331 K, T_c = 291 K, c_b = 10 % (wt.), l_l = 24 μm, u_b = 0.03 m/s, u_c = 0.00226)

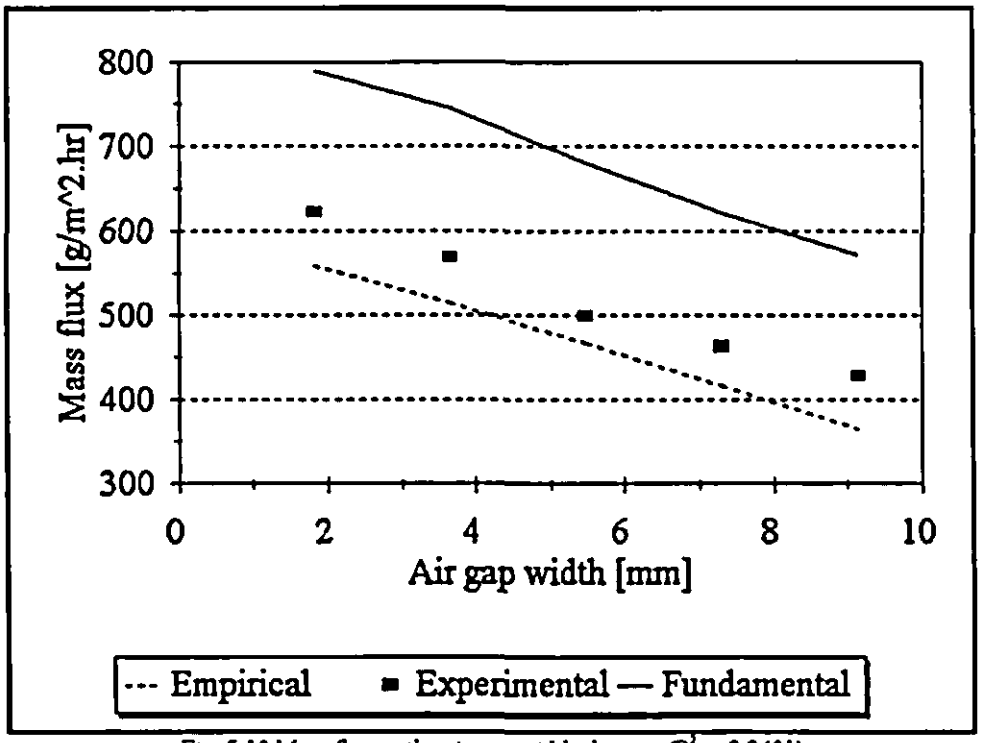

Fig. 5.13 Mass flux as the air gap width changes (R^2 = 0.9431).
(T_b = 331 K, T_c = 291 K, c_b =15 % (wt.), l_l = 24 μm, u_b = 0.03 m/s, u_c = 0.00226)

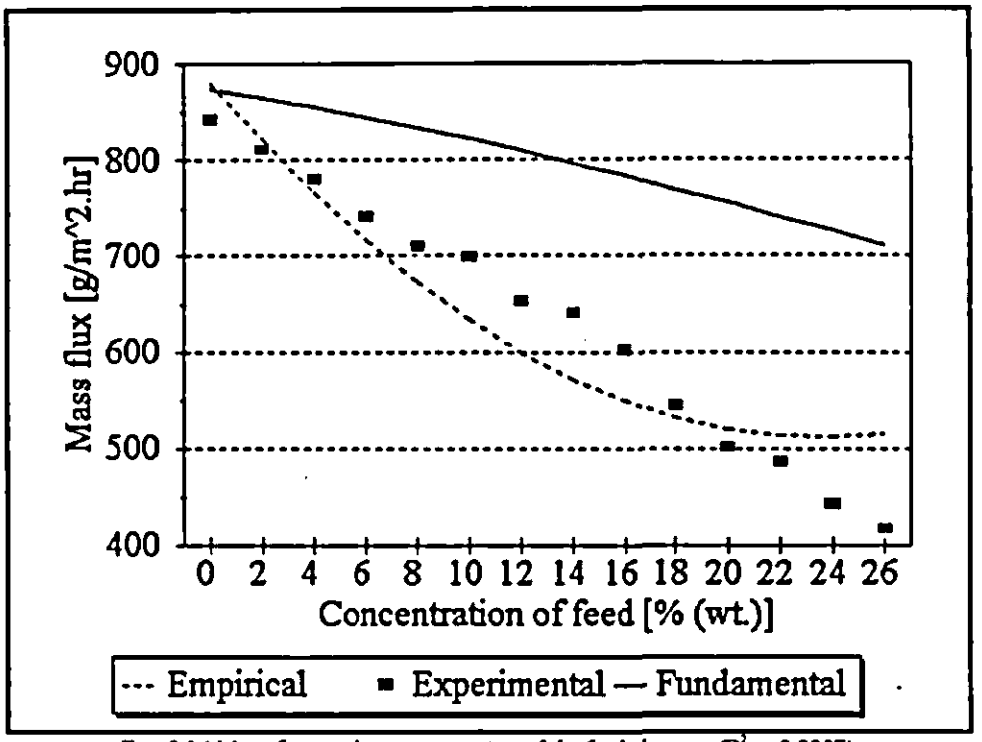

Fig. 5.14 Mass flux as the concentration of the feed changes (R^2 = 0.9937).
(T_b = 331 K, T_c = 291 K, l_1 = 24 μm, l_2 = 1.83 mm, u_b = 0.03 m/s, u_c = 0.00226)

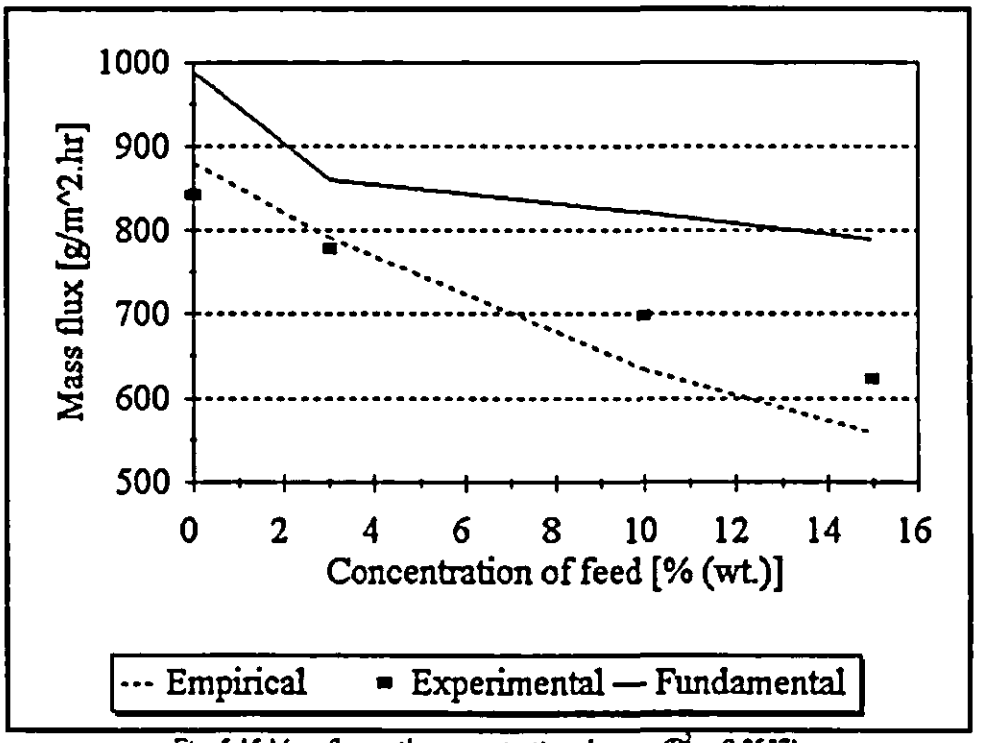

Fig. 5.15 Mass flux as the concentration changes (R^2 = 0.8537).
(T_b = 331 K, T_c = 291 K, l_1 = 24 μm, l_2 = 1.83 mm, u_b = 0.03 m/s, u_c = 0.00226 m/s)

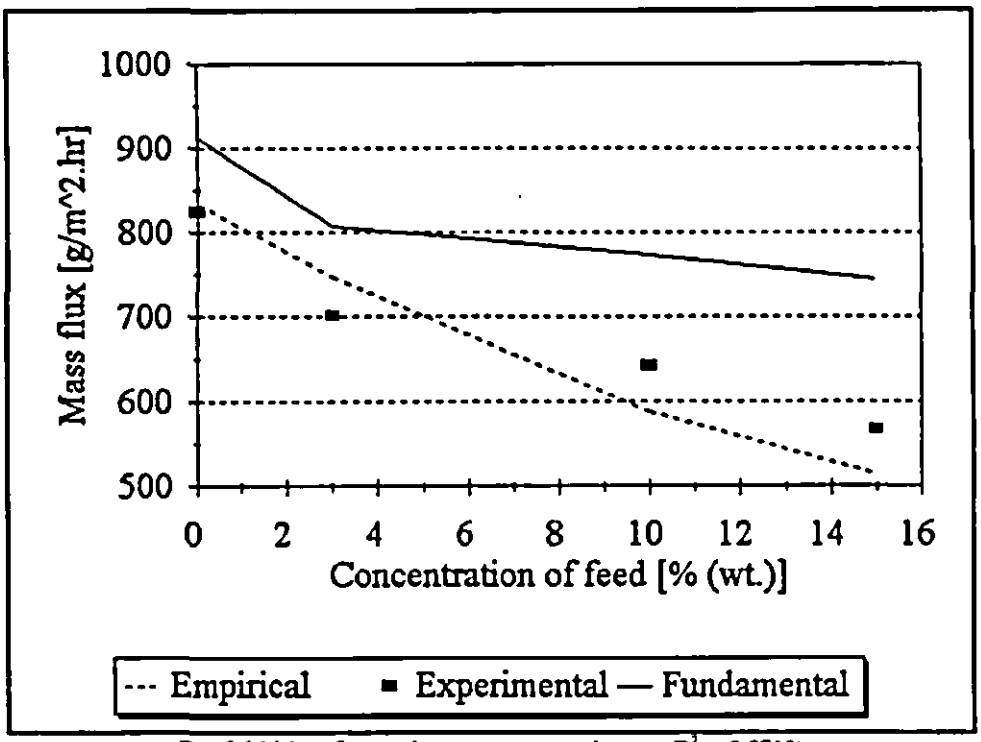

Fig. 5.16 Mass flux as the concentration changes (R^2 = 0.9710).
(T_b = 331 K, T_s = 291 K, l_1 = 24 μm, l_2 = 3.66 mm, u_b = 0.03 m/s, u_s = 0.00226 m/s)

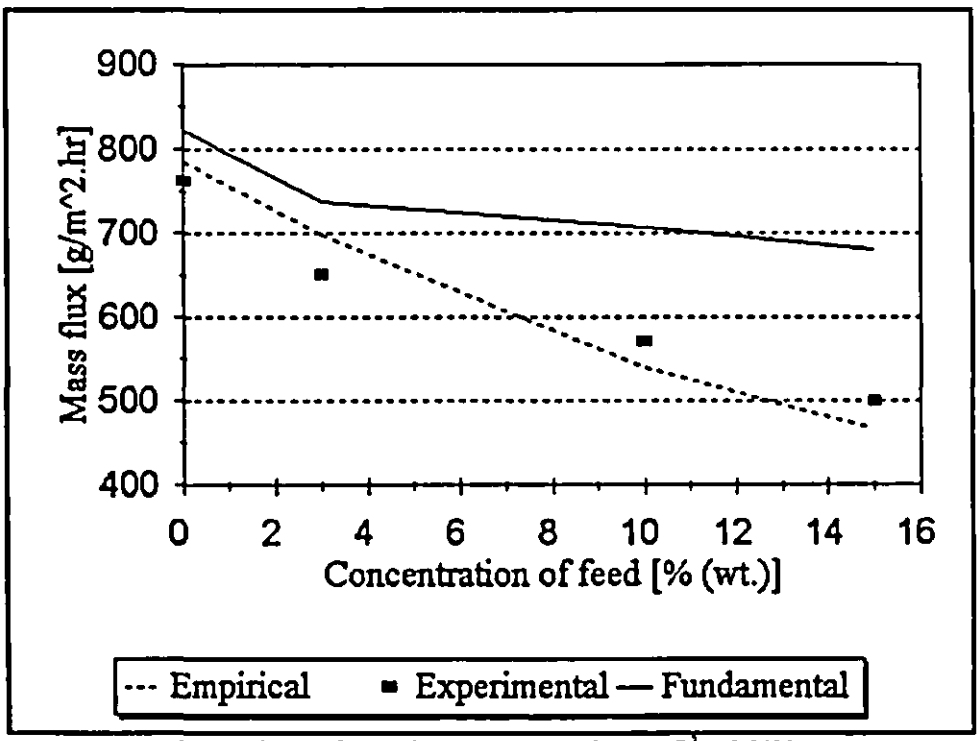

Fig. 5.17 Mass flux as the concentration changes (R^2 = 0.9620).
(T_b = 331 K, T_s = 291 K, l_1 = 24 μm, l_2 = 5.49 mm, u_b = 0.03 m/s, u_s = 0.00226 m/s)

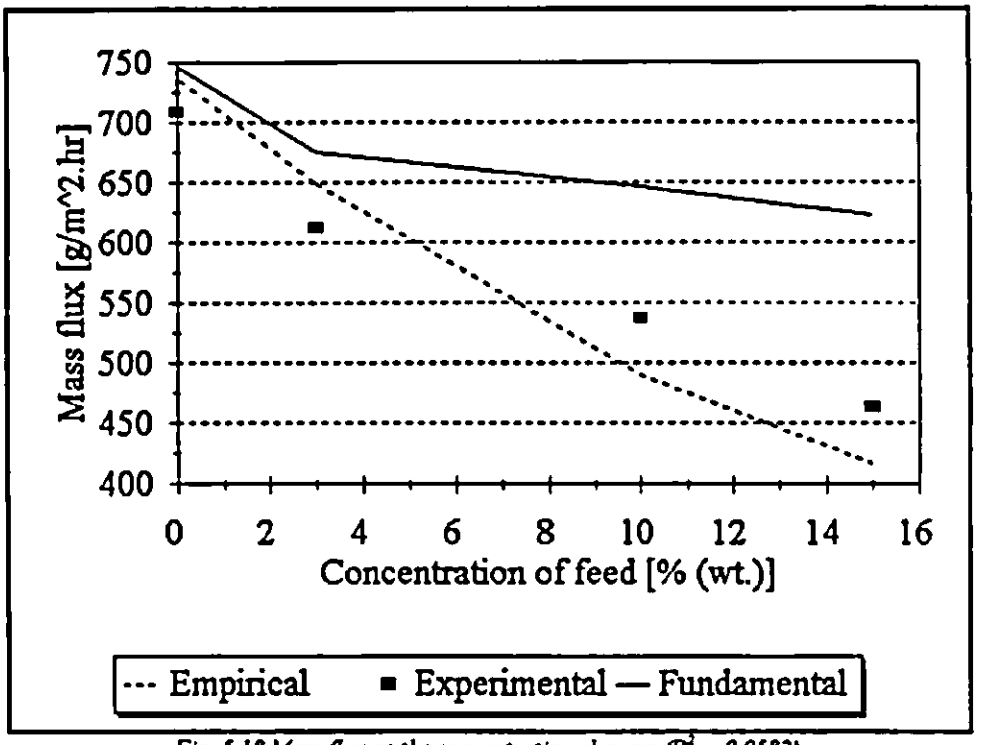

Fig. 5.18 Mass flux as the concentration changes (R^2 = 0.9582).
(T_b = 331 K, T_e = 291 K, l_1 = 24 μm, l_2 = 7.32 mm, u_b = 0.03 m/s, u_e = 0.00226 m/s).

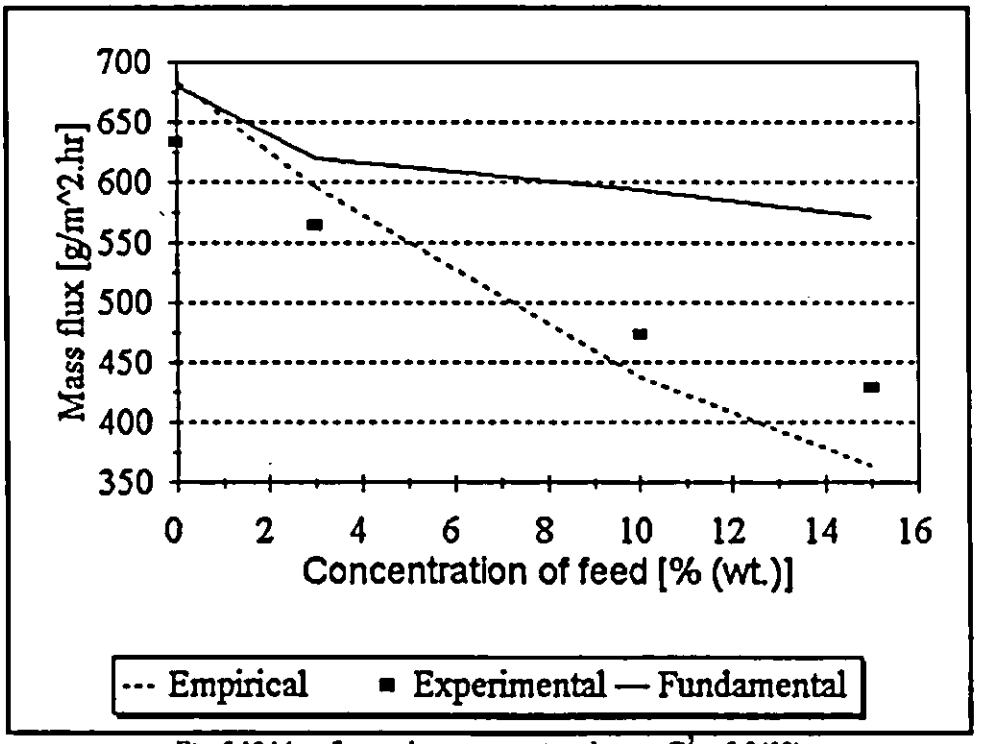

Fig. 5.19 Mass flux as the concentration changes (R^2 = 0.9430).
(T_b = 331 K, T_e = 291 K, l_1 = 24 μm, l_2 = 9.15 mm, u_b = 0.03 m/s, u_e = 0.00226 m/s)

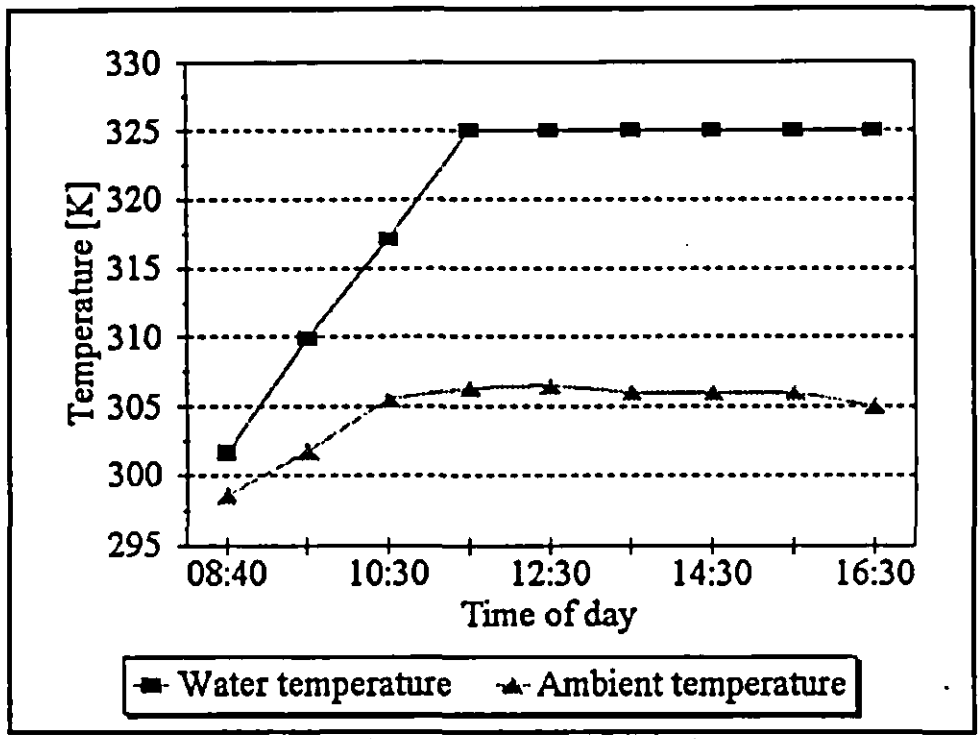

Fig. 5.20 Heating of water by direct sunlight.

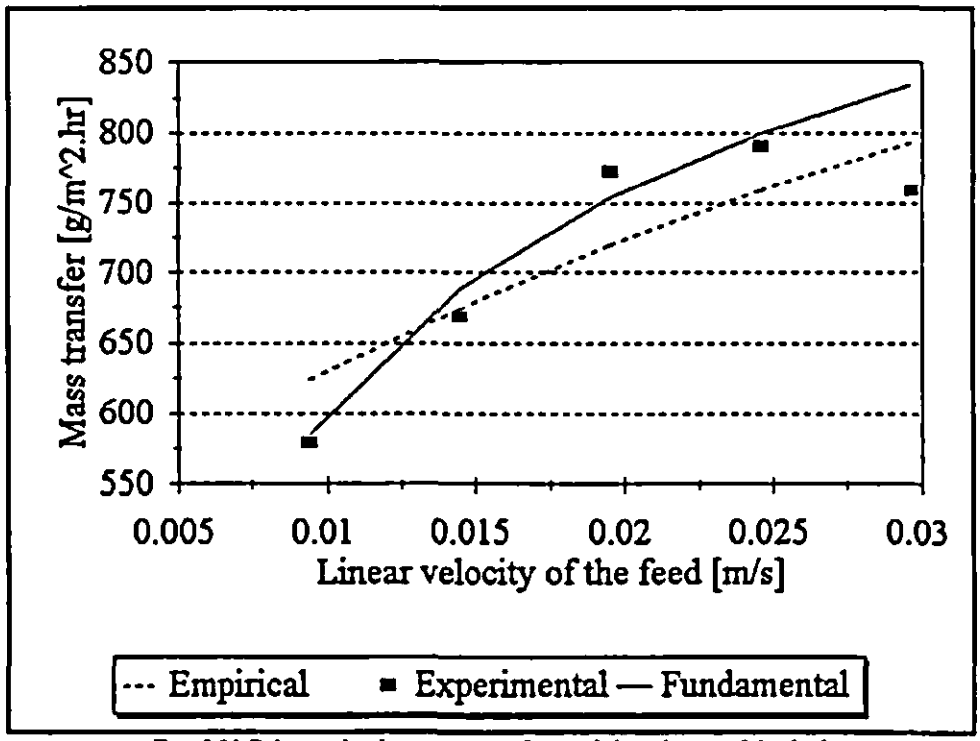

Fig. 5.21 Relationship between mass flux and the velocity of the feed.
(T_b = 331 K, T_c = 291 K, c_b = 3 % (wt.), l_1 = 24 μm, l_2 = 1.83 mm, u_c = 0.00226 m/s)

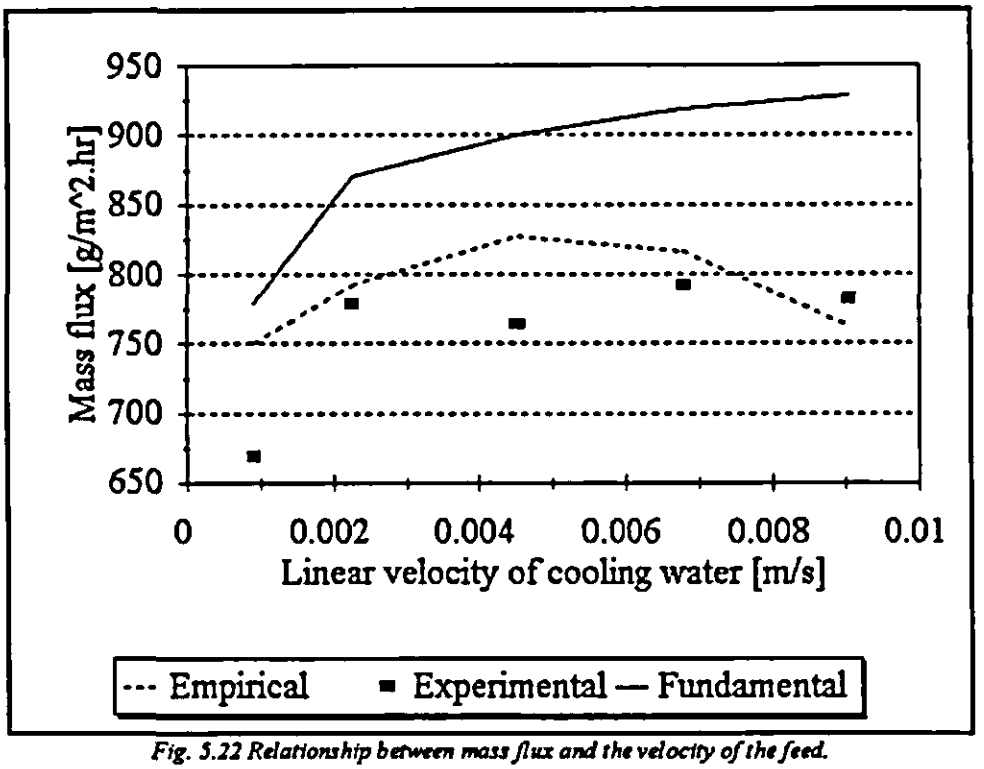

Fig. 5.22 Relationship between mass flux and the velocity of the feed.
(T_b = 331 K, T_c = 291 K, c_b = 3 % (wt.), l_1 = 24 μm, l_2 = 1.83 mm, u_b = 0.03m/s)

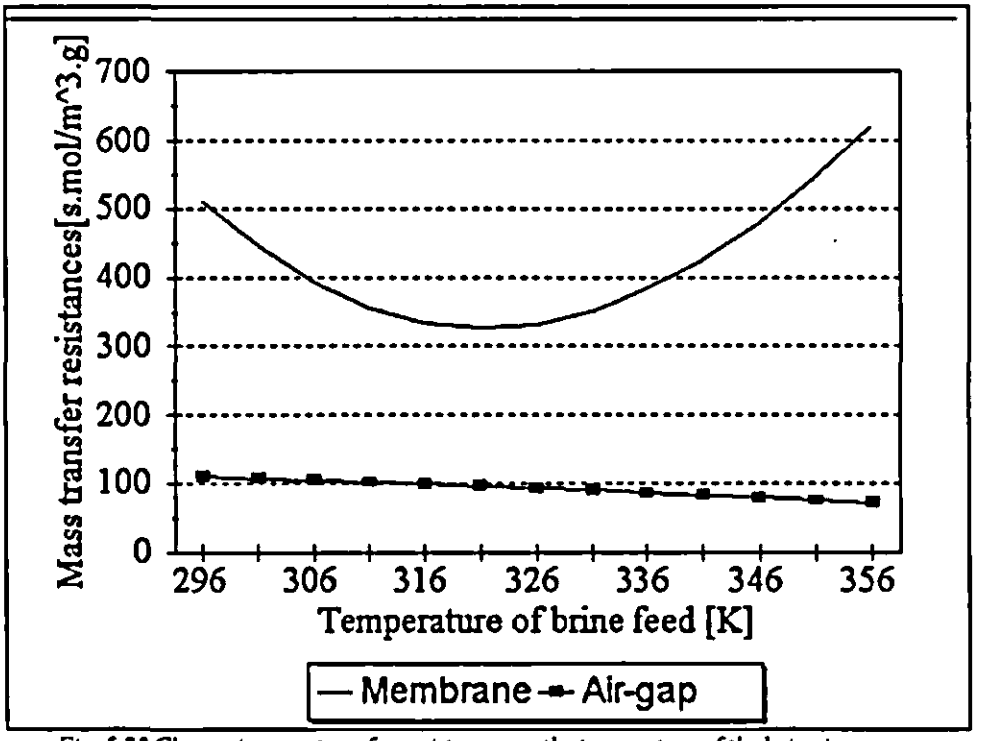

Fig. 5.23 Change in mass transfer resistances as the temperature of the brine increases.
(T_c = 291 K, c_b = 3 % (wt.) ,l_1 = 24 μm, l_2 = 1.83 mm, u_b = 0.03 m/s, u_c = 0.00226 m/s)

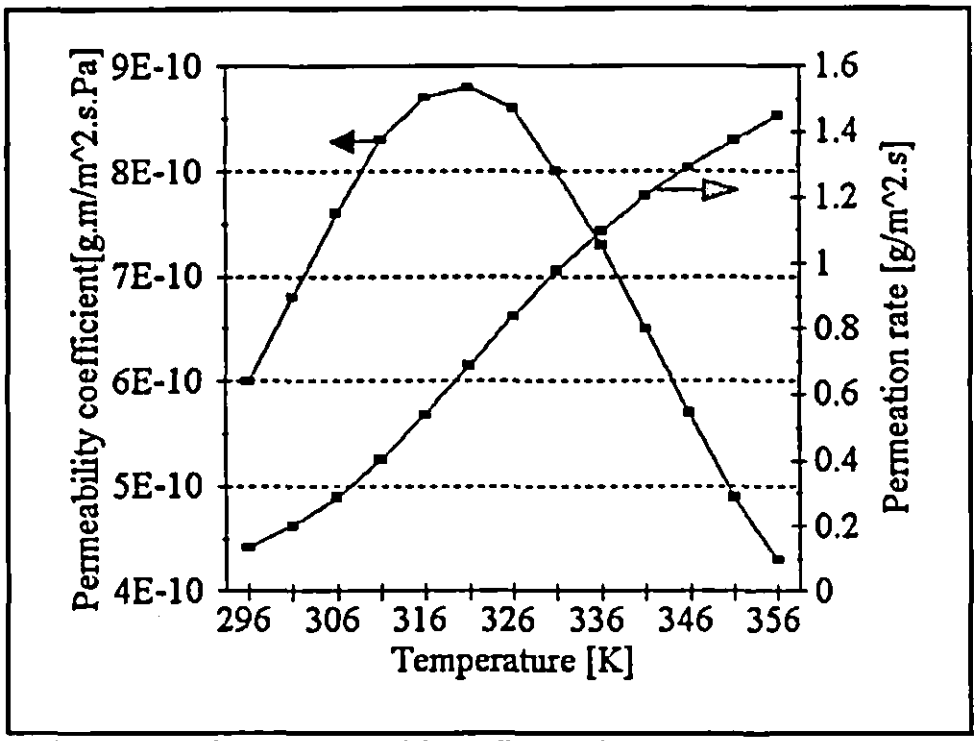

Fig.5.24 Dependency of the permeability coefficient and permeation rate on temperature.

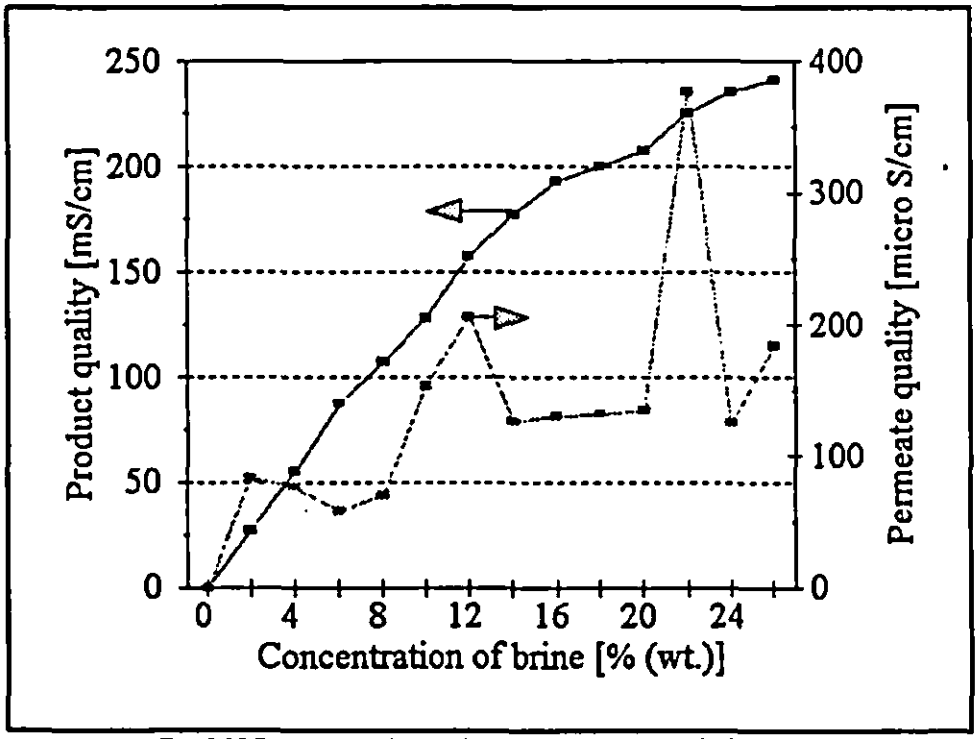

Fig. 5.25 Permeate quality as the concentration of the feed changes.

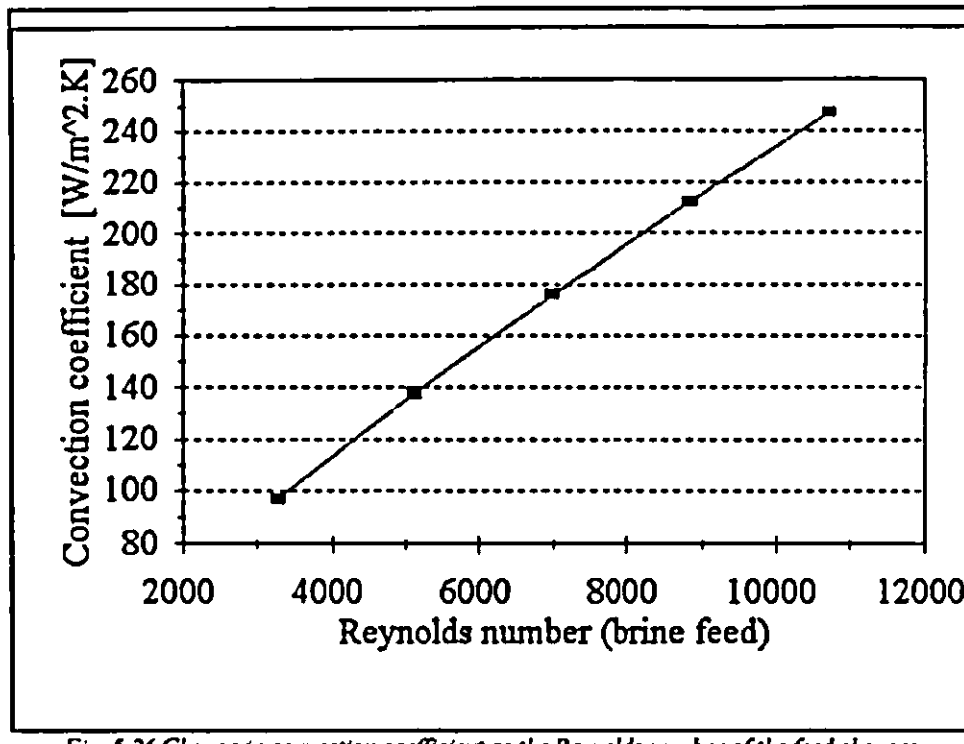

Fig. 5.26 Change in convection coefficient as the Reynolds number of the feed changes. (T_b = 331 K, T_c = 291 K, c_b = 3 % (wt.) ,l_1 = 24 μm, l_2 = 1.83 mm, u_c = 0.00226 m/s)

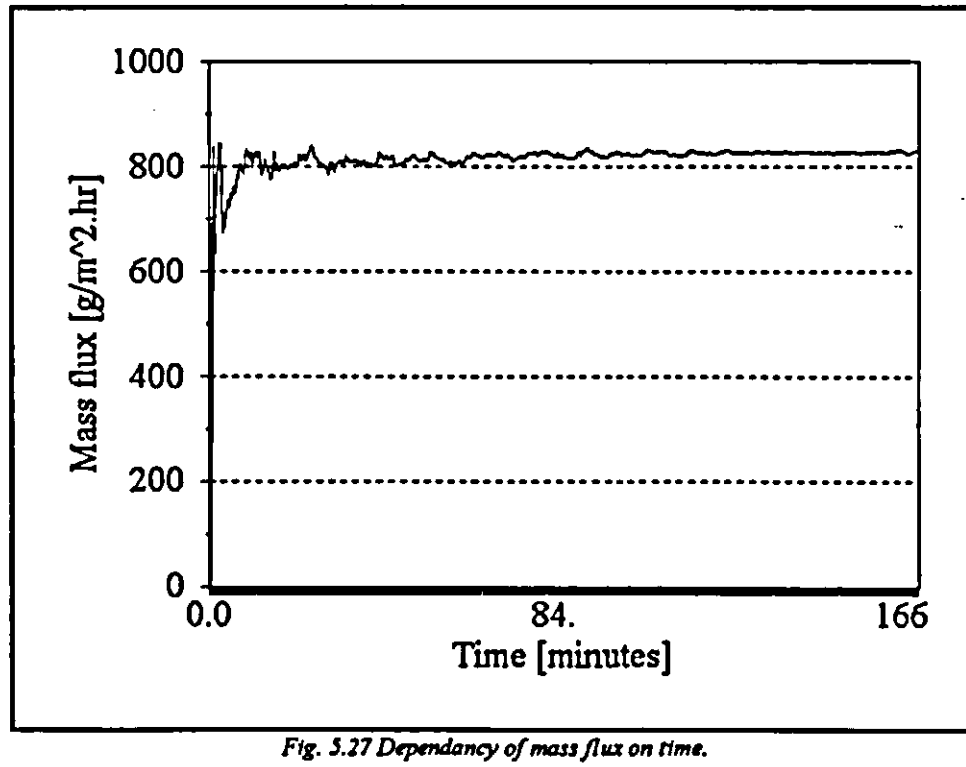

Fig. 5.27 Dependancy of mass flux on time.

CHAPTER 6

CONCLUSIONS AND RECOMMENDATIONS

The project had the drawback that the air gap membrane distillation units had variables that were difficult to control. From the data obtained from the alternative set-up, the conclusion could be drawn that this would be a viable process if a low mass flux is required and sunlight or some other source of waste heat is available. When sunlight was used as an energy source, the feed could be heated to a temperature of 52 °C. If these distillation units were to be used only for emergency purposes, this method of fresh water production would be viable. The permeate was of a quality that met the requirements for human consumption, since the salt rejection by this process was more than 99.6 % .

There was a good correlation between the predicted and experimental results. The fundamental model could be used with confidence to predict the performance of air gap membrane distillation. The fundamental model had a correlation coefficient (R^2) of 0.9156, while the empirical model had a correlation coefficient (R^2) of 0.9026. At high brine concentrations, where the fundamental model tends to deviate from the experimental data, the empirical model can be used to predict the performance of the air gap membrane distillation unit. Below 3 % (wt.) NaCl solution, both of the models correlates the experimental data quite accurately, whilst the empirical model produces better results when the air gap width is changed. Conversely, it was found that the fundamental model made better predictions of the experimental data when the flowrates of the brine solution and the cooling water were varied. The mass flux thus can be predicted very accurately when the advantages and disadvantages of both these models is taken into account.

There was a near linear relationship between the vapour pressure difference and the mass flux, showing that the vapour pressure difference was the driving force in the process.

REFERENCES

Andersson, S.I., Kjellander, N. and Rodesjö, B., 1985, Design and field tests of a new membrane distillation desalination process, *Desalination*, 56, 345-354.

Banat, F.A. and Simandl, J., 1994, Theoretical and experimental study in membrane distillation, *Desalination*, 95, 39-52.

Bandini, S., Gostolli, S. and Sarti, G.C., 1991, Role of heat and mass transfer in membrane distillation process, *Desalination*, 81, 91-106.

Barrie, J.A., Water in polymers, in: Crank, J. and Park, G.S., *Diffusion in polymers*, 1968, First edition, Academic Press, London, 452 pages.

Basini, G., D'Angelo, G., Gobbi, M., Sarti, G.C. and Gostoli, C., 1987, A desalination process through sweeping gas membrane distillation, *Desalination*, 64, 245-257.

Bird, R.B, Steward, W.E. and Lightfoot, E.N., 1960, *Transport phenomena*, Seventh Edition, Wiley, New York, 780 pages.

Carlsson, L., 1983, The new generation in sea water desalination SU distillation system, *Desalination*, 45, 221-222.

Cheng, D.Y. and Wiersma, S.J., Composite membrane for a membrane distillation system, US Patent No. 4419242, 16 pages.

Coulson, J.M., Richardson, J.F., Backhurst, J.R. and Harker, J.H., 1990, *Chemical Engineering*, 1, Fourth Edition, Pergamon Press, Oxford, 708 pages.

Coulson, J.M., Richardson, J.F., Backhurst, J.R. and Harker, J.H., 1990, *Chemical Engineering*, 2, Pergamon Press, Oxford, 968 pages.

Coulson, J.M., Richardson, J.F. and Sinnot, R.K., 1983, *Chemical Engineering - An introduction to Chemical Engineering design*, 6, Pergamon Press, U.K, 1983, 838 pages.

Deng, S., Shiyao, B., Sourirajan, S. and Matsuura, T., 1990, A study of the pervaporation of isopropyl alcohol/water mixtures by cellulose acetate membranes, *Journal of Colloid and Interface Science*, 136(1), 283-291.

Drioli, E., Wu, Y., and Calabro, V., 1987, Membrane distillation in the treatment of aqueous solutions, *Journal of Membrane Science*, 33, 277-284.

Dullien, F.A.L., 1979, *Porous media - Fluid transport and pore structure*, Academic Press, New York, NY, 396 pages.

Fabuss, B.M., Properties of sea water, in : Spiegler, K.S. and Laird, A.D.K (Ed.), 1980, *Principles of desalination*, Part B, Second Edition, Academic Press, New York, 821 pages.

Fane, A.G., Schofield, R.W., and Fell, C.J.D., 1987, The effective use of energy in membrane distillation, *Desalination*, 64, 231-243.

Feng, X. and Huang, R.Y.M., 1994, Concentration polarisation in pervaporation separation processes, *Journal of Membrane Science*, 92, 201-208.

Findley, M.E., 1967, Vaporization through porous membranes, *Ind. Eng. Chem., Process Des. Dev.*, 6, 226-230.

Findley, M.E., Tanna, V.V., Rao, Y.B. and Yeh, C.L., 1969, Mass and heat transfer relations in evaporation through porous membranes, *AIChEJ*, 15, 483-488.

Gore, D.W., 1982, Gore-Tex membrane distillation, Proc. 10th Ann. Conv. Water Supply Improvement Assoc., Honolulu, July 25-29.

Gostolli, C and Sarti, G.C., 1989, Separation of liquid mixtures by membrane distillation, *Journal of Membrane Science*, 41, 211-224.

Hanbury, W.T. and Hodgkiess, 1985, Membrane distillation - An assessment, *Desalination*, 56, 287-297.

Heintz, A. and Stephan, W., A generalized solution-diffusion model of the pervaporation process through composite membranes. Part I. Prediction of mixture solubilities in the dense active layer using the Uniquac model, 1994, *Journal of Membrane Science*, 89, 143-151.

Hogan, P.A., Sudjito, Fane, A.G. and Morrison, G.L., 1991, Desalination by solar heated membrane distillation, *Institution of Chemical Engineers Symposium Series*, 1, (125), 81-90.

Incropera, F.B. and De Witt, D.P., 1990, *Fundamentals of heat and mass transfer*, Third Edition, Wiley, New York, 919 pages.

Johnson, N.L, and Leone, F.C., 1964, "*Statistics and experimental design*", 1, First edition, Wiley, New York, 513 pages.

Jönsson, A.S, Wimmerstedt, F. and Harryson, A.C., 1985, Membrane distillation - A theoretical study of evaporation through microporous membranes, *Desalination*, 56, 237-249.

Karlsson, H.O.E. and Trägårdh, 1993 Aroma compound recovery with pervaporation - feed flow effects, *Journal of Membrane Science*, 81, 163-171.

Kimura, S and Nakoa, S., 1987, Transport phenomena in membrane distillation, *Journal of Membrane Science*, 33, 285-297.

Kubota, S., Ohta, K., Hayano, I., Hirai, M., Kikuchi, K. and Murayama, Y., 1988, Experiments on sea water desalination by membrane distillation, *Desalination*, 69, 19-26.

Kurokawa, H., Kuroda, O., Takahashi, S. and Ebara, K., 1990, Vapor permeate characteristics of membrane distillation, *Separation Science and Technology*, 25, 1349-1359.

Lochner, R.H. and Matar, J.E., 1990, *Designing for quality*, Quality Resources, New York, United States of America, 233 pages.

Löf, G.O.G., Solar Distillation, in: Spiegler, K.S. and Laird, A.D.K (Ed.), 1980, *Principles of desalination*, Part B, Second Edition, Academic Press, New York, 821 pages.

Matsuura, T., 1995, *Synthetic membranes and membrane separation processes*, CRC Press, Boca Raton, 342 pages.

Maolin, L., Lixin, Y. and Weijun, J., 1993, Studies on heat efficiency of membrane distillation, *Water Treatment*, 8, 225-233.

Mulder, M., *Basic principles of membrane technology*, 1991, Kluwer Academic Principles, Dordrecht, 363 pages.

Ohta, K., Hayano, I., Okabe, T., Goto, T., Kimura, S. and Ohya, H., 1991, Membrane distillation with Fluoro-Carbon membranes, *Institution of Chemical Engineers Symposium Series*, 1, (125), 107-115.

Ohta, K., Kikuchi, K. Hayano, I., Okabe, T., Goto, T., Kimura, S. and Ohya, H., 1990, Experiments on sea water desalination by membrane distillation, *Desalination*, 78, 177-185.

Ortiz de Zarate, J.M., Velazquez, A., Pena, L. and Mengual, J.I., 1993, Influence of temperature polarization by membrane distillation, *Separation Science and Technology*, 28(7), 1421-1426.

Sarti, G.C., Gostolli, C. and Bandini, S., 1993, Extraction of organic components from aqueous streams by vacuum membrane distillation, *Journal of Membrane Science*, 80, 21-33.

Sarti, G.C., Gostolli, C. and Matulli, S., 1985, Low energy cost desalination processes using hydrophobic membranes, Proc. Second World Congress on Desalination and Water Reuse, *Desalination*, 56, 277-286.

Schofield, R.W., Fane, A.G. and Fell, C.J.D., 1987, Heat and mass transfer in membrane distillation, *Journal of Membrane Science*, 33, 299-313.

Schofield, R.W., Fane, A.G., Fell, C.J.D., 1990a, Gas and vapour transport through Membranes .I Knudsen Poiseulle Transition, *Journal of Membrane Science*, 53, 159-172.

Schofield, R.W., Fane, A.G., Fell, C.J.D., 1990b, Gas and vapour transport through Membranes .II Membrane distillation, *Journal of Membrane Science*, 53, 173-185.

Schofield, R.W., Fane, A.G. Fell. C.J.D. and Macoun. R, 1990c, Factors affecting flux in membrane distillation, *Desalination*, 77, 279-294.

Sheng, J. and Lefebvre, M.S., 1993, Diluted brine concentration process using membrane pervaporation technique: Laboratory scale studies, *Desalination*, 93, 253-263.

Sherwood, T.K., Pigford, R.L. and Wilke, C.R., 1975, *Mass Transfer*, First Edition, McGraw-Hill, New York, 677 pages.

Weijun, J., Lixin, Y. and Maolin, L., 1993, A studies on mass and heat transfer in membrane distillation, *Water Treatment*, 8, 127-133.

APPENDIX A
(TABLES OF RESULTS)

Experimental conditions							Mass flux			Permeate
T_c [K]	T_b [K]	l_1 micron	u_b [m/s]	u_c [m/s]	L_2 [mm]	c_b [% NaCl]	Empirical [g/(h.m^2)]	Experimental [g/(h.m^2)]	Fundamental [g/(h.m^2)]	quality [micro S/cm]
296	331	24	0.030	0.00226	1.83	3	786.5	694.7	796.0	221
301	331	24	0.030	0.00226	1.83	3	754.2	660.3	718.1	30
306	331	24	0.030	0.00226	1.83	3	695.5	639.7	627.9	16
311	331	24	0.030	0.00226	1.83	3	610.3	580.1	523.1	20
316	331	24	0.030	0.00226	1.83	3	498.8	474.2	402.9	16
321	331	24	0.030	0.00226	1.83	3	360.8	328.8	267.6	16
326	331	24	0.030	0.00226	1.83	3	196.4	211.1	116.7	16
331	331	24	0.030	0.00226	1.83	3	5.6	0.0	0.0	0

Table A1 Results when the cooling water temperature is varied.

Experimental conditions							Mass flux			Permeate
T_c [K]	T_b [K]	l_1 micron	u_b [m/s]	u_c [m/s]	d [mm]	c_b [% NaCl]	Empirical [g/(h.m^2)]	Experimental [g/(h.m^2)]	Fundamental [g/(h.m^2)]	quality [micro S/cm]
298	298	24	0.030	0.00226	1.83	0	-101.4	0.0	0.0	0
298	302	24	0.030	0.00226	1.83	0	-7.2	25.8	44.7	0
298	307	24	0.030	0.00226	1.83	0	119.4	105.6	128.1	0
298	312	24	0.030	0.00226	1.83	0	255.9	261.7	241.0	0
298	317	24	0.030	0.00226	1.83	0	402.3	424.5	383.1	0
298	322	24	0.030	0.00226	1.83	0	558.6	660.0	550.1	0
298	327	24	0.030	0.00226	1.83	0	724.8	892.7	734.3	0
298	332	24	0.030	0.00226	1.83	0	900.8	1067.1	927.2	0
298	337	24	0.030	0.00226	1.83	0	1086.7	1250.4	1121.5	0
298	342	24	0.030	0.00226	1.83	0	1282.5	1450.1	1312.2	0
298	347	24	0.030	0.00226	1.83	0	1488.2	1596.4	1495.9	0
298	352	24	0.030	0.00226	1.83	0	1703.7	1729.2	1675.2	0
298	357	24	0.030	0.00226	1.83	0	1929.1	1985.8	1850.5	0

Table A2 Results when the temperature of the brine is varied for distilled water.

Experimental conditions							Mass flux			Permeate
T_c [K]	T_b [K]	l_1 micron	u_b [m/s]	u_c [m/s]	l_2 [mm]	c_b [% NaCl]	Empirical [g/(h.m^2)]	Experimental [g/(h.m^2)]	Fundamental [g/(h.m^2)]	quality [micro S/cm]
291	291	24	0.030	0.00226	1.83	3	-48.7	0.0	0.0	27
291	296	24	0.030	0.00226	1.83	3	21.8	39.3	31.3	28
291	301	24	0.030	0.00226	1.83	3	102.3	87.1	84.0	25
291	306	24	0.030	0.00226	1.83	3	192.6	148.4	159.6	243
291	311	24	0.030	0.00226	1.83	3	292.8	237.4	260.6	1149
291	316	24	0.030	0.00226	1.83	3	402.8	305.4	386.4	1257
291	321	24	0.030	0.00226	1.83	3	522.8	473.4	533.1	119
291	326	24	0.030	0.00226	1.83	3	652.6	572.1	693.3	847
291	331	24	0.030	0.00226	1.83	3	792.3	779.6	860.7	114
291	336	24	0.030	0.00226	1.83	3	941.9	969.0	1027.1	28
291	341	24	0.030	0.00226	1.83	3	1101.4	1131.2	1191.6	33
291	346	24	0.030	0.00226	1.83	3	1270.7	1352.4	1349.8	24
291	351	24	0.030	0.00226	1.83	3	1450.0	1470.2	1503.9	26
291	356	24	0.030	0.00226	1.83	3	1639.1	1568.6	1654.7	30
298	298	24	0.030	0.00226	1.83	10	-101.4	0.0	0.0	61
298	302	24	0.030	0.00226	1.83	10	184.3	31.3	20.2	73
298	307	24	0.030	0.00226	1.83	10	235.3	210.3	90.6	89
298	312	24	0.030	0.00226	1.83	10	296.2	230.0	186.0	95
298	317	24	0.030	0.00226	1.83	10	367.0	306.9	305.5	80
298	322	24	0.030	0.00226	1.83	10	447.7	432.0	445.1	63
298	327	24	0.030	0.00226	1.83	10	538.3	539.7	597.8	71
298	332	24	0.030	0.00226	1.83	10	638.7	645.7	757.2	32
298	337	24	0.030	0.00226	1.83	10	749.1	724.0	917.6	98
298	342	24	0.030	0.00226	1.83	10	869.3	822.2	1075.9	68
298	347	24	0.030	0.00226	1.83	10	999.3	874.0	1231.0	73
298	352	24	0.030	0.00226	1.83	10	1139.3	1040.6	1382.4	54
298	357	24	0.030	0.00226	1.83	10	1289.1	1149.0	1531.8	120

Table A3 Results when the temperature of the brine is varied at various NaCl concentrations.

Experimental conditions							Mass flux			Permeate quality
T_c [K]	T_b [K]	l_1 micron	u_b [m/s]	u_c [m/s]	l_2 [mm]	c_b [% NaCl]	Empirical [g/(h.m^2)]	Experimental [g/(h.m^2)]	Fundamental [g/(h.m^2)]	[micro S/cm]
291	331	24	0.030	0.00226	1.83	0	880.4	842.3	987.4	0
291	331	24	0.030	0.00226	1.83	3	792.3	779.1	860.7	114
291	331	24	0.030	0.00226	1.83	10	633.5	698.3	822.0	47
291	331	24	0.030	0.00226	1.83	15	560.0	622.4	790.1	29
291	331	24	0.030	0.00226	3.66	0	834.8	825.1	912.8	0
291	331	24	0.030	0.00226	3.66	3	746.7	701.2	808.7	76
291	331	24	0.030	0.00226	3.66	10	587.9	643.2	773.8	68
291	331	24	0.030	0.00226	3.66	15	514.4	568.5	745.1	86
291	331	24	0.030	0.00226	5.49	0	787.0	762.0	824.0	0
291	331	24	0.030	0.00226	5.49	3	698.9	652.1	738.8	118
291	331	24	0.030	0.00226	5.49	10	540.1	571.1	707.1	124
291	331	24	0.030	0.00226	5.49	15	466.6	499.9	681.1	504
291	331	24	0.030	0.00226	7.32	0	737.0	708.0	746.8	0
291	331	24	0.030	0.00226	7.32	3	648.9	612.0	675.8	122
291	331	24	0.030	0.00226	7.32	10	490.0	537.4	646.7	34
291	331	24	0.030	0.00226	7.32	15	416.5	463.2	622.8	98
291	331	24	0.030	0.00226	9.15	0	684.7	633.2	680.9	0
291	331	24	0.030	0.00226	9.15	3	596.7	565.0	620.7	67
291	331	24	0.030	0.00226	9.15	10	437.8	473.2	593.7	90
291	331	24	0.030	0.00226	9.15	15	364.3	428.7	572.1	231

Table A4 Results when the concentration of the NaCl and the air gap width is varied.

Experimental conditions							Mass flux			Permeate
T_c [K]	T_b [K]	l_1 micron	u_b [m/s]	u_c [m/s]	l_2 [mm]	c_b [% NaCl]	Empirical [g/(h.m^2)]	Experimental [g/(h.m^2)]	Fundamental [g/(h.m^2)]	quality [micro S/cm]
291	331	24	0.030	0.00226	1.83	0	880.4	842.3	987.4	0
291	331	24	0.030	0.00226	3.66	0	834.8	825.1	912.8	0
291	331	24	0.030	0.00226	5.49	0	787.0	762.0	824.0	0
291	331	24	0.030	0.00226	7.32	0	737.0	708.0	746.8	0
291	331	24	0.030	0.00226	9.15	0	684.7	633.2	680.9	0
291	331	24	0.030	0.00226	1.83	3	792.3	779.6	860.7	114
291	331	24	0.030	0.00226	3.66	3	746.7	701.2	808.7	76
291	331	24	0.030	0.00226	5.49	3	698.9	652.1	738.8	118
291	331	24	0.030	0.00226	7.32	3	648.9	612.0	675.8	122
291	331	24	0.030	0.00226	9.15	3	596.7	565.0	620.7	67
291	331	24	0.030	0.00226	1.83	10	633.5	698.3	822.0	47
291	331	24	0.030	0.00226	3.66	10	587.9	643.2	773.8	68
291	331	24	0.030	0.00226	5.49	10	540.1	571.1	707.1	124
291	331	24	0.030	0.00226	7.32	10	490.0	537.4	646.7	34
291	331	24	0.030	0.00226	9.15	10	437.8	472.3	593.7	90
291	331	24	0.030	0.00226	1.83	15	560.0	622.4	790.1	29
291	331	24	0.030	0.00226	3.66	15	514.4	568.5	745.1	86
291	331	24	0.030	0.00226	5.49	15	466.6	499.9	681.1	504
291	331	24	0.030	0.00226	7.32	15	416.5	463.2	622.8	98
291	331	24	0.030	0.00226	9.15	15	364.3	428.7	572.1	231

Table A5 Results when the concentration of the NaCl and the air gap width is varied.

Experimental conditions							Mass flux			Permeate
T_c [K]	T_b [K]	l_1 micron	u_b [m/s]	u_c [m/s]	l_2 [mm]	c_b [% NaCl]	Empirical [g/(h.m^2)]	Experimental [g/(h.m^2)]	Fundamental [g/(h.m^2)]	quality [micro S/cm]
282	297	24	0.030	0.00226	1.83	3	83.1	107.4	88.2	176
287	302	24	0.030	0.00226	1.83	3	143.9	157.3	124.1	149
292	307	24	0.030	0.00226	1.83	3	204.8	191.1	169.5	137
297	312	24	0.030	0.00226	1.83	3	265.8	211.7	221.7	163
302	317	24	0.030	0.00226	1.83	3	326.9	283.1	275.9	146
307	322	24	0.030	0.00226	1.83	3	388.2	372.1	328.0	128
312	327	24	0.030	0.00226	1.83	3	449.6	457.6	372.9	201
317	332	24	0.030	0.00226	1.83	3	511.1	592.2	408.7	170

Table A6 Results when the temperatures of the brine solution and the cooling water is varied.

Experimental conditions							Mass flux			Permeate
T_c [K]	T_b [K]	l_1 micron	u_b [m/s]	u_c [m/s]	l_2 [mm]	c_b [% NaCl]	Empirical [g/(h.m^2)]	Experimental [g/(h.m^2)]	Fundamental [g/(h.m^2)]	quality [micro S/cm]
291	331	24	0.030	0.00226	1.83	0	880.4	842.3	873.7	0
291	331	24	0.030	0.00226	1.83	2	820.4	810.0	865.3	83
291	331	24	0.030	0.00226	1.83	4	765.6	779.1	855.1	77
291	331	24	0.030	0.00226	1.83	6	716.3	740.0	844.7	58
291	331	24	0.030	0.00226	1.83	8	672.2	709.8	833.4	71
291	331	24	0.030	0.00226	1.83	10	633.5	698.3	821.9	153
291	331	24	0.030	0.00226	1.83	12	600.1	653.9	809.4	206
291	331	24	0.030	0.00226	1.83	14	572.0	640.8	796.8	126
291	331	24	0.030	0.00226	1.83	16	549.3	601.5	783.3	130
291	331	24	0.030	0.00226	1.83	18	531.8	543.6	768.7	132
291	331	24	0.030	0.00226	1.83	20	519.8	501.2	755.0	135
291	331	24	0.030	0.00226	1.83	22	513.0	485.9	740.3	376
291	331	24	0.030	0.00226	1.83	24	511.6	443.0	725.5	125
291	331	24	0.030	0.00226	1.83	26	515.5	416.7	709.7	184

Table A7 Results when the concentration of the NaCl is varied.

Experimental conditions							Mass flux			Permeate
T_c [K]	T_b [K]	l_1 micron	u_b [m/s]	u_c [m/s]	l_2 [mm]	c_b [% NaCl]	Empirical [g/(h.m^2)]	Experimental [g/(h.m^2)]	Fundamental [g/(h.m^2)]	quality [micro S/cm]
293	331	24	0.009	0.00226	1.83	3	624.1	578.8	584.7	220
293	331	24	0.014	0.00226	1.83	3	674.7	669.1	688.2	75
293	331	24	0.020	0.00226	1.83	3	719.7	772.2	754.2	64
293	331	24	0.025	0.00226	1.83	3	759.2	790.5	799.6	56
293	331	24	0.030	0.00226	1.83	3	793.2	758.8	834.5	56
291	331	24	0.030	0.00090	1.83	3	750.1	669.1	779.8	96
291	331	24	0.030	0.00226	1.83	3	792.3	779.6	870.1	87
291	331	24	0.030	0.00452	1.83	3	826.9	764.0	900.6	96
291	331	24	0.030	0.00679	1.83	3	816.7	792.2	918.5	111
291	331	24	0.030	0.00905	1.83	3	761.7	782.8	929.0	124

Table A8 Results when the linear veolcity of the cooling water and the brine solution is varied.

Experimental conditions							Mass flux			Permeate
T_c [K]	T_b [K]	l_1 micron	u_b [m/s]	u_c [m/s]	l_2 [mm]	c_b [% NaCl]	Empirical [g/(h.m^2)]	Experimental [g/(h.m^2)]	Fundamental [g/(h.m^2)]	quality [micro S/cm]
289	325	12	0.024	0.00226	3.2	3	-	826.7	816.2	12430
289	325	24	0.024	0.00226	3.2	3	-	620.8	622.7	30
289	325	36	0.024	0.00226	3.2	3	-	-	500.5	-
289	325	48	0.024	0.00226	3.2	3	-	-	417.6	-
289	325	60	0.024	0.00226	3.2	3	-	-	358.3	-
289	325	72	0.024	0.00226	3.2	3	-	-	313.6	-

Table A9 Results when the membrane thickness is varied.

Experimental conditions							Mass flux		
T_c [K]	T_b [K]	l_1 micron	u_b [m/s]	u_c [m/s]	l_2 [mm]	. c_b [% NaCl]	Empirical [g/(h.m^2)]	Experimental [g/(h.m^2)]	Fundamental [g/(h.m^2)]
297	331	24	0.030	0.00226	9.15	10	427.6	364.4	551.7
297	318	24	0.030	0.00226	9.15	10	196.5	177.3	247.9
306	318	24	0.030	0.00226	9.15	10	70.8	92.5	155.5
306	331	24	0.030	0.00226	9.15	10	340.9	287.8	456.2
306	318	24	0.030	0.00226	9.15	3	92.1	89.0	175.3
306	331	24	0.030	0.00226	9.15	3	499.8	326.3	486.9
297	331	24	0.030	0.00226	9.15	3	586.5	364.8	580.0
297	318	24	0.030	0.00226	9.15	3	217.8	164.0	265.8
297	318	24	0.030	0.00226	1.83	3	413.4	536.0	376.7
306	318	24	0.030	0.00226	1.83	3	287.8	311.4	273.4
306	331	24	0.030	0.00226	1.83	3	695.5	853.2	633.2
297	331	24	0.030	0.00226	1.83	3	782.1	1000.0	787.9
297	331	24	0.030	0.00226	1.83	10	623.3	756.4	746.2
297	318	24	0.030	0.00226	1.83	10	392.1	407.7	348.0
306	318	24	0.030	0.00226	1.83	10	266.5	140.0	203.9
306	331	24	0.030	0.00226	1.83	10	536.6	650.5	587.6

Table A10 Results from factorial design.

T_c [K]	Qcond [W]	Q [W]	Qeff	TPC	c_sur [% (NaCl)]	h [W/m^2.K]
296	11.0	30.5	0.6387	0.5863	12.9	249
301	9.3	27.2	0.6570	0.5761	12.0	250
306	7.7	23.5	0.6732	0.5657	11.0	250
311	6.1	19.5	0.6892	0.5552	9.8	251
316	4.5	15.2	0.7046	0.5447	8.4	251
321	3.0	10.5	0.7190	0.5343	6.7	252
326	1.5	5.4	0.7315	0.5242	4.7	252

Table A11 Results from the fundamental model (T_b = 331 K, c_b = 3%, l_2 = 1.83 mm l_1 = 24 micron, u_b = 0.03 m/s, u_c = 0.00226 m/s).

T_b [K]	c_b [% (NaCl)]	Qcond [W]	Q [W]	Qeff	TPC	c_sur [% (NaCl)]	h [W/m^2.K]
302	0	1.4	2.5	0.4360	0.6859	0.0	194
307	0	3.1	6.0	0.4850	0.6653	0.1	203
312	0	4.7	10.0	0.5310	0.644	0.2	212
317	0	6.2	14.6	0.5740	0.6234	0.3	221
322	0	7.7	19.6	0.6077	0.605	0.3	230
327	0	9.1	24.9	0.6329	0.5901	0.5	239
332	0	10.6	30.3	0.6498	0.5791	0.6	247
337	0	12.1	35.7	0.6602	0.5718	0.7	255
342	0	13.7	41.1	0.6667	0.5678	0.8	263
347	0	15.3	46.4	0.6694	0.5661	0.9	271
352	0	17.1	51.6	0.6696	0.5659	1.0	279
357	0	18.8	56.8	0.6690	0.5664	1.2	287
302	10	1.4	2.5	0.4360	0.6891	10.4	203
307	10	3.1	6.0	0.4817	0.6685	11.6	213
312	10	4.7	10.1	0.5327	0.6471	12.9	223
317	10	6.3	14.7	0.5748	0.6265	14.2	233
322	10	7.7	19.7	0.6071	0.6083	15.4	242
327	10	9.2	25.0	0.6320	0.5934	16.5	251
332	10	10.7	30.4	0.6487	0.5826	17.4	261
337	10	12.2	35.9	0.6599	0.5755	18.2	269
342	10	13.8	41.3	0.6659	0.5717	18.8	278
347	10	15.5	46.5	0.6675	0.5701	19.3	287
352	10	17.2	51.8	0.6683	0.57	19.6	295
357	10	19.0	56.9	0.6670	0.5706	19.9	303

Table A12 Results from the fundamental model (T_c = 298 K, l_2 = 1.83 mm, u_b = 0.03 m/s, u_c = 0.00226 m/s, l_1 = 24 micron).

T_b [K]	c_b [% (NaCl)]	Qcond [W]	Q [W]	Qeff	TPC	c_sur [% (NaCl)]	h [W/m^2.K
296	3	1.8	2.7	0.3333	0.7173	4.0	185
301	3	3.6	5.7	0.3772	0.7012	5.3	194
306	3	5.2	9.3	0.4376	0.6827	6.7	204
311	3	6.8	13.3	0.4865	0.6628	8.2	213
316	3	8.4	17.9	0.5335	0.6427	9.8	222
321	3	9.8	22.9	0.5712	0.6242	11.2	231
326	3	11.3	28.1	0.5989	0.6084	12.5	240
331	3	12.7	33.5	0.6197	0.5963	13.6	249
336	3	14.3	38.9	0.6337	0.5879	14.4	258
341	3	15.8	44.3	0.6424	0.5828	15.1	266
346	3	17.5	49.5	0.6467	0.5803	15.6	274
351	3	19.2	54.6	0.6480	0.5795	16.0	282
356	3	21.0	59.6	0.6477	0.5795	16.3	290

Table A13 Results from the fundamental model (T_c = 298 K, l_2 = 1.83 mm, u_b = 0.03 m/s, u_c = 0.00226 m/s, l_1 = 24 micron).

l_2 [mm]	c_b [% NaCl]	Qcond [W]	Q [W]	Qeff	TPC	c_sur [% (NaCl)]	h [W/m^2.K
1.83	0	12.7	33.5	0.6206	0.5953	11.9	245
1.83	3	12.7	33.5	0.6197	0.5963	13.6	249
1.83	10	12.8	33.7	0.6208	0.5983	18.1	258
1.83	15	12.8	33.8	0.6210	0.5996	21.9	264
3.66	0	7.3	26.2	0.7214	0.6828	11.2	246
3.66	3	7.3	26.2	0.7210	0.6837	12.9	250
3.66	10	7.3	26.3	0.7213	0.6857	17.6	259
3.66	15	7.4	26.3	0.7205	0.6869	21.4	265
5.49	0	5.2	22.2	0.7653	0.7317	10.3	246
5.49	3	5.2	22.1	0.7638	0.7326	12.1	250
5.49	10	5.2	22.2	0.7644	0.7344	17.0	260
5.49	15	5.2	22.2	0.7640	0.7355	20.9	265
7.32	0	4.1	19.3	0.7881	0.7656	9.6	247
7.32	3	4.1	19.3	0.7881	0.7664	11.4	251
7.32	10	4.1	19.4	0.7887	0.7681	16.4	260
7.32	15	4.1	19.4	0.7881	0.7692	20.4	266
9.15	0	3.4	17.2	0.8035	0.7911	8.9	247
9.15	3	3.4	17.2	0.8035	0.7919	10.8	251
9.15	10	3.4	17.2	0.8029	0.7935	15.9	260
9.15	15	3.4	17.2	0.8023	0.7946	19.9	266

Table A14 Results from the fundamental model (T_b = 331 K, T_c = 291 K, u_b = 0.03 m/s, u_c = 0.00226 m/s, l_1 = 24 micron).

l_2 [mm]	c_b [% NaCl]	Qcond [W]	Q [W]	Qeff	TPC	c_sur [% (NaCl)]	h [W/m^2.K]
1.83	0	12.7	33.5	0.6206	0.5953	11.9	245
3.66	0	7.3	26.2	0.7214	0.6828	11.2	246
5.49	0	5.2	22.2	0.7653	0.7317	10.3	246
7.32	0	4.1	19.3	0.7881	0.7656	9.6	247
9.15	0	3.4	17.2	0.8035	0.7911	8.9	247
1.83	3	12.7	33.5	0.6197	0.5963	13.6	249
3.66	3	7.3	26.2	0.7210	0.6837	12.9	250
5.49	3	5.2	22.1	0.7638	0.7326	12.1	250
7.32	3	4.1	19.3	0.7881	0.7664	11.4	251
9.15	3	3.4	17.2	0.8035	0.7919	10.8	251
1.83	10	12.8	33.7	0.6208	0.5983	18.1	258
3.66	10	7.3	26.3	0.7213	0.6857	17.6	259
5.49	10	5.2	22.2	0.7644	0.7344	17.0	260
7.32	10	4.1	19.4	0.7887	0.7681	16.4	260
9.15	10	3.4	17.2	0.8029	0.7935	15.9	260
1.83	15	12.8	33.8	0.6210	0.5996	21.9	264
3.66	15	7.4	26.3	0.7205	0.6869	21.4	265
5.49	15	5.2	22.2	0.7640	0.7355	20.9	265
7.32	15	4.1	19.4	0.7881	0.7692	20.4	266
9.15	15	3.4	17.2	0.8023	0.7946	19.9	266

Table A15 Results from the fundamental model (T_b = 331 K, T_c = 291 K, u_b = 0.03 m/s, u_c = 0.00226 m/s, l_1 = 24 micron).

T_c [K]	T_b [K]	Qcond [W]	Q [W]	Qeff	TPC	c_sur [% (NaCl)]	h [W/m^2.K]
282	297	5.4	7.6	0.2895	0.7237	5.7	186
287	302	5.3	8.4	0.3655	0.7031	6.2	196
292	307	5.2	9.5	0.4516	0.6771	6.8	206
297	312	5.1	10.7	0.5280	0.6471	7.4	216
302	317	4.9	12.0	0.5942	0.6158	7.9	225
307	322	4.7	13.2	0.6432	0.5862	8.2	235
312	327	4.6	14.4	0.6826	0.561	8.3	244
317	332	4.5	15.4	0.7097	0.5412	8.4	253

Table A16 Results from the fundamental model (c = 3 %, l_2 = 1.83 mm, u_b = 0.03 m/s, u_c = 0.00226 m/s, l_1 = 24 micron).

C_b [% NaCl]	Qcond [W]	Q [W]	Qeff	TPC	c_sur [% (NaCl)]	h [W/m^2.K]
0	12.7	33.5	0.6206	0.5953	11.9	245
2	12.7	33.5	0.6200	0.596	13.0	248
4	12.7	33.6	0.6208	0.5966	14.2	250
6	12.8	33.6	0.6202	0.5972	15.4	253
8	12.8	33.6	0.6199	0.5978	16.7	256
10	12.8	33.7	0.6208	0.5983	18.1	258
12	12.8	33.7	0.6205	0.5989	19.6	261
14	12.8	33.7	0.6199	0.5994	21.1	263
16	12.8	33.8	0.6207	0.5998	22.6	265
18	12.8	33.8	0.6204	0.6003	24.2	267
20	12.8	33.8	0.6201	0.6007	25.9	269
22	12.9	33.8	0.6198	0.6012	27.5	271
24	12.9	33.9	0.6206	0.6016	29.2	273
26	12.9	33.9	0.6206	0.6019	30.9	275

Table A17 Results from the fundamental model (T_b = 331 K, T_c = 291 K, l_2 = 1.83 u_b = 0.03 m/s, u_c = 0.00226 m/s, l_1 = 24 micron).

u_b [m/s]	Qcond [W]	Q [W]	Qeff	TPC	c_sur [% (NaCl)]	h [W/m^2.K]
0.009	10.6	26.8	0.6063	0.5236	20.0	97
0.014	11.2	29.3	0.6174	0.5538	17.5	138
0.020	11.6	30.7	0.6225	0.5715	15.7	176
0.025	11.9	31.6	0.6250	0.5834	14.4	212
0.030	12.0	32.3	0.6272	0.5919	13.4	247

Table A18 Results from the fundamental model (T_b = 331 K, T_c = 293 K, l_2 = 1.83 c_b = 3% (NaCl), u_c = 0.00226 m/s, l_1 = 24 micron).

u_c [m/s]	Qcond [W]	Q [W]	Qeff	TPC	c_sur [% (NaCl)]	h [W/m^2.K]
0.00090	10.7	29.8	0.6426	0.4955	12.7	250
0.00226	13.0	34.0	0.6171	0.5963	13.6	249
0.00452	14.0	35.6	0.6062	0.6595	14.0	249
0.00679	14.7	36.5	0.5984	0.6909	14.2	249
0.00905	15.1	37.1	0.5941	0.7105	14.3	249

Table A19 Results from the fundamental model (T_b = 331 K, T_c = 291 K, l_2 = 1.83 c_b = 3% (NaCl), u_b = 0.03 m/s, l_1 = 24 micron).

l_1 [micron]	Qcond [W]	Q [W]	Qeff	TPC	c_sur [% (NaCl)]	h [W/m^2.K]
12	6.62	27.31	0.7576	0.6077	15.8	199
24	7.37	22.31	0.6697	0.6791	13.2	199.6
36	7.79	19.45	0.5995	0.72	11.4	200
48	8.06	17.61	0.5423	0.7464	10.2	200.2
60	8.24	16.32	0.4951	0.7649	9.3	200.3
72	8.37	15.37	0.4554	0.7785	8.6	200.5

Table A20 Results from the fundamental model (T_b = 325 K, T_c = 289 K, l_2 = 3.2 c_b = 3% (NaCl), u_b = 0.024 m/s, u_c = 0.00226 m/s).

	Mass transfer resistances		
T_c [K]	Membrane	Air gap [s.mol/m^3.g]	Boundary layer
296	352.26	87.23	353786
301	353.73	84.84	352448
306	355.58	82.44	351007
311	357.83	80.03	349454
316	360.54	77.6	347788
321	363.74	75.15	346020
326	367.46	72.68	344150

Table A21 Mass transfer resistances
(T_b = 331 K, c_b = 3%, l_2 = 1.83 mm
u_b = 0.03 m/s, u_c = 0.00226 m/s, l_1 = 24 micron).

		Mass transfer resistances		
T_b [K]	c_b [% (NaCl)]	Membrane	Air gap [s.mol/m^3.g]	Boundary layer
296	3	511	110	754006
301	3	444	107	664882
306	3	393	105	590390
311	3	356	102	527636
316	3	334	99	474337
321	3	327	96	428693
326	3	332	93	389280
331	3	351	90	355008
336	3	383	86	325000
341	3	426	83	298610
346	3	481	79	275287
351	3	547	76	254608
356	3	622	72	236214

Table A22 Mass transfer resistances
(T_c = 291 K, l_2 = 1.83 mm, l_1 = 24 micron
u_b = 0.03 m/s, u_c = 0.00226 m/s).

		Mass transfer resistances		
T_b [K]	c_b [% (NaCl)]	Membrane	Air gap	Boundary layer
			[s.mol/m^3.g]	
302	0	423	103	0
307	0	377	101	0
312	0	346	98	0
317	0	329	95	0
322	0	326	92	0
327	0	335	89	0
332	0	358	86	0
337	0	393	82	0
342	0	439	79	0
347	0	497	75	0
352	0	564	71	0
357	0	640	67	0
302	10	423	103	630379
307	10	377	101	560409
312	10	346	98	501355
317	10	329	95	451117
322	10	326	92	408027
327	10	336	89	370769
332	10	359	86	338327
337	10	395	82	309907
342	10	442	79	284886
347	10	500	75	262767
352	10	569	72	243140
357	10	646	68	225669

Table A23 Mass transfer resistances
(T_c = 291 K, l_2 = 1.83 mm, l_1 = 24 micron
u_b = 0.03 m/s, u_c = 0.00226 m/s).

		Mass transfer resistances		
l_2 [mm]	c_b [% (NaCl)]	Membrane	Air gap	Boundary layer
		[s.mol/m^3.g]		
1.83	0	351	90	0
1.83	3	351	90	355008
1.83	10	352	90	346127
1.83	15	352	90	340684
3.66	0	353	179	0
3.66	3	353	179	351987
3.66	10	354	180	343245
3.66	15	354	180	337884
5.49	0	355	269	0
5.49	3	355	269	350364
5.49	10	356	270	341697
5.49	15	356	270	336380
7.32	0	357	359	0
7.32	3	357	360	349273
7.32	10	358	360	340659
7.32	15	358	361	335370
9.15	0	358	450	0
9.15	3	358	450	348459
9.15	10	359	451	339881
9.15	15	359	452	334620

Table A24 Mass transfer resistances
(T_b = 331 K, T_c = 291 K, l_2 = 1.83 mm, l_1 = 24 micron u_b = 0.03 m/s, u_c = 0.00226 m/s).

		Mass transfer resistances		
l_2 [mm]	c_b [% (NaCl)]	Membrane	Air gap	Boundary layer
		[s.mol/m^3.g]		
1.83	0	351	90	0
3.66	0	353	179	0
5.49	0	355	269	0
7.32	0	357	359	0
9.15	0	358	450	0
1.83	3	351	90	355008
3.66	3	353	179	351987
5.49	3	355	269	350364
7.32	3	357	360	349273
9.15	3	358	450	348459
1.83	10	352	90	346127
3.66	10	354	180	343245
5.49	10	356	270	341697
7.32	10	358	360	340659
9.15	10	359	451	339881
1.83	15	352	90	340684
3.66	15	354	180	337884
5.49	15	356	270	336380
7.32	15	358	361	335370
9.15	15	359	452	334620

Table A25 Mass transfer resistances
(T_b = 331 K, T_c = 291 K, l_2 = 1.83 mm, l_1 = 24 micron u_b = 0.03 m/s, u_c = 0.00226 m/s).

		Mass transfer resistances		
T_c [K]	T_b [K]	Membrane	Air gap	Boundary layer
		[s.mol/m^3.g]		
282	297	511	114	741897
287	302	438	109	651530
292	307	383	104	576432
297	312	347	98	513419
302	317	327	93	460055
307	322	325	88	414502
312	327	339	82	375308
317	332	368	76	341372

Table A26 Mass transfer resistances
(c = 3 % (NaCl), l_2 = 1.83 mm, l_1 = 24 micron u_b = 0.03 m/s, u_c = 0.00226 m/s).

c_b [% (NaCl)]	Mass transfer resistances		
	Membrane	Air gap	Boundary layer
	[s.mol/m^3.g]		
0	350.77	89.57	0
2	351.01	89.61	356404
4	351.23	89.64	353639
6	351.45	89.67	351010
8	351.65	89.71	348505
10	351.85	89.75	346127
12	352.04	89.79	343863
14	352.21	89.83	341718
16	352.38	89.88	339678
18	352.54	89.92	337740
20	352.69	89.97	335919
22	352.83	90.02	334194
24	352.97	90.07	332570
26	353.1	90.12	331035

Table A27 Mass transfer resistances
(T_b = 331 K, T_c = 291 K, l_2 = 1.83 mm
u_b = 0.03 m/s, u_c = 0.00226 m/s, l_1 = 24 micro

u_b [m/s]	Mass transfer resistances		
	Membrane	Air gap	Boundary layer
	[s.mol/m^3.g]		
0.009	331.45	92.13	934373
0.014	338.4	90.63	649783
0.020	344.65	89.62	505621
0.025	348.51	89.07	417476
0.030	351.54	88.67	357583

Table A28 Mass transfer resistances
(T_b = 331 K, T_c = 293 K, l_2 = 1.83 mm,
c_b = 3 % (NaCl), u_c = 0.00226 m/s, l_1 = 24 m

u_c [m/s]	Mass transfer resistances		
	Membrane	Air gap	Boundary layer
	[s.mol/m^3.g]		
0.00090	352.55	86.72	353502
0.00226	351.12	89.62	355196
0.00452	350.46	91.4	355834
0.00679	350.2	92.26	356227
0.00905	350.05	92.8	356462

Table A29 Mass transfer resistances
(T_b = 331 K, T_c = 291 K, l_2 = 1.83 mm
c_b = 3 % (NaCl), u_b = 0.03 m/s, l_1 = 24 micro

	Mass transfer resistances		
l_1 [micron]	Membrane	Air gap	Boundary layer
	[s.mol/m^3.g]		
12	163.29	164.63	477277
24	328.36	165.64	473893
36	494.32	166.22	471991
48	660.75	166.59	470776
60	827.48	166.85	469944
72	994.38	167.04	469331

Table A30 Mass transfer resistances
(T_b = 325 K, T_c = 289 K, l_2 = 3.2 mm
c_b = 3 % (NaCl), u_b = 0.03 m/s,
u_c = 0.00226 m/s, l_1 = 24 micron).

T_c [K]	R11 [K/W]	R12 [K/W]	R1t [K/W]	Rc1 [K/W]	Rc2 [K/W]	R22 [K/W]	R221 [K/W]	R23 [K/W]	R2t [K/W]	R3 [K/W]	R4 [K/W]	R5 [K/W]
296	0.125	30.20	0.125	0.013	1.85	74.52	75.09	1.067	0.675	0.0090	0.0030	0.338
301	0.125	33.47	0.125	0.013	1.84	82.51	83.06	0.979	0.638	0.0084	0.0030	0.332
306	0.125	38.28	0.124	0.013	1.83	94.26	94.81	0.901	0.603	0.0078	0.0030	0.326
311	0.125	45.94	0.124	0.013	1.82	113.01	113.54	0.831	0.570	0.0072	0.0030	0.321
316	0.124	59.63	0.124	0.013	1.81	146.54	147.07	0.768	0.539	0.0065	0.0030	0.316
321	0.124	89.76	0.124	0.013	1.80	220.36	220.91	0.712	0.511	0.0056	0.0029	0.312
326	0.124	205.76	0.124	0.013	1.79	504.59	505.22	0.662	0.484	0.0044	0.0029	0.308

Table A31 Heat transfer resistances (T_b = 331 K, c_b = 3%, l_1 = 24 micron, l_2 = 1.83 mm, u_b = 0.03 m/s, u_c = 0.00226

T_b [K]	R11 [K/W]	R12 [K/W]	R1t [K/W]	Rc1 [K/W]	Rc2 [K/W]	R22 [K/W]	R221 [K/W]	R23 [K/W]	R2t [K/W]	R3 [K/W]	R4 [K/W]	R5 [K/W]
296	0.169	785.91	0.169	0.013	1.98	1929.34	1930.66	4.147	1.344	0.0045	0.0031	0.353
301	0.161	291.54	0.161	0.013	1.96	716.33	717.40	3.234	1.225	0.0057	0.0031	0.352
306	0.153	153.08	0.153	0.013	1.94	376.49	377.39	2.556	1.107	0.0066	0.0031	0.351
311	0.147	93.49	0.146	0.013	1.93	230.16	230.95	2.061	0.997	0.0074	0.0031	0.350
316	0.141	62.85	0.140	0.013	1.91	154.88	155.58	1.705	0.901	0.0080	0.0031	0.348
321	0.135	45.41	0.135	0.013	1.89	112.00	112.64	1.454	0.822	0.0086	0.0030	0.347
326	0.130	34.80	0.130	0.013	1.88	85.89	86.49	1.281	0.760	0.0091	0.0030	0.346
331	0.125	27.93	0.125	0.013	1.86	68.98	69.57	1.166	0.715	0.0095	0.0030	0.344
336	0.121	23.33	0.121	0.013	1.84	57.63	58.21	1.092	0.683	0.0099	0.0030	0.343
341	0.117	20.03	0.117	0.013	1.83	49.51	50.10	1.047	0.663	0.0102	0.0030	0.341
346	0.114	17.62	0.113	0.013	1.81	43.55	44.15	1.022	0.650	0.0104	0.0030	0.340
351	0.111	15.75	0.110	0.013	1.80	38.94	39.56	1.009	0.642	0.0106	0.0030	0.339
356	0.108	14.26	0.107	0.013	1.78	35.25	35.90	1.002	0.637	0.0108	0.0030	0.338

Table A32 Heat transfer resistances (T_c = 291 K, l_1 = 24 micron, l_2 = 1.83 mm, u_b = 0.03 m/s, u_c = 0.00226 m/s).

T_b [K]	R11 [K/W]	R12 [K/W]	R1t [K/W]	Rc1 [K/W]	Rc2 [K/W]	R22 [K/W]	R221 [K/W]	R23 [K/W]	R2t [K/W]	R3 [K/W]	R4 [K/W]	R5 [K/W]
302	0.161	547.79	0.161	0.013	1.94	1345.22	1346.11	2.597	1.114	0.0041	0.0030	0.342
307	0.154	190.65	0.154	0.013	1.92	468.60	469.34	2.076	1.001	0.0055	0.0030	0.341
312	0.147	101.03	0.147	0.013	1.91	248.54	249.18	1.697	0.899	0.0064	0.0030	0.340
317	0.141	63.34	0.141	0.013	1.89	155.96	156.53	1.424	0.813	0.0072	0.0030	0.339
322	0.136	43.97	0.135	0.013	1.87	108.35	108.87	1.233	0.743	0.0078	0.0030	0.337
327	0.131	32.83	0.130	0.013	1.86	80.94	81.44	1.103	0.691	0.0084	0.0030	0.336
332	0.127	25.91	0.126	0.013	1.84	63.90	64.39	1.017	0.653	0.0088	0.0030	0.335
337	0.122	21.34	0.122	0.013	1.83	52.66	53.15	0.963	0.628	0.0092	0.0030	0.334
342	0.119	18.18	0.118	0.013	1.81	44.86	45.34	0.931	0.612	0.0095	0.0030	0.333
347	0.115	15.88	0.114	0.013	1.80	39.20	39.71	0.915	0.603	0.0098	0.0030	0.331
352	0.112	14.13	0.111	0.013	1.78	34.87	35.39	0.907	0.597	0.0101	0.0030	0.330
357	0.109	12.74	0.108	0.013	1.77	31.44	31.98	0.905	0.594	0.0103	0.0030	0.329
302	0.154	1210.06	0.154	0.013	1.94	2971.59	2973.56	2.596	1.114	0.0041	0.0030	0.342
307	0.147	269.45	0.147	0.013	1.92	662.28	663.33	2.073	1.001	0.0055	0.0030	0.341
312	0.140	130.90	0.140	0.013	1.91	322.02	322.85	1.693	0.898	0.0064	0.0030	0.340
317	0.134	79.43	0.134	0.013	1.89	195.55	196.27	1.421	0.812	0.0072	0.0030	0.339
322	0.129	54.34	0.129	0.013	1.87	133.89	134.54	1.230	0.743	0.0078	0.0030	0.337
327	0.124	40.32	0.124	0.013	1.86	99.41	100.03	1.101	0.691	0.0084	0.0030	0.336
332	0.120	31.73	0.120	0.013	1.84	78.25	78.85	1.015	0.653	0.0088	0.0030	0.335
337	0.116	26.08	0.115	0.013	1.83	64.36	64.95	0.962	0.629	0.0092	0.0030	0.334
342	0.112	22.17	0.112	0.013	1.81	54.70	55.30	0.932	0.613	0.0096	0.0030	0.333
347	0.109	19.30	0.108	0.013	1.79	47.63	48.24	0.916	0.604	0.0098	0.0030	0.331
352	0.106	17.12	0.105	0.013	1.78	42.24	42.88	0.909	0.599	0.0101	0.0030	0.330
357	0.103	15.39	0.102	0.013	1.76	37.96	38.62	0.906	0.596	0.0103	0.0030	0.329

Table A33 Heat transfer resistances (T_c = 291 K, l_1 = 24 micron, l_2 = 1.83 mm, u_b = 0.03 m/s, u_c = 0.00226 m/s).

l_2 [mm]	C_b [% NaCl]	R11 [K/W]	R12 [K/W]	R1t [K/W]	Rc1 [K/W]	Rc2 [K/W]	R22 [K/W]	R221 [K/W]	R23 [K/W]	R2t [K/W]	R3 [K/W]	R4 [K/W]	R5 [K/W]
1.83	0	0.128	27.52	0.127	0.013	1.86	67.96	68.53	1.167	0.715	0.0095	0.0030	0.344
1.83	3	0.125	27.93	0.125	0.013	1.86	68.98	69.57	1.166	0.715	0.0095	0.0030	0.344
1.83	10	0.121	29.25	0.121	0.013	1.86	72.23	72.85	1.164	0.714	0.0095	0.0030	0.344
1.83	15	0.118	30.43	0.118	0.013	1.86	75.14	75.78	1.163	0.714	0.0095	0.0030	0.344
3.66	0	0.127	29.27	0.127	0.013	3.73	72.10	72.84	1.476	1.051	0.0089	0.0030	0.346
3.66	3	0.125	29.72	0.125	0.013	3.73	73.20	73.95	1.475	1.050	0.0089	0.0030	0.346
3.66	10	0.121	31.06	0.120	0.013	3.73	76.50	77.29	1.474	1.050	0.0089	0.0030	0.346
3.66	15	0.118	32.25	0.118	0.013	3.73	79.43	80.26	1.473	1.050	0.0089	0.0030	0.346
5.49	0	0.127	32.02	0.126	0.013	5.60	78.76	79.66	1.769	1.334	0.0085	0.0031	0.347
5.49	3	0.125	32.52	0.124	0.013	5.60	80.01	80.92	1.769	1.334	0.0085	0.0030	0.347
5.49	10	0.120	33.98	0.120	0.013	5.60	83.59	84.54	1.768	1.334	0.0085	0.0030	0.347
5.49	15	0.118	35.28	0.117	0.013	5.60	86.78	87.77	1.768	1.334	0.0085	0.0030	0.347
7.32	0	0.127	35.01	0.126	0.013	7.47	86.05	87.09	2.059	1.600	0.0082	0.0031	0.348
7.32	3	0.125	35.55	0.124	0.013	7.47	87.39	88.44	2.058	1.600	0.0082	0.0031	0.348
7.32	10	0.120	37.15	0.120	0.013	7.47	91.32	92.42	2.058	1.600	0.0082	0.0031	0.348
7.32	15	0.118	38.57	0.117	0.013	7.47	94.82	95.97	2.058	1.601	0.0082	0.0031	0.348
9.15	0	0.127	38.08	0.126	0.013	9.35	93.58	94.75	2.347	1.858	0.0079	0.0031	0.348
9.15	3	0.125	38.71	0.124	0.013	9.35	95.10	96.30	2.346	1.858	0.0079	0.0031	0.348
9.15	10	0.120	40.46	0.120	0.013	9.35	99.42	100.67	2.347	1.859	0.0079	0.0031	0.348
9.15	15	0.118	41.99	0.117	0.013	9.35	103.17	104.48	2.347	1.860	0.0079	0.0031	0.348

Table A34 Heat transfer resistances (T_b = 331 K, T_c = 291 K, l_1 = 24 micron, u_b = 0.03 m/s, u_c = 0.00226 m/s).

l_2 [mm]	C_b [% NaCl	R11 [K/W]	R12 [K/W]	R1t [K/W]	Rc1 [K/W]	Rc2 [K/W]	R22 [K/W]	R221 [K/W]	R23 [K/W]	R2t [K/W]	R3 [K/W]	R4 [K/W]	R5 [K/W]
1.83	0	0.128	27.52	0.127	0.013	1.86	67.96	68.53	1.167	0.715	0.0095	0.0030	0.344
3.66	0	0.127	29.27	0.127	0.013	3.73	72.10	72.84	1.476	1.051	0.0089	0.0030	0.346
5.49	0	0.127	32.02	0.126	0.013	5.60	78.76	79.66	1.769	1.334	0.0085	0.0031	0.347
7.32	0	0.127	35.01	0.126	0.013	7.47	86.05	87.09	2.059	1.600	0.0082	0.0031	0.348
9.15	0	0.127	38.08	0.126	0.013	9.35	93.58	94.75	2.347	1.858	0.0079	0.0031	0.348
1.83	3	0.125	27.93	0.125	0.013	1.86	68.98	69.57	1.166	0.715	0.0095	0.0030	0.344
3.66	3	0.125	29.72	0.125	0.013	3.73	73.20	73.95	1.475	1.050	0.0089	0.0030	0.346
5.49	3	0.125	32.52	0.124	0.013	5.60	80.01	80.92	1.769	1.334	0.0085	0.0030	0.347
7.32	3	0.125	35.55	0.124	0.013	7.47	87.39	88.44	2.058	1.600	0.0082	0.0031	0.348
9.15	3	0.125	38.71	0.124	0.013	9.35	95.10	96.30	2.346	1.858	0.0079	0.0031	0.348
1.83	10	0.121	29.25	0.121	0.013	1.86	72.23	72.85	1.164	0.714	0.0095	0.0030	0.344
3.66	10	0.121	31.06	0.120	0.013	3.73	76.50	77.29	1.474	1.050	0.0089	0.0030	0.346
5.49	10	0.120	33.98	0.120	0.013	5.60	83.59	84.54	1.768	1.334	0.0085	0.0030	0.347
7.32	10	0.120	37.15	0.120	0.013	7.47	91.32	92.42	2.058	1.600	0.0082	0.0031	0.348
9.15	10	0.120	40.46	0.120	0.013	9.35	99.42	100.67	2.347	1.859	0.0079	0.0031	0.348
1.83	15	0.118	30.43	0.118	0.013	1.86	75.14	75.78	1.163	0.714	0.0095	0.0030	0.344
3.66	15	0.118	32.25	0.118	0.013	3.73	79.43	80.26	1.473	1.050	0.0089	0.0030	0.346
5.49	15	0.118	35.28	0.117	0.013	5.60	86.78	87.77	1.768	1.334	0.0085	0.0030	0.347
7.32	15	0.118	38.57	0.117	0.013	7.47	94.82	95.97	2.058	1.601	0.0082	0.0031	0.348
9.15	15	0.118	41.99	0.117	0.013	9.35	103.17	104.48	2.347	1.860	0.0079	0.0031	0.348

Table A35 Heat transfer resistances (T_b = 331 K, T_c = 291 K, l_1 = 24 micron, u_b = 0.03 m/s, u_c = 0.00226 m/s).

T_c [K]	T_b [K]	R11 [K/W]	R12 [K/W]	R1t [K/W]	Rc1 [K/W]	Rc2 [K/W]	R22 [K/W]	R221 [K/W]	R23 [K/W]	R2t [K/W]	R3 [K/W]	R4 [K/W]	R5 [K/W]
282	297	0.168	278.32	0.168	0.013	2.00	683.86	685.09	4.964	1.429	0.0067	0.0031	0.367
287	302	0.160	197.31	0.160	0.013	1.97	485.07	486.11	3.400	1.250	0.0066	0.0031	0.358
292	307	0.152	144.09	0.152	0.013	1.94	354.42	355.29	2.387	1.072	0.0066	0.0031	0.349
297	312	0.145	109.80	0.145	0.013	1.91	270.15	270.89	1.733	0.910	0.0066	0.0030	0.341
302	317	0.139	87.95	0.139	0.013	1.88	216.42	217.07	1.311	0.774	0.0066	0.0030	0.334
307	322	0.133	73.72	0.133	0.013	1.86	181.37	181.95	1.039	0.666	0.0066	0.0030	0.327
312	327	0.128	64.61	0.128	0.013	1.83	158.89	159.44	0.863	0.587	0.0065	0.0030	0.321
317	332	0.124	58.75	0.123	0.013	1.80	144.35	144.88	0.749	0.529	0.0065	0.0030	0.315

Table A36 Heat transfer resistances (c_b = 3 % (NaCl), l_1 = 24 micron, l_2 = 1.83 mm, u_b = 0.03 m/s, u_c = 0.00226 m/s).

C_b [% NaCl]	R11 [K/W]	R12 [K/W]	R1t [K/W]	Rc1 [K/W]	Rc2 [K/W]	R22 [K/W]	R221 [K/W]	R23 [K/W]	R2t [K/W]	R3 [K/W]	R4 [K/W]	R5 [K/W]
0	0.128	27.52	0.127	0.013	1.86	67.96	68.53	1.167	0.715	0.0095	0.0030	0.344
2	0.126	27.78	0.126	0.013	1.86	68.61	69.19	1.166	0.715	0.0095	0.0030	0.344
4	0.125	28.12	0.124	0.013	1.86	69.43	70.02	1.165	0.715	0.0095	0.0030	0.344
6	0.123	28.46	0.123	0.013	1.86	70.28	70.88	1.165	0.715	0.0095	0.0030	0.344
8	0.122	28.85	0.122	0.013	1.86	71.24	71.85	1.164	0.714	0.0095	0.0030	0.344
10	0.121	29.25	0.121	0.013	1.86	72.23	72.85	1.164	0.714	0.0095	0.0030	0.344
12	0.120	29.70	0.119	0.013	1.86	73.34	73.97	1.163	0.714	0.0095	0.0030	0.344
14	0.119	30.17	0.118	0.013	1.86	74.50	75.13	1.163	0.714	0.0095	0.0030	0.344
16	0.118	30.69	0.117	0.013	1.86	75.79	76.44	1.163	0.714	0.0095	0.0030	0.344
18	0.117	31.27	0.117	0.013	1.86	77.22	77.88	1.162	0.714	0.0095	0.0030	0.344
20	0.116	31.84	0.116	0.013	1.86	78.62	79.30	1.162	0.714	0.0095	0.0030	0.344
22	0.115	32.47	0.115	0.013	1.86	80.18	80.87	1.162	0.714	0.0095	0.0030	0.344
24	0.115	33.14	0.114	0.013	1.86	81.82	82.52	1.161	0.714	0.0095	0.0030	0.344
26	0.114	33.87	0.113	0.013	1.86	83.64	84.36	1.161	0.714	0.0095	0.0030	0.344

Table A37 Heat transfer resistances (T_b = 331 K, T_c = 291 K, l_1 = 24 micron, l_2 = 1.83 mm, u_b = 0.03 m/s, u_c = 0.00226 m/s).

u_b [m/s]	R11 [K/W]	R12 [K/W]	R1t [K/W]	Rc1 [K/W]	Rc2 [K/W]	R22 [K/W]	R221 [K/W]	R23 [K/W]	R2t [K/W]	R3 [K/W]	R4 [K/W]	R5 [K/W]
0.009	0.322	41.19	0.320	0.013	1.87	101.81	102.49	1.237	0.744	0.0088	0.0030	0.343
0.014	0.227	34.97	0.225	0.013	1.87	86.38	87.01	1.182	0.722	0.0090	0.0030	0.342
0.020	0.178	31.90	0.177	0.013	1.86	78.77	79.38	1.154	0.711	0.0092	0.0030	0.342
0.025	0.147	30.07	0.146	0.013	1.86	74.25	74.85	1.137	0.704	0.0092	0.0030	0.342
0.030	0.126	28.81	0.126	0.013	1.86	71.12	71.70	1.125	0.699	0.0093	0.0030	0.341

Table A38 Heat transfer resistances (T_b = 331 K, T_c = 293 K, c_b = 3 % (NaCl), l_1 = 24 micron, l_2 = 1.83 mm, u_c = 0.0

u_c [m/s]	R11 [K/W]	R12 [K/W]	R1t [K/W]	Rc1 [K/W]	Rc2 [K/W]	R22 [K/W]	R221 [K/W]	R23 [K/W]	R2t [K/W]	R3 [K/W]	R4 [K/W]	R5 [K/W]
0.0009	0.125	30.83	0.125	0.013	1.85	76.04	76.61	1.047	0.667	0.0088	0.0030	0.540
0.00226	0.125	27.93	0.125	0.013	1.86	68.98	69.57	1.166	0.715	0.0095	0.0030	0.344
0.00452	0.126	26.69	0.125	0.013	1.87	65.96	66.56	1.247	0.746	0.0099	0.0030	0.245
0.00679	0.126	26.18	0.125	0.013	1.87	64.71	65.31	1.289	0.761	0.0101	0.0031	0.200
0.00905	0.126	25.88	0.125	0.013	1.87	63.99	64.60	1.316	0.771	0.0102	0.0031	0.174

Table A39 Heat transfer resistances (T_b = 331 K, T_c = 291 K, c_b = 3 % (NaCl), l_1 = 24 micron, l_2 = 1.83 mm, u_b = 0.0

l_1 [micron]	R11 [K/W]	R12 [K/W]	R1t [K/W]	Rc1 [K/W]	Rc2 [K/W]	R22 [K/W]	R221 [K/W]	R23 [K/W]	R2t [K/W]	R3 [K/W]	R4 [K/W]	R5 [K/W]
12	0.16	29.586	0.156	0.007	3.3000	72.911	73.445	1.073	0.806	0.009	0.003	0.349
24	0.16	38.765	0.156	0.013	3.3040	95.529	96.308	1.665	1.102	0.009	0.003	0.35
36	0.16	48.224	0.156	0.02	3.3070	118.834	119.858	2.265	1.340	0.008	0.003	0.351
48	0.16	57.789	0.156	0.026	3.3090	142.403	143.673	2.869	1.534	0.008	0.003	0.352
60	0.16	67.345	0.156	0.033	3.3100	165.947	167.461	3.475	1.695	0.008	0.003	0.352
72	0.16	76.947	0.156	0.039	3.3110	189.606	191.366	4.083	1.831	0.008	0.003	0.352

Table A40 Heat transfer resistances (T_b = 325 K, T_c = 289 K, c_b = 3 % (NaCl), l_2 = 3.2 mm, u_b = 0.03 m/s, u_c = 0.002

APPENDIX B
(FIGURES)

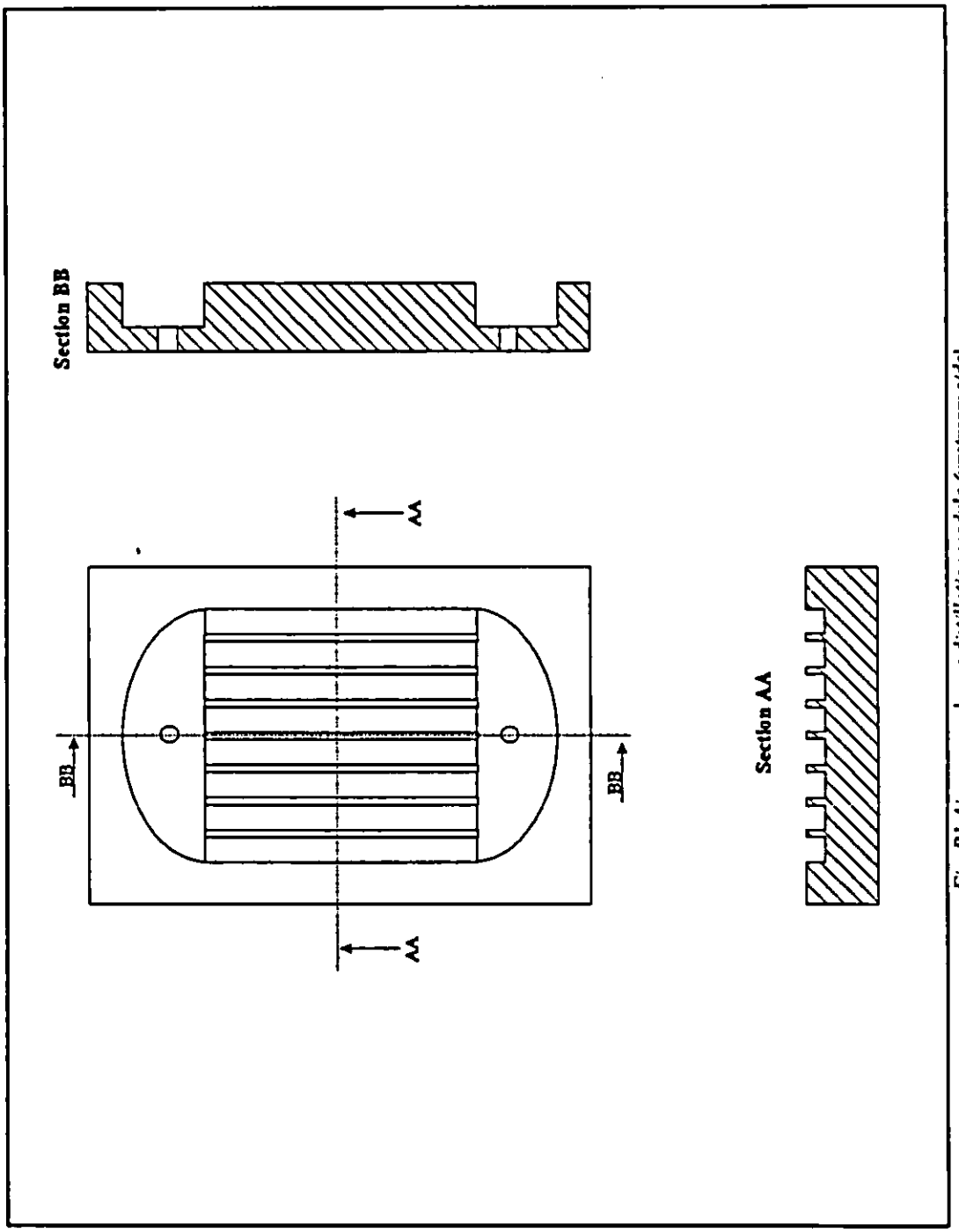

Fig. B1 Air gap membrane distillation module (upstream side).

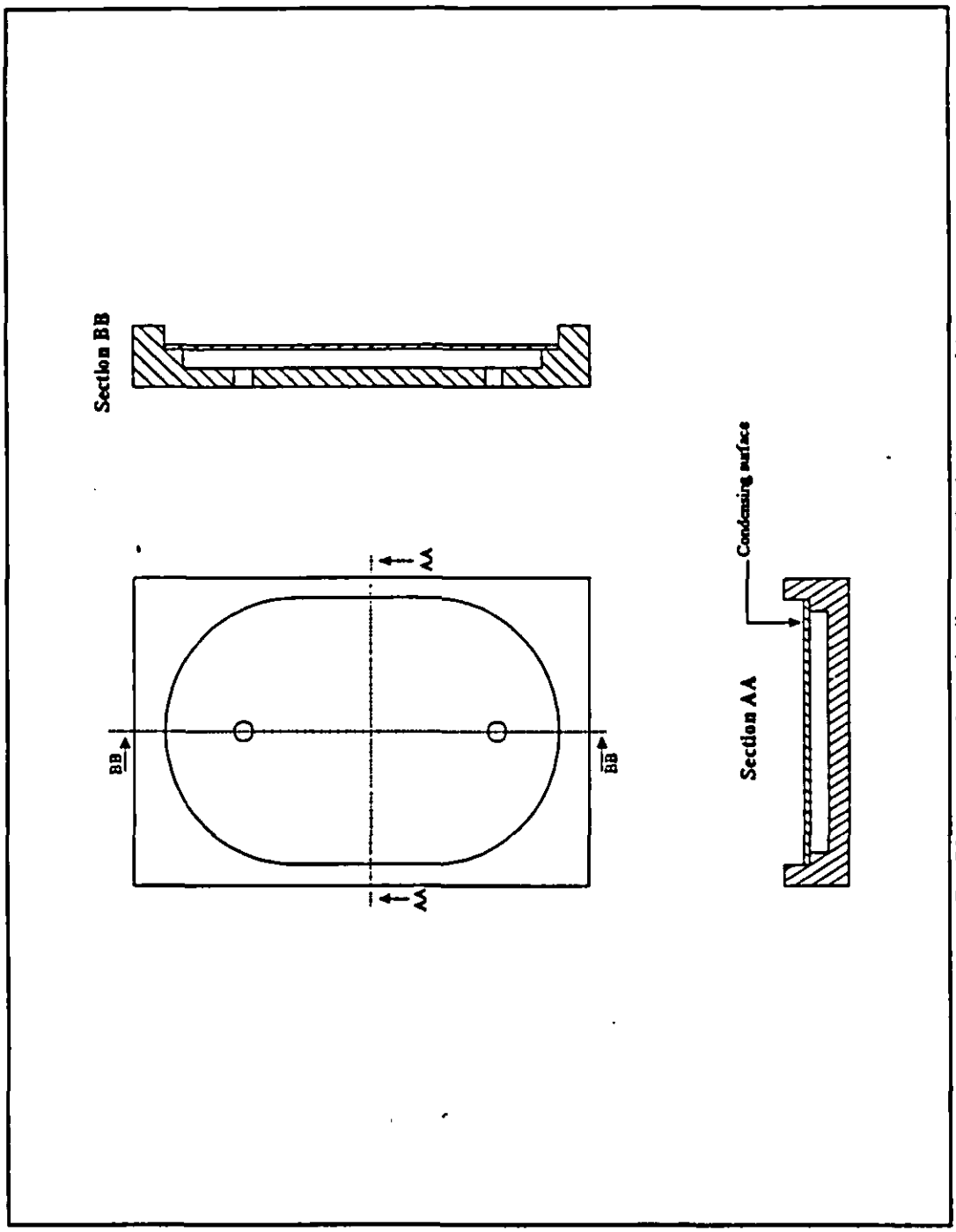

Fig. B2 Air gap membrane distillation module (downstream side).

APPENDIX C
(TURBO PASCAL PROGRAM)

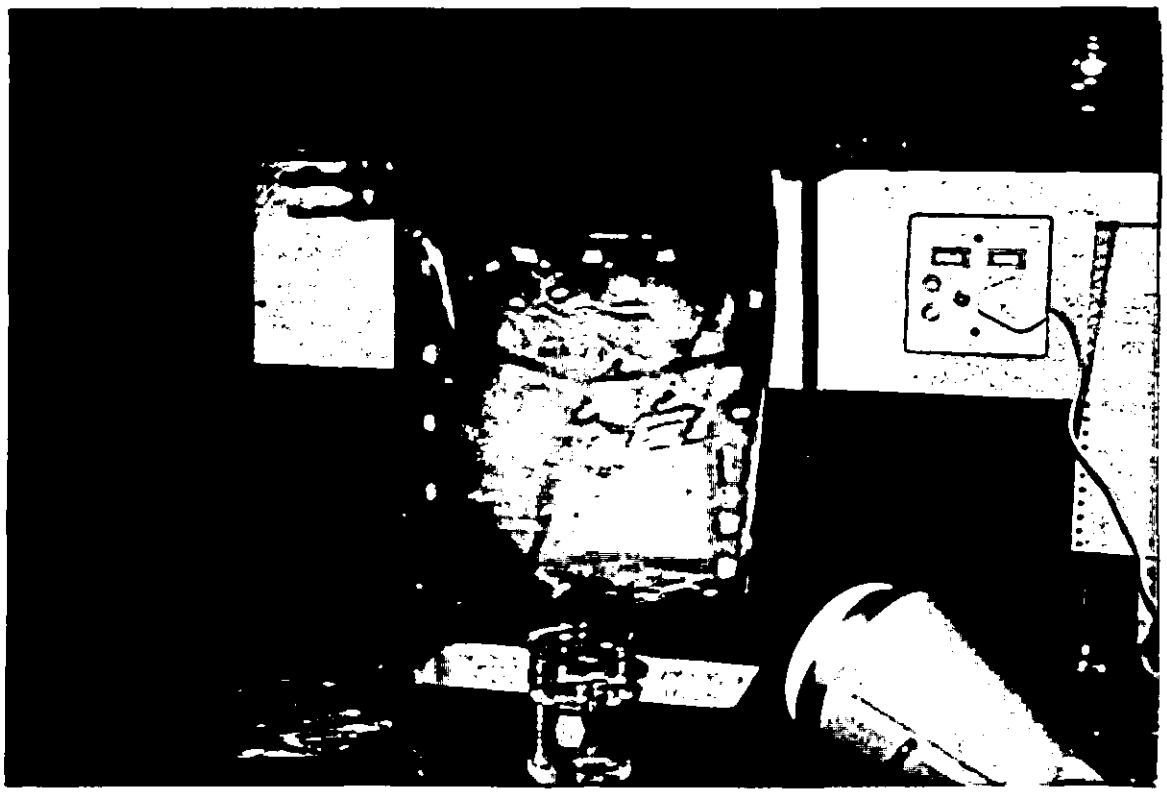

Fig. B3 Photograph of air gap membrane distillation unit.

```
program AGMD;
{$N+}        Emulates a math co-processor
uses Crt;
var
      Re,Nu,Sh,Pam,TPC,Q,Qcond,k,c21,c22,c1,c4,x21,
      T1,T7,T2,T3,T4,T5,T6, Ta1,Ta2,Ta3,Ta4, Ta5,Ta6,
      Rc1,Rc2,Rm1,Rm2,Rm3,Rm4,R11,R12,R1t,
      R21,R22,R23,R2t,R3,R3t,R4,R5,Rt,N,Np,
      R221, f1,f2,kss,z,cb,l2,ub,uc,fa,fb,csur,t,        : extended;
      InFile                                             : Text;
const
      A1    = 0.032;      Transfer area of membrane [m]
      A2    = 0.04*0.9;   Condensing surface area [m]
      cc    = 0;          Concentration of salt in cooling water [% (wt.)]
      cp    = 0;          Concentration of salt in permeate [% (wt%)]
      d1    = 1.6E-3;     Thickness of condensing surface [m]
      dH    = 0.2;        Characteristic length of membrane[m]
      dH2   = 0.2;        Characteristic length of condensing plate [m]
      g1    = 9.81;       Gravitational acceleration [m/s2]
      km    = 0.0576;     Thermal conductivity of membrane [W/m.K]
      l1    = 24E-6;      Thickness of membrane [m]
      M     = 18;         Molecular mass of H2O [g/mol]
      Mn    = 58.5;       Molecular mass of NaCl [g/mol]
      P     = 101325;     Total pressure [Pa]
```

```
R     = 8.314;     Universal gas constant [J/mol.K]
x     = 0.2;       [m]
```

To calculate the latent heat of evaporation for H_2O [J/g]

```
function hfg(T :real) : real;
begin
  hfg := 3168.2772-2.4353676*T;
end;
```

To calculate the spesific heat of water [J/g.K]

```
function cpf(T : real) : real;
begin
cpf:=  45.358904-0.49160618*T+0.002205092*sqr(T)-4.3807394E-
       6*sqr(T)*T+3.2759702E-9*sqr(sqr(T));
end;
```

To calculate the spesific. heat of H_2O vapour [J/g.K]

```
function cpg(T : real) : real;
begin
  cpg := 2.134852-1.1795944E-5*sqr(T)+2.952599E-8*T*sqr(T);
end;
```

Vapour pressure of NaCl as a function of concentration and temperature [Pa]

```
function VP(T,c : real) : real;
var
```

```
 a,b : real;
begin
 a := exp(-29.247931+0.15905282*T-0.00016886801*sqr(T));
 b := -3349.03+8.39513*T+376967/T-1.58194E-5*sqr(T)*T;
 VP := (a+b*c/Mn/0.1)/760*101325;
end;
```

To calculate the permeability coefficient of H_2O in membrane [g.m/(s.m^2.Pa)]

```
function Perm(T :real) : real;
 var
        f1 : real;
 const

 a = 1.1970891517;
 b = -1.08389038116;
begin
 f1 := exp(-sqr(T-317)/(2*sqr(67.2872925)));
 Perm := (1/(a+b*f1))/1E10;
 end;
```

Diffusion coefficient of H_2O-vapour in air [m^2/s]

```
function Dw(T : real) : real;
 begin
   Dw := exp(ln(0.26E-4)+2.334*ln(T/298));
 end;
```

Used in Clausius-Clapeyron equation [Pa/K]

```
function PMRT(T,c : real) : real;
begin
  PMRT := VP(T,c)*M*hfg(T)/(R*sqr(T));
end;
```

Density of brine solution as function of concentration and temperature [kg/m^3]

```
function dens(T,c : real) : real;
var
  a,b,ca : extended;
const
a1 = 1.47809652056;        a2 = 0.0985569923901;       a3 = -9.48586704271;
b1 = -0.00116210231391;    b2 = -0.000264393965564;    b3 = 0.144299456262;
c1 = -11942.9335297;       c2 = 7.53043492004E-10;     c3 = -0.000877534860513;
                           d2 = 3.99473928633E123;     d3 = 2.66598287932E-6;
                                                       e3 = -4.04541368844E-9;
                                                       f3 = 2.45238734929E-12;
begin
 a := a1+b1*T+c1/sqr(T);
 b := a2+b2*T+c2*sqr(T)*T+d2*exp(-T);
 ca := a3+b3*T+c3*sqr(T)+d3*T*sqr(T)+e3*sqr(sqr(T))+f3*T*sqr(sqr(T));
 dens := (a+b*(c/Mn/0.1)+ca*sqr(c/Mn/0.1))*1000;
end;
```

Viscosity of brine solution as function of concentration and temperature [N.s/m^2]

```
function viscb(T,c : real) : real;
var
        I,a01,b01,viscw,m : real;
const
        a1 =  0.03550;
        a2 =  0.00231;
        a3 = -0.00003;
        b1 = -0.04753;
        b2 =  0.01598;
        b3 = -0.00194;
 begin
  m := (c/Mn)/0.1;
        I := 0.5*(m*1+m*1);
         a01 := a1+a2*I+a3*sqr(I);
         b01  := b1+b2*I+b3*sqr(I);
        viscw := exp((-1.64779+262.37/(139.18+T-273))*ln(10)); Viscosity of pure water
  viscb := (exp(A01*ln(10)+B01*ln(viscw)))*viscw/1000;   Viscosity of brine solution
 end;
```

Thermal conductivity of H_2O [W/m.K]

```
function k12(T : real) : real;
 begin
  k12 := (577+1.522+(T-273)-0.00581*sqr(T-273))/1000;
 end;
```

Thermal conductivity of air [W/m.K]

```
function kair(T : real) : real;
 begin
  kair := (3.27+0.0764*T)/1E3;
 end;
```

Calculation of the Prandtl number

```
function Pr(T,c : real) : real;
 begin
  Pr := cpf(T)*viscb(T,c)/k12(T)*1000;
 end;
```

Diffusion coefficient of NaCl in water [m^2/s]

```
function Dab(T : real) : real;
 begin
  Dab := 1.9E-9*viscb(298,(cb+x21*100)/2)/viscb(T,(cb+x21)/100)*T/298;
 end;
```

Calculating the Schmidt number

```
function Sc(T,c : real) : real;
 begin
  Sc := viscb(T,c)/(Dab(T)*dens(T,c));
 end;
```

Calculation of the convection heat transport coefficient [W/m².K]

```
function h(T,c,u,dH : real) : real;
 begin
  Re := dens(T,c)*u*dH/viscb(T,c);          Reynolds number
 if Re <= 2400 then
  begin                  For laminar conditions
        Nu := exp(ln(0.644)+0.5*ln(Re)+1/3*ln(Pr(T,c)));  Nusselt number
        h := k12(T)*Nu/x;                          Convection heat transfer coefficient
  end
       else
  begin        For turbulent conditions
        Nu':= exp(ln(0.0296)+0.8*ln(Re)+1/3*ln(Pr(T,c)));        Nusselt number
        h := k12(T)*Nu/x;                          Convection heat transfer coefficient
   end;
end;
```

Mass transport coefficient [m/s]

```
function kmass(T,c,u,dH : real) : real;
 begin
   Re := dens(T,c)*u*dH/viscb(T,c);          Reynolds number
 if Re <= 2400 then
  begin        for laminar conditions
        Sh := exp(ln(0.644)+0.5*ln(Re)+1/3*ln(Sc(T,c)));        Sherwood number
        kmass := Dab(T)*Sh/x;                        Mass transfer coefficient
  end
```

```
      else
 begin        for turbulent conditions
      Sh := exp(ln(0.0296)+0.8*ln(Re)+1/3*ln(Sc(T,c)));        Sherwood number
      kmass := Dab(T)*Sh/x;                                    Mass transfer coefficient
 end;
end;
```

To determine the magnitude of the resistances against heat and mass transfer

```
procedure Resistances;
 begin
  Ta1 := (T1+T2)/2;          Average temperature across the temperature
                             boundary layer
  Ta2 := (T2+T4)/2;          Average temperature across diffusion path
  Ta3 := (T4+T5)/2;          Average temperature across condensate
  Ta4 := (T6+T7)/2;          Average temperature across the condensing plate
  Ta5 := (T2+T3)/2;          Average temperature across the membrane
  Ta6 := (T3+T4)/2;          Average temperature across the air-gap
 Pam := P-((VP(T2,cb)-VP(T4,cp))/(ln(VP(T2,cb)/VP(T4,cp))));   log-mean pressure
      kss := 0.02*(T5+T6)/2+8.6; Thermal conductivity of stainless steel
t:=0;
```

Iteration used to determine the concentration of the salt at the membrane surface

```
      repeat
            t := t+1;
            c1 := dens(T1,cb)*(1-cb/100)/M*1000;
```

```
c22 := VP(T2,x21*100)/(R*Ta2);
c4 := VP(T4,cp)/(R*Ta2);
c21 := c1-(Rm3*R*Ta2/Rm4)*(c22-c4);
repeat
    z:= z+1;
    x21 := x21+0.001;
    f1 := c21/1000*M;
    f2 := (1-x21)*dens(T2,x21*100);
until f2<=f1;
until t = 15;
```

```
Rm1 := l1/(Perm(T2)*A1);                    Membrane mass transfer resistance
Rm2 := Pam*R*Ta2*l2/(Dw(Ta2)*P*M*A2);       Air-gap resistance
if cb=0 then
 Rm3 := 0
else
 begin
    Rm3 := 1/((kmass(Ta1,cb,ub,dH)*A1*M));  Boundary layer mass transfer resistance
 end;
Rm4 := Rm1+Rm2;
R11 := 1/(h(Ta1,cb,ub,dH)*A1);              Bounary layer heat transfer resistance
R12 := 1/(Np*cpf(Ta1));                     Enthalpy change heat transfer resistance
Rc1 := l1/(km*A1);                          Resistance due to conduction through membrane
```

```
Rc2  := l2/(kair(Ta2)*A2);          Air-gap heat transfer resistance

R22  := 1/(Np*cpg(Ta5));            Enthalpy change heat transfer resistance

R221 := 1/(Np*cpg(Ta6));            Enthalpy change heat transfer resistance

R23 := 1/(1/(Rm1+Rm2)*hfg(Ta5)*PMRT(Ta2,cp)); Heat transfer resistance
                                              due to evaporation process

R3 := 1/(A2*exp(ln(0.943) + 0.25*ln(g1*k12(Ta3)*sqr(k12(Ta3))*hfg(Ta3)*
      sqr(dens(Ta3,cp))/(x*viscb(Ta3,cp)*(T4-T5))))); Heat transfer
                                                      resistance through
                                                      condensate

R4 := d1/(A2*kss);                  Conduction heat transfer resistance through
                                    condensing plate

R5 := 1/(A2*h(Ta4,cc,uc,dH2));      Convection heat transfer resistance of
                                    boundary layer

Np := (1/(Rm1+Rm2)*(VP(T2,x21*100)-VP(T4,cp)))*3600/A1; Mass flux [g/m².hr]

end;
```

Calculation of the temperature polarisation

```
procedure TempPol;

R1t := 1/(1/R11+1/R12);             Total heat transfer resistance through
                                    boundary layer

R2t := 1/(1/(1/(1/Rc1+1/R22)+1/(1/Rc2+1/R221))+1/R23);  Total heat transfer
                                                       resistance through
                                                       diffusion path

Rt := R1t+R2t+R3+R4+R5;             Total heat transfer resistance


TPC := R2t/Rt;                      Temperature polarisation coefficient

Q  := 1/Rt*(T1-T7);                 Heat flux [W]

Qcond := 1/(Rc1+Rc2)*(T2-T4);       Conduction heat losses through diffusion
                                    path
```

```
    T2 := T1-Q*R1t;                    Temperature at membrane surface
                                       (upstream)

    T3 := T2-Q*R2t*(1/(Rc1+R22)+1/(Rc2+1/R221)); Temperature at membrane
                                                 surface (downstream)

    T4 := T2-Q*R2t;                    Temperature of condensate
                                       surface

    T5 := T4-Q*R3;                     Temperature of condensing
                                       surface (condensate side)

    T6 := T5-Q*R4;                     Temperature of condensing
                                       surface (cooling water side)

end;

begin

 ClrScr;

 l2 := 1.83E-3;          Air-gap thickness [m]

 ub := 0.003;            Linear velocity of brine solution [m/s]

 uc := 0.00226;          Linear velocity of cooling water [m/s]

 cb := 3;                Concentration of feed [% (wt.)]

 T1 := 326;              Temperature of feed [K]

 T7 := 291;              Temperature of cooling water [K]

 T2 := T1;               Initial conditions

 T3 := T2-1;             Initial conditions

 T4 := T7+2;             Initial conditions

 T5 := T7+1;             Initial conditions

 T6 := T7;               Initial conditions

 Np := 1;                Initial conditions

 Rm3 := 10000;           Initial conditions

 Rm4 := 10000;           Initial conditions
```

```
z := 0;
Assign(Infile,'c:\AG');Creates and writes data to a file
ReWrite(InFile);              Creates and writes data to a file
```

Iteration used to calculate heat and mass flux

```
repeat
      T1 := T1 + 5;
      k:=0;
 repeat
       k:=k+1;
       x21 := 0;      Initial condition
       Resistances;
       TempPol;
 until k=10;
      csur := 0;      Initial condition
      repeat
            csur := csur+0.001;
            fa := c21;
            fb := dens(T2,csur)*(1-csur/100)/M*1000;
           until fb<=fa;
 WriteLn(InFile,T1:0:4,',T1:10:3,',Q:10:4,',N:10:1);
 WriteLn(T1:0:4,',T1r:10:3,',Q:10:4,',N:10:1);
 until T1 >= 356;                                   End of iteration
Close(InFile);
ReadLn;
```

APPENDIX D
(PUBLICATIONS)

MODELLING OF THE TRANSPORT PHENOMENA IN AN AIR GAP MEMBRANE DISTILLATION UNIT

BF Chemaly, RD Sanderson*, C Aldrich, L Lorenzen

Department of Metallurgical Engineering, University of Stellenbosch, Private Bag X5018, Stellenbosch, 7600
South Africa, Fax 27/21/082059

* Institute for Polimer Science, University of Stellenbosch, Stellenbosch, 7600, South Africa

SYNOPSIS

The main objective of this project was to demonstrate the feasibility of a membrane distillation unit which is made to use the abundant supply of solar energy to produce potable water from brackish or sea water.

The aims of the project involve:

- The development of the appropriate theory behind the system
- The design and optimisation of the unit with the aid of a computer simulation which is developed from the theory.
- The construction of a prototype unit with which the simulation results can be compared to the practical results

From the preliminary results that were obtained, it was observed that the temperature of the salt water solution was the most important variable in the process. As the temperature increased, the flux increased exponentially. Another variable which played a role in the mass transfer flux, but not as significantly, is the temperature of the cooling water.

KEYWORDS: Solar powered membrane distillation(SPMD) , Air Gap Membrane Distillation (AGMD)

Theory

In order to produce a distillate of quality, energy is required to separate the different species which are to be found in the feed to the distillation unit. The principle factor is the cost of the energy needed to produce the thermal driving force. Generally, membrane distillation is found to be competitive in situations where some source of waste energy is available or where electricity is expensive. The advantage of using a solar distillation unit to produce water which is safe for human consumption, lies in the fact solar energy is used as the only source of energy and it is readily available. In most areas where there is a lack or shortage of reliable water, there is access to large quantities of brackish, non-potable water. The combination of abundant quantities of solar energy as well as non-potable water, gives rise to the possibility to economically desalinate the water in order to produce potable water.

Membrane distillation[1] is a process in which water in a salt solution is evaporated through a porous membrane. The vapour condenses on a coolant surface on the other side of the membrane. The two liquid surfaces, the heated salt solution and the condensate, are separated by a porous hydrophobic membrane. Surface tension forces withhold liquids from the pores and prevent contact of the two streams. It can be said that the main purpose of the membrane in membrane distillation is as a physical support for the vapour-liquid interface[2]

The temperature difference, causing a corresponding vapour pressure difference across the membrane, provides the driving force of the membrane distillation process. Evaporation will occur at the solution surface if the vapour pressure on the solution side is greater than the vapour pressure at the condensate surface. Vapour then diffuses through the pores to the cooler surface, where it condenses.

There are basically two categories into which membrane distillation (MD) can be categorised. These are Direct Contact Membrane Distillation (DCMD) and Air Gap Membrane Distillation (AGMD)[3]. In both cases the liquid feed flows over one side of the membrane and the evaporation surface is immobilised at one membrane surface. In DCMD the condensation surface is localised at the opposite side of the membrane, while in AGMD condensation of the distillate takes place over a cold surface separated from the membrane by the additional gap of an inert gas, typically air. Clearly, in DCMD the distance between the evaporation and the condensing surface is separated only by the membrane, so that low mass and heat transfer are obtained. In AGMD, on the contrary, the evaporation and condensing surfaces are separated by a much larger distance, giving rise to a much larger heat and mass resistance. The very narrow gas gap in DCMD gives rise to a small temperature difference between the two surfaces and consequently a small driving force for mass transfer. The larger air gap in AGMD, on the other hand, gives rise to a larger temperature difference and consequently a large partial pressure difference. An increase in the air gap thickness is beneficial in all cases as far as the heat losses are concerned; however, it can result in an increase or in a decrease of the water distillation rate from a salt solution. Indeed as far as the separation is concerned an optimum air gap thickness is obtained which increases the salt concentration of the feed increases.[3]

Heat and mass transfer

Mass transfer in MD occurs by convective and diffusive transport[2] of water vapour across the dry microporous membrane, for which the driving force is the difference in water vapour pressure on either side of the membrane.

Heat transfer within the membrane occurs by two principle mechanisms[4] : firstly there is the latent heat transfer accompanying vapour flux and secondly there is heat transfer by conduction across the gas filled membrane.

Of the total quantity of heat consumed by the process, only 50 to 80% is consumed as latent heat, whilst the remainder is lost by thermal conduction. The amount of heat lost by thermal conduction can be minimised by the incorporation of an air-gap between the membrane and the condensing surface. Unfortunately, this increases the mass transfer inefficiency and limits the control of the temperature polarisation.

Mass transfer inefficiency can be seen as the presence of air between the evaporating and condensing surfaces that hinders the diffusion of vapour through the membrane and results in the flux being lower than the maximum achievable flux for the specific membrane and conditions. Hence, it is obvious that there is an optimum thickness for the air gap.

The Air Gap Membrane Distillation (AGMD) unit

The unit comprises of a membrane which is in the form of a bag. One side of the bag is black in order to maximise the absorption of radiation. To prevent the membrane from damaging, the top surface is covered with a transparent PVC sheet. This sheet will allow sunlight to enter the unit so that the black membrane surface will be able to absorb the radiation. At the back of the membrane bag, the surface is separated from the condensing surface by means of highly porous spacing material. The condensing surface is a black PVC sheet. This surface can be placed against a cold surface or in a pool of water to induce a thermal gradient between the condensing surface and the heated non-potable solution. The PVC sheets are in the form of a pocket. The one great advantage of this unit is that it can be tilted to an optimum angle, so that the incoming radiation is maximised.

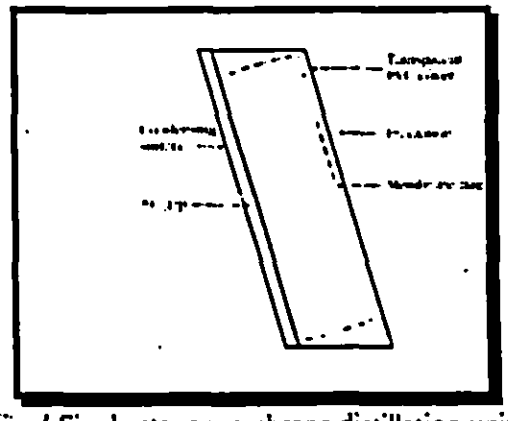

Fig. 1 Single stage membrane distillation unit

Where multistage distillation is operational, the condensing surface of the first unit is in contact with the top surface of the second membrane bag. Each stage has its' own condensing surface.

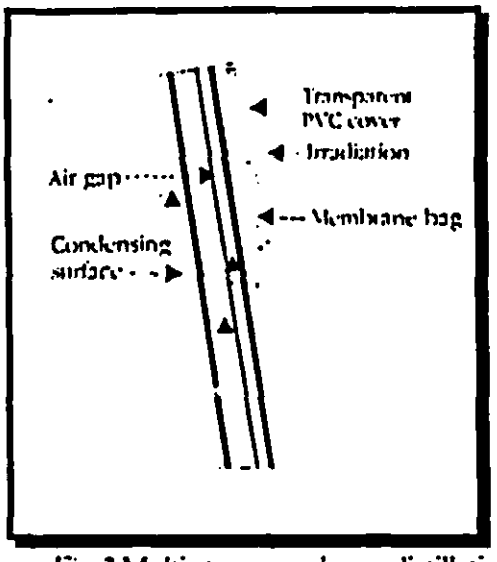

Fig 2 Multi stage membrane distillation unit

Advantages of MD compared to conventional distillation[5]

- The configuration of the evaporation surface can be made similar to various membrane modules, with a compact area density
- Mist can be eliminated, and the product is very pure
- Corrosion and/or fouling may be less than with metal surfaces
- It is able to operate at low temperatures, that is temperatures below the boiling point of the liquid

Properties of the membranes[6]

Economy of the operation calls for long life membranes, which therefore should have the following attributes:

- Chemically resistance
- Structurally strong
- Heat resistant
- Repellent to impurities in the mother liquid

Re-using of energy[7]

One of the major advantages of MD is its ability to recover the latent heat of vaporisation for re-use. As the vapour condenses on the condensing surface, the heat of condensation is used to heat

up the feed in the next stage in a multistage system. The proportion of heat transferred during distillation that can be re-used depends primarily on the approach temperatures of the streams in the MD module. The heat recovery factor is defined as the maximum possible heat recoverable in the main heat recovery exchanger divided by the heat transferred in the membrane module

$$HRF = \frac{Q_{max}}{Q_{MD}}$$

Modelling

The basis for the calculations is the assumption that membrane distillation can be described as a process in which a hot condensable vapour is diffusing at steady state through a stagnant film of non-condensable gas to a cold surface where the vapour condenses.

The molar flux, N, of a vapour diffusing at steady state through a stagnant air film is given by[1]

$$N = -\frac{cD}{1-x}\frac{dx}{dz}$$

where x is the mole fraction of the water, z is the thickness of the diffusion path and D is the diffusion coefficient.

Even though the molar flux is only affected to a minor degree by the simultaneous heat transfer, the rate of heat transfer is directly affected by the simultaneous mass transfer.
The sensible heat, E, is made up of one term describing the conductive energy flux and one term describing the energy flux caused by diffusion

$$E = -k\frac{dT}{dz} + N C_p (T - T_o)$$

where k is the thermal conductivity, C_p is the thermal conductivity.

An initial model, in the form of a TURBO PASCAL program, was developed with the aim of testing such a model against the experimental results. From the modelling of the process it was clear that a large number of variables would influence the final result, namely the production rate of potable water. Factors that are most likely to influence the production rate are :

- The amount of solar energy absorbed by the experimental system
- The temperature of the feed stream and the condensing surface

- The flowrates of the salt solution and the cooling water
- The length of the diffusion path

The theoretical model comprises mass and energy balances and uses appropriate correlations for the heat transfer, diffusion rate of the vapour, as well as the heat generated due to the condensation of the vapour. Models for both the single and double effects were developed, making it possible to determine the influence and importance of the different variables on the distillation process.

Materials for construction

The two most important requirements for the distillation unit are its portability and simplicity of operation. The latter would make it acceptable for a wider variety of applications; these could vary from emergency equipment on seacraft to the production of potable water in remote deserts.

The material of construction should be very light, but must provide the necessary protection to the membrane to prevent any damage to it.

Experimental

In the first experimental set-up that was built, canvas was used as the membrane bag. Problems arose due to the hydrostatic pressure of the water and in the controlling of the different parameters. For example, it was difficult heating the salt solution evenly, consequently a temperature gradient formed in the membrane bag and this would have influenced the production rate considerably. Other problems that arose were the uneven cooling of the condensing surface and the collecting of the permeate. One of the greatest disadvantages of the whole system was that the experimental set-up had to be re-build from scratch if anything went wrong.

To overcome these problems, a plate-and-frame type of system was built. The greatest advantage of this set-up is that there is better control over the different parameters and that different membranes can be tested. Each time the membrane needs to be replaced, the whole set-up does not have to be re-built. The heating by sunlight was simulated by heating the water with electrical heaters. The salt water, as well as the cooling water, are circulated by means of pumps.

Results

The preliminary tests delivered some results on the production rate of potable water as a function of the temperature of the heated water, as well as the cooling water.

Two types of membranes were used. One with laminated cloth on both sides of the membrane and one with cloth only on one side.

In the first experiment that was conducted, the cooling water temperature was kept constant at 14°C, while the salt water's temperature varied. The membrane that was used was laminated at either side of the membrane.

The following results were obtained:

$T_{salt\ water}$ [°C]	Condensate [ml/(h.m^2)]
50	74.1
54	78
60	160.7
62	183.5
65	192.7
76	330.3

In the second experiment the influence of the temperature of the condensing surface was investigated, keeping the temperature of the salt water constant at 65 ± C.

The following results were obtained:

$T_{condensing\ surface}$ [°C]	Condensate [ml/(h.m^2)]
13	204.5
15	192.7
19	183.5

Further experiments were done to see the effects of the laminated cloth on the permeate flux. In other words, it had to be seen whether the laminated cloth acts as extra resistance for the mass transfer through the membrane.

The following results were obtained:

$T_{salt\ solution}$ [°C]	Condensate [ml/(h.m^2)]
48	517.1
57	587.2
61	652.4

Discussion of the results

The results confirmed the idea that the temperature of the salt water plays one of the most important roles in the production rate. On thermodynamic grounds the amount of vapour that was formed would increase if the temperature of the salt water was increased.

The above results indicate that the laminated cloth has a definite effect on the diffusion rate of the water-vapour. Thus, the laminated support cloth adds to the resistance against mass transfer through the membrane. Ideally, a membrane without any protective cloth should be used, but since the membrane has a thickness of only 12 micron, it would not be possible to use the membrane without any protection.

The effect of changes in the temperature of the condensing surface is not as significant as changes in the temperature of the salt solution. If the air gap is saturated with water-vapour, it is obvious that the temperature of the condensing surface would have a noticeable effect on the production rate. The lower the temperature of the condensing surface, the faster the water-vapour would condense. This will influence the saturation of the water-vapour in the air-gap, and diffusion would be able to take place at a faster rate through the specific membrane and under the specific conditions.

Conclusions

Changes in the temperature of the condensing surface does not have such a great effect on the mass flux as the salt water's temperature. It does, however have a noticeable effect on the mass flux.

The salt water's temperature is the parameter with the greatest effect on the permeate flux. The flux increases exponentially as the temperature increases.

One of the most important changes to the current model would be to change the model to a model with multiple stages. As the vapour condenses on the condensing surface, the heat of condensation is used to heat up the feed in the next stage.

References

1. AS Jonsson, R Wimmerstedt, AC Harryson, "Membrane distillation - A theoretical study of evaporation through microporous membranes". Desalination Elsevier Science Publishers, 56(1985), pp.237-249
2. S. Bandini, C. Gostoli, GC Sarti, "Role of heat and mass transfer in membrane distillation process", Desalination, Elsevier Science Publishers, 81(1991, pp.91-105
3. I Basini, G D'Angelo, M Gobbi, GC Sarti, C Gostoli, "A desalination process through sweeping gas membrane distillation, Desalination, Elsevier Science Publishers, pp.245-257
4. AG Fane, RW Schofield, CJD Fell," The efficient use of energy in membrane distillation", Desalination, Elsevier Science Publishers, 64(1987), pp.231-243
5. Shoji Kimura, Shin-Ichi Nakoa, "Transport phenomena in membrane distillation", Desalination, Elsevier Science Publishers, pp.285-297
6. SI Andersson, R Kjellander, B Rodesjo, " Design and field tests of a new membrane distillation desalination process". Desalination, Elsevier Science Publishers, 56(1985), pp.345-354
7. PA Hogan, Sudjito, AG Fane GL Morrison, "Desalination by Solar heated membrane distillation"

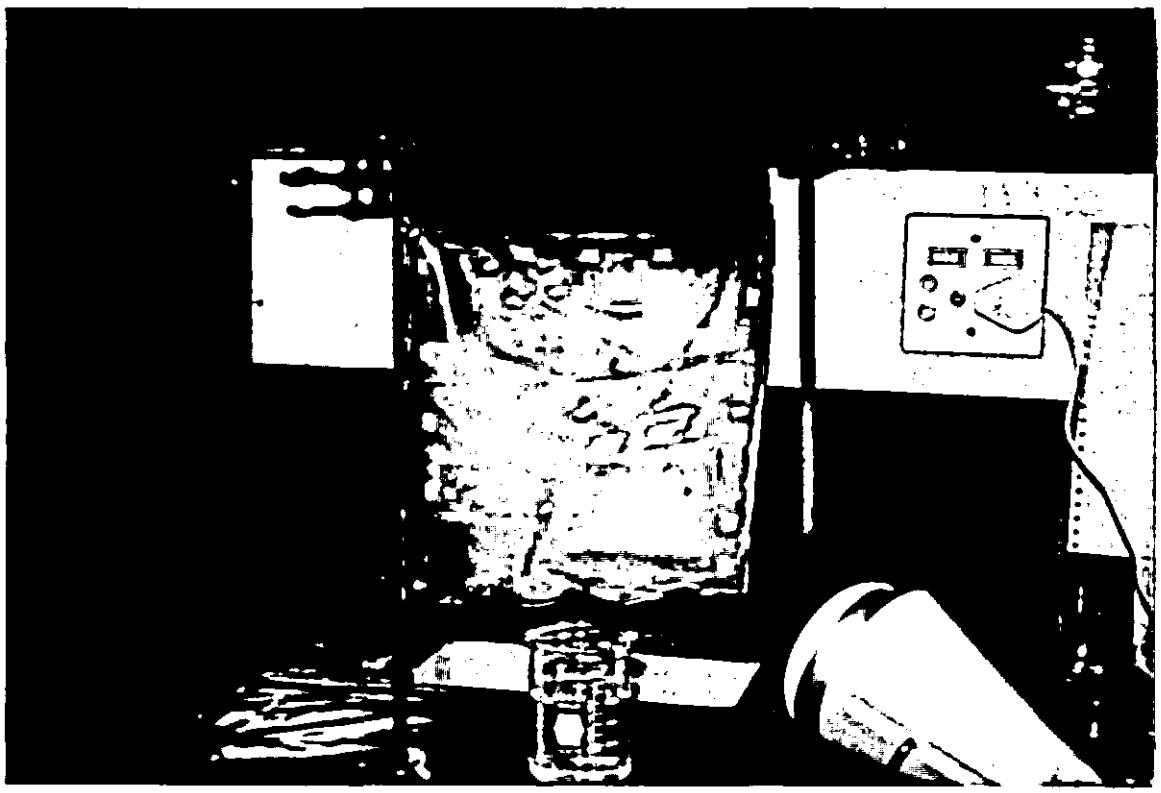

Fig. B3 Photograph of air gap membrane distillation unit.